Dysregulated TGF-β signaling and oxidative stress as the cause for osteoporosis in the progeroid disorder Gerodermia Osteodysplastica

A dissertation submitted to the

Department of Biology, Chemistry and Pharmacy

Freie Universität Berlin

in partial fulfillment of the requirements for the degree of

doctor rerum naturalium

– Dr. rer. nat. –

by

Magdalena Steiner

Born in Tristach / Lienz in Austria

Berlin 2015

This study was carried out from April 2011 until June 2015 at the Department for Medical Genetics and Human Genetics at the Charitè and in the Max Planck Institute for Molecular Genetics under the supervision of Prof. Dr. Uwe Kornak and Prof. Dr. Stefan Mundlos.

1. First Examiner: Prof. Dr. Uwe Kornak
Charitè Universitätsmedizin
Institute for Medical Genetics and Human Genetics
Augustenburgerplatz 1, 13353 Berlin
Tel.: +49 30 450 569 134
Email: uwe.kornak@charite.de

2. Second Examiner: Prof. Dr. Silke Sperling
Charitè Universitätsmedizin and Max Delbrück Zentrum
Cardiovascular Genetics
Lindenberger Weg 80, 13125 Berlin
Tel: +49 30 450 540122
Email: silke.sperling@charite.de

Date of defense: 10th of May 2016

Eidesstattliche Erklärung

Ich erkläre eidesstattlich, dass ich die vorliegende Arbeit selbstständig angefertigt und keine anderen, als die angegebenen Hilfsmittel und Literaturquellen verwendet habe. Diese schriftliche Arbeit wurde noch an keiner Stelle vorgelegt.

Berlin, den 30. November 2015 _____

Abstract

Gerodermia Osteodysplastica (GO) is a premature ageing disorder characterized by wrinkled, lax skin and premature osteoporosis. GO is caused by loss-of-function mutations in GORAB, a novel Golgin with poorly understood function. This study is focused on in vitro and in vivo studies in order to get insight into the molecular pathomechanism of GO. A conditional *Gorab* mouse model was created and crossed with Runx2cre to inactivate *Gorab* in osteoblast and chondrocyte lineage. The GorabRunx2cre mutants displayed growth retardation, a reduction of trabecular and cortical bone volume, mineralization defects, and spontaneous fractures mostly in the long bones. Further analysis revealed a significant increase of osteoblasts with a delay in osteocyte differentiation.

To identify the reason for the impaired osteoblast differentiation, expression analyses on primary osteoblast isolated from the calvaria of GorabRunx2cre mice, were conducted. An increase of early osteoblasts markers together with a delayed osteocyte maturation was found. In addition, an incrased expression of the cell cycle inhibitor p21 and TGF-β were observed.

In vitro, GorabRunx2cre mutant bone cells and GORAB-deficient fibroblasts exhibited increased levels of reactive oxygen species (ROS) leading to an accumulation of oxidative DNA damage and subsequently to increased cellular senescence markers. The increase of ROS in *Gorab*-deficient cells and bone tissue is correlated with excessive TGF-β - Nox4 signaling. These enhanced TGF-β levels in *Gorab*-deficient tissues were correlated with a striking decrease in decorin glycanation known to modulate the activity of TGF-β. The organization of collagen fibers in the cortical bone of GorabRunx2cre mice was highly altered, showing thin and fragmented fibers. Taken together, these results demonstrate that oxidative DNA damage and cellular senescence are triggered by elevated TGF-β signaling which is caused by abnormal glycanation of extracellular matrix components. This pathomechanism is suggested to play a dominant role in the development of GO.

Zusammenfassung

Gerodermia osteodysplastica (GO) ist eine autosomal rezessiv vererbte segmental progeroide Erkrankung, die durch frühzeitige Osteoporose und Faltenbildung der Haut gekennzeichnet ist. Die molekulare Ursache sind Mutationen im Gen GORAB. Die hier beschriebene Studie befasste sich mit in vitro und in vivo Untersuchungen zur molekulare Pathophysiologie von GO. Ein konditionelles *Gorab* Mausmodell wurde etabliert und durch die Kreuzung mit der Runx2cre Linie führt dies zu einer Inaktivierung des Gens in Osteoblasten und Chondrozyten. GorabRunx2cre Mutanten zeigten Wachstumsverzögerung, eine Reduktion des trabekulären und kortikalen Knochenvolumens, verzögerte Mineralisierung und spontane Frakturen vor allem in den langen Röhrenknochen. Zudem wurde eine deutliche Veränderung der Osteozytenmorphologie festgestellt. In 4 Wochen alten Tieren konnte zudem eine starke Zunahme von unreifen Osteoblasten beobachtet werden. Dieses Ergebnis deutet darauf hin, dass Differenzierung von Osteozyten aus Osteoblasten beeinträchtigt ist. Zur näheren Untersuchung dieser Osteoblastenfehlfunktion wurde die Genexpression, von aus der Schädeldecke der GorabRunx2cre Maus gewonnenen primären Osteoblasten, untersucht. Dies zeigte zuerst eine Erhöhung der frühen Osteoblastenmarker und später eine verlangsamte Osteozytenreifung. Zusätzlich konnten eine verstärkte Expression des Zellzyklus-Inhibitors p21 und von TGF-β beobachtet werden. Die erhöhte Aktivität des TGF-β Signalweges konnte auch in GO Hautfibroblasten bestätigt werden.

Außerdem zeigten GorabRunx2cre und GORAB defiziente humane Fibroblasten eine vermehrte Produktion von Reaktiven Sauerstoff Spezies (ROS) welche zu vermehrten DNA Schäden führte und in weiterer Folge zu erhöhter zellulärer Seneszenz. Die Erhöhung von ROS in den verschiedenen Geweben war verursacht durch den gesteigerten TGF-β - Nox4 Signalweg. Die erhöhten TGF-β Werte im Gorab defizienten Gewebe korrelierte stark mit einer verminderten Glykanierung von Decorin, welches die Aktivität von TGF-β moduliert. Die Kollagenstruktur im kortikalen Knochen wies starke Veränderungen auf, mit dünnen und fragmentierten Fasern. Zusammengefasst zeigen die Experimente eine erhöhte Anzahl von DNA Schäden und in weiterer Folge zelluläre Seneszenz in GO. Dies wird verursacht durch eine Verstärkung des TGF-β Signalweges auf Grund einer veränderten Glykanierung des Proteoglykans Decorin verursacht wird.

List of contents

List of Figures

List of Tables

1. Introduction

1.1 Gerodermia Osteodysplastica

Gerodermia Osteodysplastica (GO, MIM231070) is a rare autosomal recessive disorder characterized by wrinkled and lax skin, which is most prominent in the face and at the dorsum of the hands and feet. Patients with GO appear to be older than the normal physiological age and bones show severe osteoporosis in early childhood. The disorder was first named and described by Bamatter et al. in 1950 in five members of a Swiss family. A more detailed study was published by Hunter et al. (1987) including two consanguin families with six affected children. Up to date, not more than 100 GO cases were diagnosed. GO can be considered as a segmental progeroid disorder involving bone and skin [1], [2], [3].

1.1.1 Clinical features of GO

GO patients in general have a decreased height and weight when they are born. Its main clinical features are lax and wrinkled skin and prominent veins most marked over the extremities, especially on the dorsum of the hands and feet. GO patients have a specific facial appearance which include craniofacial variations with a droopy, jowly face, large ears, a large bulbous nose, a broad prominent forehead, malar hypoplasia and a mandibular prognathism (Figure 1). Other characteristics include joint hyperextensibility and radiological manifestations including Wormian bones [2]. Histological abnormalities include excessive fragmentation of the elastic fibers [1]. These characteristics give the patients a premature aged appearance. One major characteristic of GO patients is the early onset of osteoporosis in the long bones and vertebrae. Patients suffer from spontaneous fractures and hip dislocations.

1.1.2 GO in comparison to other Cutis laxa syndromes

Debré et al. (1937) were the first ones using the term cutis laxa (CL;CLGDD; OMIM 219200) to describe a rare disorder characterized by hanging loose skin, pre- and post-natal growth deficiency, mental retardation, large fontanels, hip dislocation and dysmorphic facial features, as well as radiological signs consisting of osteoporosis and Wormian bones [4]. Other histological findings include aggregation, fragmentation and clumping of elastic fibers. Today we know that cutis laxa is a group of connective tissue disorders. The lax skin is often most prominent in the face which results in a premature aged appearance. CL does not only affect the skin; other organs including the skeleton, muscles, heart and lungs can be affected. The features of GO are corresponding to the ones of autosomal recessive cutis laxa type II (Debrè

type, ARCL2A) and recessive cutis laxa with progeroid features (ARCL2B). ARCL2A and ARCL2B share many common features like generalized lax and wrinkled skin, osteopenia, developmental delay and microcephaly. In contrast to ARCL2B, ARCL2A patients show defects in N- and O- linked glycosylation in plasma transferring and apolipoprotein CIII [5]. GO patients generally have osteoporosis and resulting bone fractures whereas ARCL2A and ARCL2B patients have only mildly increased fracture risk. Taken together, GO shares a lot of common features with ARCL2A and ARCL2B, which makes a diagnosis only based on phenotypical appearance challenging (see Table 1).

Table 1: Phenotype comparison in GO, ARCL2A and ARCL2B. [6]

Characteristics	**GO**	**ARCL2A**	**ARCL2B**
Causative Gene	GORAB	ATP6V0A2	PYCR1
Generalized Cutis Laxa	-	+	+
Wrinkled skin at birth	+	+	+
Osteopenia	+	+/?	+/?
Fractures	+	-	-
Spinal deformity	+	+	+
Mental retardation	-	+	+
Abnormal N- and O- glycosylation	-	+	-
Delayed motor development	+	+	+/?
Maxillary Hypoplasia	+	-	-

1.1.3 GORAB, the causative gene for GO

GORAB was found to be the causative gene for Gerodermia Osteodysplastica [6]. The study involved patients from 13 families, all showing typical GO features like osteoporosis which frequently resulted in fractures of long bones or the vertebrae. A genome wide scan in all affected patients from a Mennonite pedigree identified a homozygous region on chromosome 1q24. By a candidate sequencing approach a homozygous nonsense mutation in a gene called *GORAB* (also known as Scyl1bp1, NTKLBP1) was found in all four Mennonite families. In nine other patients with GO features from Germany, Italy, Oman, Pakistan, Libya, Mexico and the United States they were able to identify eight other mutations including five nonsense mutations, one splice-site mutation and one mutation affecting the methionine start codon. The GORAB protein was completely absent in immunoblot analysis of patient-derived cells (Figure 1.E). Staining with markers for different subcellular locations showed a clear localization at the Golgi apparatus. GO patients show no other Golgi abnormalities comparing to controls. Nevertheless gene expression analyses in different tissues revealed a ubiquitous expression of *Gorab* with highest gene expression in the lung, skin and bone. This expression

pattern correlates with the disease phenotype. Gene expression of *Gorab* increases with progressing osteoblast development [6].

Another group described one missense mutation in the *GORAB* gene of GO patients where the alpha helix structure containing the two coiled-coil domains of the GORAB protein was disrupted [7]. Both groups concluded that the loss of function mutation in the gene *GORAB* is the cause for Gerodermia osteodysplastica [6], [7].

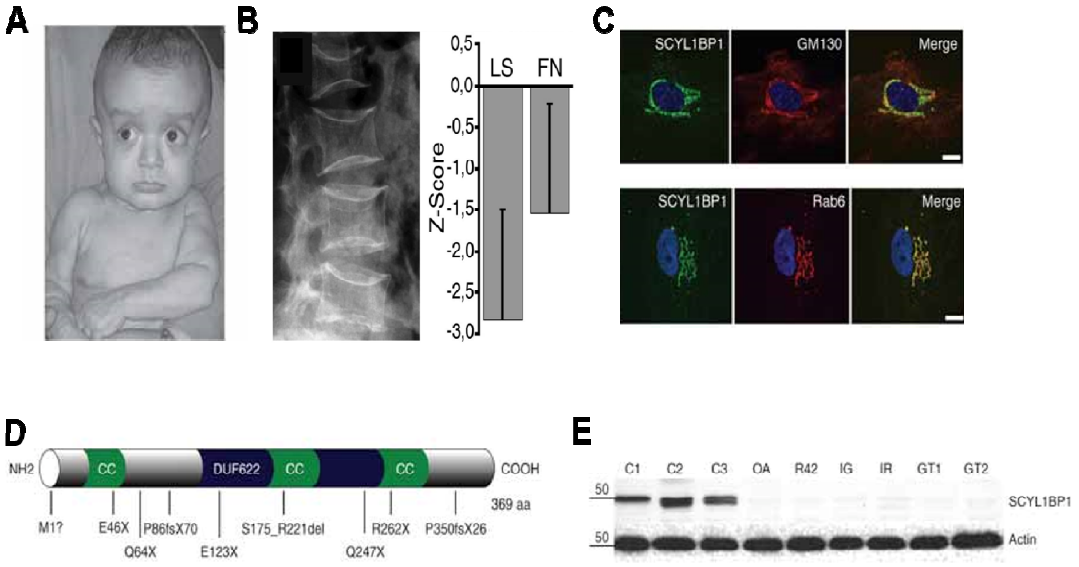

Figure 1: *GORAB (Scyl1bp1)* is the causative gene of GO. (A) Gerodermia osteodysplastica is chararcterized by a premature aged appearance with wrinkled skin, triangular face (B) and osteoporosis. (C) GORAB is a novel Golgin, located at the Golgi apparatus (co-localizing with the Golgi marker GM130) and interacts with Rab6. (D) Schematic diagram showing different positions of mutations found in GO patients and the different domains in the GORAB protein (CC- coiled-coil; DUF622-an uncharacterized domain). (E) Immunoblot analysis showing GORAB (Scyl1bp1) protein with a size of around 50kDA in human fibroblasts whereas in GO patients a complete loss of the protein was observed. Pictures modified and adopted from [6].

1.2 GORAB and its interacting partners

Gorab is a highly conserved gene that can be found in a variety of species including human, mouse, dog, chimpanzee, zebrafish and xenopus [8]. It is located on chromosome 1 and according to Ensemble the distinct position is: 170,532,129 - 170,553,446. The full-length cDNA sequence of the *Gorab* gene consists of 2,537 bp, which encodes 368 amino acids (aa). In human two transcripts are known. The longer version of GORAB has 394aa and another shorter isoform that contains 368aa; the predicted protein size is 44993 dalton (Da). In silico analysis of GORAB predicted three coild-coil regions on following positions: 130-170aa, 200-250aa and 270-300aa [9].

GORAB was originally named and described as a binding partner of NTKL (N-terminal kinase-like protein) and therefore it was named NTKL binding protein 1. This NTKL protein was renamed into Scyl1, therefore also NTKL1bp1 was changed into Scyl1bp1. Scy1lbp1 underwent another name change into GORAB (Golgin, RAB-6 interacting) because it was described as the causative gene of Gerodermia Osteodysplastica (GO). Up do date several interaction partners of GORAB have been described. Note that GORAB is the notation for the human protein and Gorab is the notation for the murine protein.

Scyl1

Scyl1 mRNA is found ubiquitously in human tissues; it is located on 11q13 and is mapped around chromosomal breakpoints. Scyl1 was identified as a high affinity partner of COPI coats acting as a regulatory element in COPI mediated retrograde trafficking [10]. Moreover it was reported that Scyl1 knockdown leads to an increased size of the Golgi apparatus [11]. Scyl1 mutations are found in several types of cancer, suggesting that Scyl1 dysfunction may be involved in carcinogenesis. Scyl1 shows a cell-cycle-dependent centrosomal localization suggesting a role in centrosome-related cellular functions [12]. Loss-of-function mutations in Scyl1 revealed that it is essential for neuronal and, particularly, Purkinje cell survival. Mutations in Scyl1 lead to an early-onset and progressive neurodegenerative disorder with muscle atrophy [13], [14]. However, this neuromuscular phenotype is not overlapping with GO.

Pirh2

Pirh2 is an E3 ligase with central roles in the regulation of cell cycle, DNA damage response, and differentiation. Pirh2 has been reported to polyubiquitylate p53 and to mediate its proteasomal degradation [15]. Moreover it is important for the in vivo regulation of p53 stability in response to DNA damage [16]. Zhang et al. found GORAB as a new interacting protein of Pirh2 in their yeast two-hybrid system. The specific interaction of GORAB and Pirh2 was confirmed by immunoprecipitation in vitro and in vivo. Contransfection of SMMC 7721 cells with hPirh2 and GORAB showed clearly a colocalization in the cytoplasm surrounding the nucleus. [17].

MDM2

MDM2 is a proto-oncogene and a nuclear localized E3 ubiquitin ligase. MDM2 is known to promote tumor formation by targeting tumor suppressor proteins such as p53 for proteasomal degradation. Overexpression is associated with different kinds of cancer [18],[19]. In 2010 it

was found that GORAB promotes p53 protein stabilization and affects the transcriptional activity of p53 but also the ubiquitination and subsequent proteasome-mediated degradation of MDM2. GORAB overexpressin also resulted in cell proliferation and increased apoptosis. GORAB might possibly form a complex with P53 and MDM2. The authors speculate that GORAB directly inhibits MDM2 mediated p53 ubiquitination by competing with p53 for binding sites on MDM2 [20].

Liu et al. (2012) reported that GORAB has a transcriptional activator domain (nuclear localizing domain). Overexpression of GORAB inhibits nerve outgrowth in PC12 cells and affects morphogenesis of primary cortical neurons by strongly decreasing the p53 protein level in vitro. The authors suggest that GORAB is a novel transcriptional activator by directly modulating the Mdm2/p53-dependent pathway [21].

Rab6 and Arf5

The localization at the Golgi apparatus as well as the presence of coiled-coil domains and the interaction with the small GTPase Rab6 defines GORAB as a Golgin. Rab proteins represent the largest branch of the GTPase superfamily. 3 isoforms of Rab6 are known: Rab6A, Rab6A`and Rab6B [22]. Rab proteins are involved in the regulation of intracellular membrane trafficking. Each Rab targets to an organelle and specifies therefore a specific transport step (exocytic, endocytic, or recycling pathways). Through protein-protein interactions, Rab proteins control membrane budding and formation of transport vesicles, vesicle movement along cytoskeleton, and membrane fusion at the target compartment. The huge number of Rab proteins reflect the complexity in these signaling pathways [23],[24].

In a yeast-two hybrid experiment our group could prove the interaction of Rab6 and Arf5 with the activated GTP bound domain [6]. It was shown that Arf5 and Rab6 bind to GORAB via the same internal Golgi-targeting domain (IGRAB). Two GO patients carrying a missense mutation within the IGRAB domain failed to interact with both, Rab6 and Arf5 [9].

Interestingly, siRNA knockdown of Rab6 blocks the cell in the metaphase suggesting a role of Rab6 in cell cycle progression. At the beginning of each metaphase Rab6 becomes upregulated, exactly when the Golgi apparatus fragments into numerous tubulo-vesicular structures known as mitotic Golgi fragments [23],[25].

Arf5, one member of the Arf family (ADP-ribosylation factors), are highly conserved GTPases belonging to the Ras superfamily. Arf5 is found on COPI vesicles with potential roles in vesicle coat formation [26].

Among the five mentioned potential interacting partners of GORAB: Scyl-1, Rab6 and Arf5 have been reported to play a role in retrograde transport. In addition, the location of GORAB at the Golgi suggests a role in vesicular trafficking. Nevertheless, Scyl-1, Rab6, Pirh2 and MDM2 have been reported to play a role in cell cylcle progression. The nuclear signaling domain of GORAB is another important hint for the involvement of GORAB in cytokinesis.

1.3 The Skeletal System

Even though the skeleton seems rigid and unchanging, it is a living, metabolically active organ. Each bone of the body is a complex living system that is made up of many cells, fibres and minerals. The skeleton acts as a scaffold that gives the body the stature, provides support and protects the inner organs. New blood cells are produced by the red bone marrow inside of our bones. The skeletal system also provides attachment sites for muscles to allow movements of the joints. The adult skeletal system consists of 206 bones, 32 teeth and a number of structures that connect the bones together.

1.3.1 Embryonic Development of the Skelton

In vertebrates, bones arise from three distinct lineages. The somites generate the axial skeleton, the lateral plate mesoderm generates the limb skeleton, and the cranial neural crest gives rise to the branchial arch and craniofacial bones and cartilage [27]. First, the mesenchyme arises where the initial ossification takes place. This occurs by two independent mechanisms: 1.) intramembranous ossification and 2.) endochrondral ossification. Intramembranous ossification occurs primarily in the bones of the skull. Other bones are formed by endochondral ossification.

Intramembranous ossification

Intramembranous ossification is the direct bone formation in which the mesenchyme is directly transformed into bone without an intermediate step. The ossification of the calvaria in the skull is one example for intramembranous ossification. In detail, the mesenchyme differentiates into osteoblasts which then begin to produce osteoid (unmineralized matrix). Then they start to deposit calcium phosphate into the osteoid tissue which leads to the differentiation of ostoblast to osteocytes and to the formation of mineralized mature bone matrix around the mature osteocytes. Some osteoblasts though remain on the bone surface and continue to lay down lamellae.

Endochondral ossification

Endochondral ossification is the bone formation in which the mesenchymal cells give first rise to an intermediate cartilage. The cartilage is gradually replaced and becomes bone in a next step. Endochondral ossification happens in long bones of the limbs, in the basal bones of the skull, the vertebral column and the ribs.

Endochondral bone is formed first by mesenchymal cells that differentiate into chondrocytes where they start to condense. Afterwards the cells enlarge in size, get more round in shape and start to produce matrix which is characterized by the presence of collagen type II and aggrecan. These chondrocytes continue proliferating until they get into cell hypertrophy. These hypertrophic chondrocytes secrete a collagen X matrix and direct mineralization of their surrounding matrix and blood vessel invasion. As soon as the blood vessels are formed, perichondreal precursor cells (Osx+) invade the cartilage with blood vessels and begin the formation of the primary spongiosa. Round chondrocytes continue to proliferate and form columns of proliferating chondrocytes. Bone lengthening occurs by chondrocyte proliferation, synthesis of matrix proteins and cell hypertrophy [28].

Post-natally secondary ossification sites are formed. Certain chondrocytes stop dividing, undergo hypertrophy and create a new vascularized primary spongiosa [28]. Chondrocytes express osteoblast markers like ALP, osteonectin, osteocalcin and osteopontin (Figure 2.H) [29], [30], [31].

1.3.2 Runx2 in Bone Development

Runx2 is a member of the Runt domain family of transcription factors that regulates transcription of several genes in cooperation with other cofactors and thereby controls osteoblast and chondrocyte differentiation [32]. *Runx2* expression starts in early bone development, by E13.5 it is expressed in areas of cartilaginous condensation as well as in the perichondreal region and in the tendons [33], [34], [35], [36]. After ossification has started, *Runx2* is most abundant in pre-hypertrophic and hypertrophic chondrocytes and in all osteoblasts at the trabecular as well as the cortical bone. Also desmal ossification depends on *Runx2* as indicated by the ossification defects in the calvaria and the clavicula found in patients with *Runx2* mutations [34], [37]. In in vitro ossification assays *Runx2* expression starts to rise at day 3 after osteogenic stimulation [38].

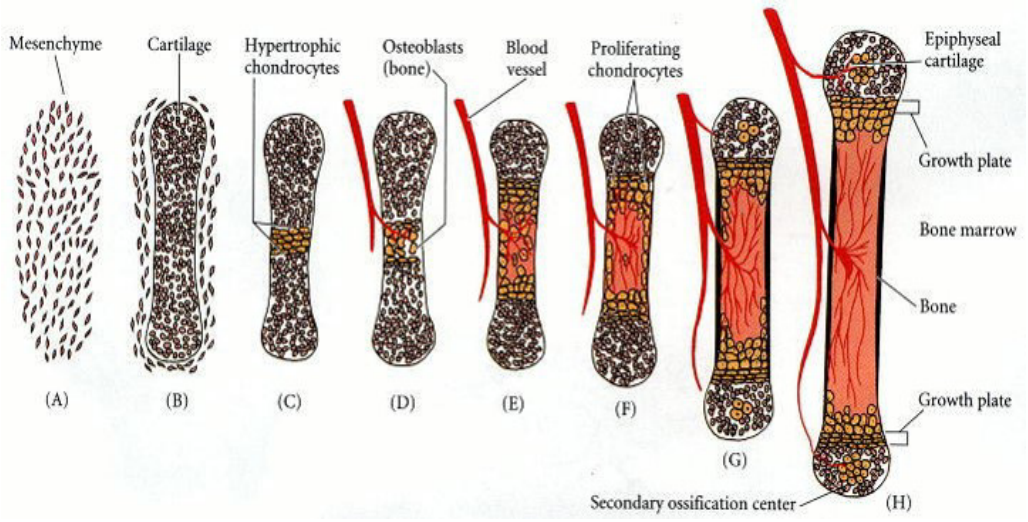

Figure 2: Schematic diagram of endochondral ossification. (A, B) Cells from the mesenchyme condense and differentiate first into chondrocytes to form the cartilage of the bone. (C) Chondrocytes, in the center of the shaft, undergo hypertrophy and apoptosis while they change and mineralize their extracellular matrix. This controlled cell death allows blood vessels to enter. (D, E) In the primary ossification center osteoblasts are brought in trough the blood vessels. (F-H) Bone formation and growth takes place in a controlled order of proliferating, hypertrophic and mineralizing chondrocytes. (H) Secondary ossification starts by the penetration of blood vessels near the tips of the bone. Picture modified adopted from [31].

1.3.3 Bone compositions

The inorganic part of the bone is composed of mainly crystalline phosphate salts which are present in form of hydroxyapatite. This serves as a reservoir for the bone of calcium and phosphate that can be mobilized in a controlled way. Bone also contains carbonate, fluoride, acid phosphate, magnesium and citrate [31].

The organic component of the bone makes up about 40% of the dry weight of the bone. Most of the organic component is type I collagen, which is synthesized intracellular as tropocollagen and then exported as collagen fibrils. Osteogenesis imperfect (OI) is caused by a defect in type I collagen which results in a less organized bone with loss of the normal osteon structure. With the failure in osteons the bone fractures with just a minimum amount of loading [39]. The other organic part of the bone is composed of proteoglycans (PGs), glycoproteins, glycosaminoglycans (GAGs) phospholipids and phosphoproteins as well as various growth factors including osteocalcin, osteonectin and bone sialoprotein [31]. Decorin is a small leucin-rich proteoglycan characterized by the presence of one chondroitin sulfate/dermatan sulfate chain [40]. It is known to be directly involved in the control of matrix organization and cell growth. In the skeletal system it is mainly located in the ECM of the

articular cartilage. Decorin is mainly required for assembling the collagen fibers [41]. The decorin core protein has a size of 36 kDA and has 6-11 leucine rich repeats and a GAG chain of chrondroitin/dermatan sulfate with additionally 50 kDA. Decorin is known to interact with type I and type II collagens. The binding site of decorin to collagen I is very close to the intermolecular cross-linking sites of collagen heterodimers [41]. Decorin is also known to interact with TGF-β1 which results in an inhibitory effect on proliferation.

1.3.4 Bone cells

There are two categories of bone cells. 1.) The osteoblast family consists of osteoblasts that form bone and osteocytes that help maintain bone as well as lining cells that cover the surface of the bone. 2.) Osteoclasts, the bone resorbing cells. Both osteoblasts and osteoclasts are originating from bone marrow derived precursors. The precursors of osteoblasts are multipotent mesenchymal stem cells, which also give rise to bone marrow stromal cells, chondrocytes, muscle cells, and adipocytes [42].

Old bone is continuously replaced by newly formed bone. This process is called bone remodelling which is necessary to keep bone volume and strength constant. Old cells are resorped and new bone is formed and integrated. Osteoblasts are appointed to bone formation. They are round in shape and build a line on the bone surface. In general, newly formed bone is calcified immediately therefore uncalcified osteoid is rare. Osteoblasts have in addition a supporting role in osteoclast differentiation. They express RANKL on their surface and osteoclast precursors are known to express RANK. RANKL recognizes RANK trough cell-cell interaction and lead to the activation of differentiation in osteoclast precursors [43].

In bone formation, longitudinal growth of long bones depends on proliferation and differentiation of cartilage cells at the growth plate. Growth in width and thickness is achieved by formation of bone at the periosteal surface with resorption at the endosteal surface. Remodelling is a lifelong process whereby the mechanical properties of the bone are maintained.

The morphology and properties of osteoblasts can differ substantially in different developmental stages. Active osteoblasts are plump, cuboidal, mononuclear cells lying on the bone matrix which they have synthesized [44]. They are highly active and have therefore a large Golgi complex as well as high mitochondria content. They synthesize and secrete type I collagen, glycoproteins such as osteopontin, osteocalcin, cytokines and growth factors into the osteoid between the cell body and the mineralized matrix [45]. Osteoblasts have receptors and respond to parathyroid hormone (PTH), 1,25-dihydroxyvitamin D3 [1,25(OH)2D3],

prostaglandins (PGs), epidermal and transforming growth factors (EGFs, TGFs) and tumour necrosis factors (TNFs) [44]. With progression into the mineralization stage, cells become positive for ALP (alkaline phosphatse). Other osteoblast related genes are also upregulated in the following differentiation process: bone sialoprotein (BSP), osteopontin (OP), and osteocalcin (OC) [44].

In order to become an osteocyte, the cell undergoes a dramatic transformation, from a polygonal cell to a cell extending dendrites in a polarized manner toward the mineralizing front. This process is followed by dendrites extending toward the vascular space of the bone surface (Figure 3) [39]. Osteocytes are the terminally differentiated and mature cell type of the bone which have become trapped within the bone matrix they have secreted previously. They are able to communicate with each other through their complex canaliculi network. When the skeleton undergoes mechanical stress, osteocytes are able to locate and sense the pressure from mechanical loading of the bone and respond by bone formation or resorption [46].

Osteoclasts are multinucleated cells that are responsible for bone resorption. They use an acidic fluid to dissolve mineralized bone and provide the environment for enzymatic degradation of demineralised extracellular matrix of the bone [30]. The activity of osteoclasts is maintained by calcitonin for which they have a high number of receptors [47].

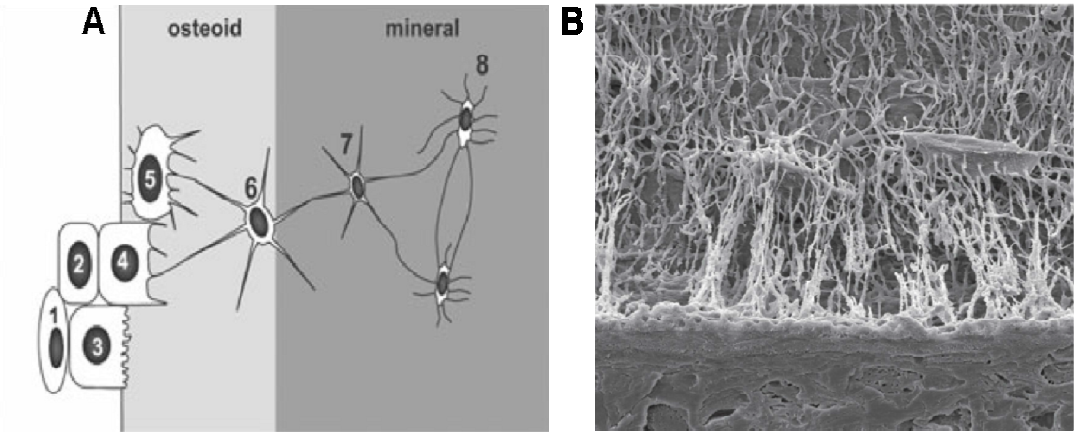

Figure 3: (A) Schematic illustration showing the transitional stages from osteoblasts to mature osteocytes. During this process, the volume of the cell body and the number of cell organelles decreases. (1) Proliferating preosteoblasts (2) preosteoblastic osteoblast (3) osteoblast (4) osteoblastic osteocyte (type I preosteocyte) (5) osteoid osteocyte (type II preosteocyte) (6) type III preosteocyte (7) young osteocyte (8) mature osteocyte. (B) Complex osteocyte canaliculi network. Figure modified and adapted from [46], [39].

1.3.5 TGF-β in bone development

TGF-β is a growth factor which is involved in the development of various bone-related diseases including Marfan syndrome and Osteogenesis Imperfecta (OI). Osteoblast differentiation is regulated by numerous secreted growth factors including the following: transforming growth factor beta (TGF-β), bone morphogenic proteins (BMPs) and fibroblast growth factors (FGFs). TGF-β is an abundant protein that controls proliferation, cellular differentiation and apoptosis in most cell types. Bone and cartilage contain large amounts of TGF-β [48]. Five different TGF-β isoforms are known, TGF-β1, -β2, and –β3 as well as two heterodimers containing one type 2 subunit, known as TGF-β1.2 and TGF-β2.3 [49]. Homodimers are in general more abundantly expressed. The TGF-β family is also part of the TGF-β superfamily that consists of nearly 30 members that share a significant sequence homology like growth and differentiation factors (GDFs) inhibin, activin and BMPs [49],[50]. TGF-β signals are passed on trough type I and type II receptors, both of them are transmembrane serine-threonine (Ser-Thr) kinases, to specific intracellular mediators known as Smad proteins. Vertebrates have at least eight different Smad proteins that are divided into three different functional classes: (a) receptor activated Smads (R-Smad) Smad 1, Smad2, Smad3, Smad5, Smad8; (b) the co-mediator Smad4 (c) the inhibitory Smads, 6 and 7 [50]. The Smad complex translocates to the nucleus and interacts with other co-activators, repressors or transcription factors to regulate gene transcription [49],[51],[52].

TGF-β is known to maintain bone mass and quality in response to a variety of biological conditions. It participates in the anabolic response to mechanical loading. An in vivo hind limb loading model revealed that mechanical loading represses TGF-β signalling trough Smad2/3 [53].

1.4 Research Aims

Gerodermia Osteodysplastica (GO) is a rare genetic disorder characterized by lax, wrinkled skin and premature osteoporosis. GORAB is a highly conserved golgin with many unknown functions.

To understand the role of Gorab in bone development different mouse models were generated. The genetrap mouse model displayed delayed ossification in long bones at E14.5. Moreover, mutant mice showed abnormal expression of osteoblast and osteocyte specific marker genes. Since the genetrap animals died at birth, several conditional mouse models were generated to study the specific effect of Gorab in postnatal bone development (GorabPrx1cre, GorabRunx2cre, GorabCol2a1cre and GorabDmp1cre).

In this study the bone phenotype of the GorabRunx2cre conditional mouse line in different postnatal stages will be analyzed. In addition, in vitro experiments on primary calvaria osteoblasts followed by a candidate gene expression profiling will help to get insight into the osteoblast to osteocyte transition process and the development of premature osteoporosis in GO.

Moreover, preliminary in vitro studies indicated increased reactive oxygen species (ROS) after the loss of Gorab. Therefore, human skin fibroblasts and primary calvaria osteoblasts from GorabRunx2cre animals will be used to test for total and mitochondrial ROS levels and DNA damages.

2. Material and Methods

2.1 Instruments

All material and instruments used in this study are listed in table 2.

Table 2: Material	
Name	**Supplier**
Centrifuges	
Centrifuge 5415 C	Eppendorf
Megafuge 2R	Heraues Instruments
Perfect Spin 24R Refrigerated Centrifuge	PeqLab
Thermo Cycler/qPCR	
9700 PCR Systems	Applied Biosystems
7500 Real Time PCR	Applied Biosystems
Microscopes, High Content Screener	
LSM 700 inverted confocal microscope	Zeiss
DX60 fluorescent microscope	Olympus
Axio cam HrC	Zeiss
Operetta	Perkin Elmer
Microtomes	
Microtome Cool Cut HM355S	Microm
Leica RM2255	Leica
Leica CM1950	Leica
Other Instruments	
PerfectBlue Semi-dry electro blotter	PeqLab
FUSION-FX7 Advance	PeqLab
Nano Photometer	Implen
CO2 Incubator	Forma Scientific
Thermomixer Comfort	Biometra
TB1 Thermoblock	Biometra

2.2 Kits

All kits used in this study are listed in table 3.

Table 3: Kits	
Name	**Supplier**
cDNA synthesis kit	Fermentas
BCA Protein Assay Kit	Pierce
Peroxidase Substrate Kit	Vector Laboratories
Direct Zol RNA mini prep	Zymo Research
Vectastain Mouse ABC Kit	Biozol

2.3 Software

Table 4 includes all software and programs used in this study.

Table 4: Software	
Name	**Supplier**
Microsoft Office	Data analysis, text processing, statistics
Inkscape	Image processing
Columbus	Evaluation of HCS data
Ostemeasure	Histomorphometry, Cell Count
7500 Real Time	qPCR analysis
Skyscan software package	CT analysis
Image J	Image processing, Immunoblot Quantification

2.4 Cell Culture Methods

2.4.1 Human Fibroblasts

Human skin fibroblasts and from GO patients and from controls were cultured in DMEM Medium (Hyclone 4.5g/L D-Glucose) with 10% fetal calf serum, 1% Ultraglutamine (Bio Wittaker) and 1% Pen-Strep (Bio Wittaker).

2.4.2 Mouse Primary Osteoblasts

Mouse primary osteoblasts were cultured in alpha-MEM (Hyclone 4.5g/L D-Glucose) 10% fetal calf serum, 1% Ultraglutamine and 1% Pen-Strep.

All ROS experiments were performed in DMEM culture medium instead of alpha-MEM. The reason is, alpha-MEM contains additionally L-Ascorbic Acid, which could lead to an indirect rescue effect in patient cells.

2.4.3 Primary Osteoblast Calvaria Preparation

Adult mice were dissected and decapitated. The calvaria was obtained; skin and muscles were carefully removed from the bone. A short step in 70% ethanol was used in order to maintain the tissue sterile. Afterwards, the bone was washed in sterile PBS; then the sample was brought twice into 4mM EDTA for 5 minutes at 37°C. Supernatant was removed and then washed 3 times in PBS. First, the bone was incubated with 0.1% Collagenase for 5 minutes. The supernatant, containing contamination of outer skin or muscles, was discarded. Then Collagenase IV was used 3-5 times for 30 minutes to digest the calvaria stepwise. Cells were passed through a 0.44µm cell sieve and stored in a medium containing 10% FBS to deactivate

the collagenase. Before seeding cells were centrifuged for 5 minutes at 1200RPM. The pellet was then lysed in alpha-MEM containing 10% FCS und 1% glutamine and1% pen/strep.

2.4.4 BMP-2 Stimulation of Mouse Primary Osteoblasts

$4x10^4$ primary osteoblasts (P1) were seeded in 12 well plates. One day after seeding cells reached confluency and were stimulated with 100ng/ml BMP-2 (Biomol) in osteogenic medium (alpha-MEM, 10% FBS, 1% Pens-Strep, 1% Ultraglutamine, 50µg/ml Vitmin C and 10mM β-glycerolphosphate). Medium was changed every 2-3 days and new ostegenic medium with 100ng/ml BMP-2 was added to each well. Cells were harvested at day 0, 1, 3, 7, 10, 14 for RNA and Protein and Alizarin and ALP Assays were performed. Specific mouse qPCR primers used for this study are listed in table 5.

2.4.5 Alizarin Staining

Alizarin Staining was performed in order to test calcium deposition in vitro. First, cells were washed with PBS and then fixed with 4% PFA for 10 minutes at 4^0C. Afterwards cells were washed three times. Then, 2% Alizarin Red S powder was dissolved in A.dest and incubated for 10 minutes at room temperature. The wells were then washed three times with PBS. Red staining showed a positive calcium deposition within the cultured cells. Staining intensities were qualitatively compared.

2.4.6 ALP Staining

Alkaline phosphatase staining was used to identify ALP expressing cells (osteoblasts) in culture. First, cells were washed with PBS and then fixed with 4% PFA for 10 minutes at 4^0C. Afterwards cells were washed three times. Then, 0.5ml CHAP Buffer (100mM Tris pH 9,5; 100mM NaCl; 50mM $MgCl_2$) was added to a 12 well plate and incubated for 30 minutes. Afterwards the buffer was removed and replaced by 0.5ml detection buffer (10ml H_2O; 45µl 4-Nitro blue tetrazolium chloride; 35µl –Bromo-4-chloro-3-indolyl-phosphate). This was incubated for 30 minutes at room temperature.

2.4.7 Cell passaging or cell splitting

Cells were washed with 1xPBS to eliminate the influence of the serum to the activity of trypsin. PBS was removed after 5-10 minutes then pre-warmed Trypsin/EDTA (Gibco) was added to the cell culture and incubated for 5 minutes. Cells were checked under the microscope until they were detached. Then the cells were resuspended with medium containing FBS and in the desired concentration used for experiments.

2.4.8 Cell freezing

Cells were trypsinized and resuspended in normal cell culture medium. Then cells were centrifuged (5min 1000RPM) and the cell pellet was resuspended in freezing medium containing 40%FBS, 10%DMSO and 50% DMEM. Initially cells were stored at -80ºC (either in a polysterene or isopropanol box) and then transferred into the liquid nitrogen tank.

2.4.9 siRNA knock down of GORAB in HeLa Cells

$7x10^4$ HeLa cells were seeded in a 6 well plate to reach a confluency of 50-70%. One day after seeding, the cells were transfected twice with siRNA against GORAB (5'-CCAUGAUGGUCACAACAAUTT-3') or control scrambled siRNA (Ambion Cat. # AM4635) using INTERFERin™ (Polyplus transfection) as a transfection reagent. According to the manufacturers protocol, 200nM siRNA was mixed with 2µl interferin in 100 µl OptiMEM (Gibco) for 10 minutes before adding to the cell culture. This allows the complexes of siRNA duplexes and interferin to form, before adding it to the cells. Eight hours after the first transfection, the cells were transfected a second time with the standard protocol. The cells were then harvested 72 hours after the first transfection for immunofluorescence, RNA extraction or protein lysates.

2.4.10 Hydrogen Peroxide Treatment

Cells were seeded at 70% confluence either on cover slips, or for protein or RNA extraction. Cells were washed 3-4 times to ensure the complete removal of serum in the wells. Then 200µM or 1mM hydrogen peroxide (Sigma Aldrich) was added to starvation medium (5mg/ml BSA in DMEM) for maximum 1 hour. Then the hydrogen peroxide was replaced by normal cultivation medium for up to 3 hours or overnight. The standard time points used for this study were 0, 30, 60, 120 and 180 minutes and/or overnight.

2.4.11 Immunofluorescence

Cells were plated onto glass cover slips at 50 % - 70% confluency. The cells were then fixed in 4% paraformaldehyde (PFA) at 4ºC for 10 minutes. After the fixation the cells were washed 3-4 times with 1xPBS and permeabilized with 0.1% Triton X-100 (TX-100) in 3%BSA in PBS at RT. The cells were then blocked with 3% BSA for 30 minutes at RT. This was followed by the primary antibody incubation at 4ºC overnight. Then the cells were washed 3-4 times with PBS and stained with the matching secondary antibody for one hour at room temperature. The cells were then counterstained with DAPI and washed 3-4 times with PBS. The cover slips were then mounted with Fluoromount ™ on a glass slide. Images were

taken either with the Olympus Bx60 microscope and the Olympus fluorescent light (U-RFC-T) or with a confocal microscope LSM700 from Zeiss. Specific primary and secondary antibodies that were used in this study are listed below in table 6.

Table 5: Primary Antibodies

Antibody	Manufacturer	Ordering Number	Dilution
Gorab	Abcam	ab128110	1:200
Gorab	Sigma Aldrich	HPA027208	1:300
GM130	BD	610823	1:500
Rab6	Santa Cruz	SC-310	1:300
p-Smad2	Cell Signaling	3101	1:300
Decorin	R&D	AF143	1:300
Collagen I	Abcam	34710	1:200
Lamin A/C	Santa Cruz	sc-6215	1:500
Calnexin	Santa Cruz	sc-6465	1:500
TGN46	Serotech	AHP500G	1:500
EEA1	BD	610457	1:500
Goat-αMouse Alexa 555	Invitrogen	A-21422	1:500
Goat-αMouse Alexa 488	Invitrogen	A-21428	1:500
Goat-αRabbit Alexa 488	Invitrogen	A-11008	1:500
Goat-αRabbit Alexa 555	Invitrogen	A-21428	1:500
Donkey-αGoat Alexa 555	Invitrogen	A-21432	1:500
DAPI	Lifetechnologies	D1306	1:3000

2.5 RNA extraction, cDNA synthesis and qPCR analysis

2.5.1 RNA extraction

RNA extraction from cell culture plates was done by using TRIzol® reagent (Invitrogen) followed by RNA isolation using Direct-zol ™ RNA mini preparation kit. 1µg of RNA was then used for cDNA synthesis using the RevertAid kit (Fermentas) according to the manufacturer's protocol.

2.5.2 Real time qPCR on cDNA

Quantitative real time PCR was performed with an ABI 7500 real time PCR system (Applied Biosciences) using EvaGreen (Solis). All the primers that were used in qPCR analysis are listed in Table 5.

The expression levels of specific genes were quantified by real time PCR. Eva green, binds to dsDNA and during the PCR reaction cycle the fluorescence intensity increases proportionally.

The increase in fluorescent signals of the PCR product is measured in real time. Primers for real time PCR were designed with primer3 (http://bioinfo.ut.ee/primer3-0.4.0/). qPCR reaction was performed in 96 well plates in a volume of 20µl on an 7900 Real-time Cycler from Applied Biosystems. The data analysis was performed with the 7900 software SDS 2.1. Expression levels of candidate genes were measured compared to Gapdh, which is a housekeeping gene (relative expression) (Table 6, Table 7). 1 ng cDNA, 2.5pmol of forward and reverse primer and Eva Green qPCR master mix were used for the reaction. The presented data are averages and standard deviations of triplicates of one representative experiment out of at least three.

Table 6: Primers used for qPCR analysis of human samples

Name	Sequence 5'à 3'
qh_GORAB	F: GGCTAAAGCTATTGCAGAAAGATCC
	R: CCTCAGCCCTGTCAAACCGCT
qh_Decorin	F: GTGTCATCTTCGAGTGGTGCAG
	R: GCCTCTGGACTGATTTTGCTGATC
qh_p16/CDKN2A	F: CACTGCTGGAAGCCGGGGTT
	R: GTTCGAATCTGCACCGTAGTTGAG
qh_DDITL4	F: CTCTCTGGGTGATAGCCACAG
	R: TGGCAGCGCTCAGGAAAGGC
qh_SOD2	F: AAGTACCAGGAGGCGTTGGCCA
	R: CTTTGGGTTCTCCACCACCGTTAG
qh_TGFβ1	F: ACCCGCGTGCTAATGGTGGTGGAA
	R: GTACCGCTTCTCGGAGCTCT
qh_TGFβ2	F: ATGTAGCGCTGGGTTGTTGGAGATGT
	R: ATGCCATCCCGCCACTTTCTAC
qh_p21	F: GCAATACTTCTGGAGATCTGTACC
	R: TGACAAAGGAACAATTAAACTGG
qh_Serpine	F: CCCATAGGGTGAAACCACTGT
	R: GAACTTGAGGATGCAGATGTCTC

2.6 Animal handling

2.6.1 GorabRunx2cre conditional mouse model

Gorab (Scyl1bp1) floxed animals were created by a former colleague (WL Chan) of our lab. Briefly, a BAC clone containing the mouse Gorab locus was obtained from Geneservice Ltd containing Exon2 and Exon 4 of the Gorab flanking regions. LoxP sites were then inserted into the targeting vector, flanking Exon2 and 3 by homologous recombination. Runx2cre expressing mice were obtained from J. Tuckermann from the University of Jena. Briefly, a 150 kb BAC clone covering the *Runx2* locus was modified by inserting a codon-improved

Cre-recombinase at the translational start site of the bone-specific site of the distal promoter (P1) of the *Runx2* gene by ET recombination (J. Tuckermann). *Runx2* cre expressing female mice were bred with Scyl1bp1 homozygous male mice. Scyl1bp1 (flox/flox) Cre positive animals were used as Gorab deficient mice and compared to Scyl1bp1 (flox/-) Cre positive animals that served as control. All mice were kept in our animal facility at the Max-Planck Institute of Molecular Genetics in Berlin under standard housing conditions.

Table 7: Primers used for qPCR analysis of mouse samples

Name	**Sequence 5'à 3'**
qm_GAPDH	F: GGGAAGCCCATCACCATCTT
	R: CGGCCTCACCCCATTTG
qm_Gorab	F: CGGATGGCTCAGGATTGG
	R: CGAGTTTTCTTCACAGGAATTCG
qm_Osterix	F: GAGGCCTTTCGTCTGCAACT
	R: TTCTTCTCCCGGGTGTGAGT
qm_p16/CDKN2Aa	F: CGCAGGTTCTTGGTCACTG
	R: TCTGCACCGTAGTTGAGCAG
qm_p21/CDKN1A	F: TGACAGATTTCTATCACTCCAAGCG
	R: CACACAGAGTGAGGGCTAAGGC
qm_Osteocalcin	F: CCTGGCTGCGCTCTGTCT
	R: TGCTTGGACATGAAGGCTTTG
qm_XBP1	F: TGGCCGGGTCTGTGCTGGGTCCG
	R: GTCCATGGGAAGATGTTCTGG
qm_XBP1spliced	F: TGGCCGGGTCTGTGCTGGGTCCG
	R: GTCCATGGGAAGATGTTCTGG
qm_TGFb1	F: ATACGCCTGAGTGGCTGTCT
	R: GCTGAATCGAAAGCCCTGTA
Qm_TGFb2	F: CGAGGAGTACTACGCCAAGG
	R: CAA TGAGCCAGAGGGTGTTG
qm_Nox4	F: CCAGAGTATCACTACCTCCACCA
	R:TCAGAGGTAAGCCAAGAGTGTTC

2.6.2 *Runx2* Cre Genotying

For genotyping, genomic DNA was extracted from mouse tail cuts. The PCR protocol, the primers and the cycler temperature program are listed below.

3 Primer strategy by binding of the 5´primer (24) to the cbfa1 promoter of the endogenous gene and the transgene and binding of one 3´primer (25) to the cre sequence and one 3´primer (30) to the endogenous cbfa-1 sequence. Thereby a wildtype product 24-30 of 780 bp will be generated and a transgene product 24-25 of 600 bp. The corresponding primers and sequences are listed in table 8.

Table 8: Runx2 Primer Sequences	
Name	**Sequence 5' à 3'**
Gorab 1F	CGACACAGGACACAATTTTTGA
Gorab 1R	GAAGATAAAACAATCACAGGGAT
Gorab 2F	TCATGTGCTATGCCATACTGC
Gorab 2R	ATCTCCCTCTCACCATTTCTG
Runx2_24	CCAGGAAGACTGCAAGAAGG
Runx2_25	TGGCTTGCAGGTACAGGAG
Runx2_30	GGAGCTGCCGAGTCAATAAC

Template DNA was mixed with the PCR master mix that is described in table 9.

Table 9: Runx2 PCR Master Mix	
Reagent	**Volume per Sample**
Firepol 12.5M $MgCl_2$	2.50 µl
dNTPs	1.00µl
F24 Primer	0.75µl
R30 Primer	0.75µl
R25 Primer	0.75µl
DNA 1µg	2.00µl

The Gorabfl/fl; PCR was implemented on a GeneAmp PCR System 9600 (Applied biosystems under following conditions (see table 10):

Table 10: PCR Cycler Programm		
Repeats	**Time**	**Temperature**
1x	5 min	95ºC
35x	30sec	95ºC
	30 sec	59ºC
	1 min	72ºC
1x	10 min	72ºC

2.6.3 X-Gal Staining

To detect all time point and regions of *Runx2* promoter activity, *Runx2* mice were crossed with a RosaLacZ reporter mouse. Embryonic stages 10.5, 12.5, 14.5 and P2 were taken to study the *Runx2* activity in embryonic development. Whole embryos or the tibia and femur were fixed with PBS containing 5mM EGTA, 2mM $MgCl_2$ and 0.25 Glutaraldehyde. Before the staining, the tissue was permeabilized with 0.01% deoxycholate and 0.02% NP-40 for either 3x5 minutes or 3x15 minutes, depending on the age of the animal. The X-gal staining

buffer contained 2mM $MgCl_2$, 5mM $K_4Fe(CN)_6$-H2O and 5mM $K_3Fe(CN)_6$. The samples were incubated for 2-4 hours at 37ºC and then overnight at 4ºC.

2.6.4 Enrichment of osteocytes from mouse long bone for RNA extraction

Osteocytes from cortical bone of mouse long bones were enriched by sequential collagenase digestion. This protocol was similar to the protocol used by Kramer et al, 2010. Mouse bones were first cleared from surrounding muscles. Then the epiphysis was cut off and the bone marrow was flushed out using a syringe with PBS. The bone shaft was then digested twice with 0.2% collagenase in isolation buffer at 37Cº.

Isolation buffer: 70mM NaCl, 10mM $NaHCO_3$, 60mM Sorbitol, 30mM KCl, 3mM KCl, 3mM K_2HPO_4, 1mM $CaCl_2$, 0.1% BSA, 0.5% Glucose, 25mM HEPES

2.6.5 Mouse Osteoblast extraction from GorabRunx2cre Calvaria

Mouse primary osteoblasts (POBs) were prepared from the calvaria of E18.5 embryos or 2 week old adult GorabRunx2cre mice. The animal was dissected and further processed to remove skin, muscles and blood vessels from the calvaria. Then, a pre-digestion followed using 0.1% collagenase for 10 minutes at 37ºC. These first cells were discarded. Then, 3-4 incubations in collagenase/trypsin followed for 45 minutes. These cells were rinsed trough a cell sieve and collected in a 50ml Falcon. Collagenase/trypsin was inactivated by a medium containing 10% FBS.

2.7 Biochemical Methods

2.7.1 Protein extraction from tissue

Tissue samples were prepared and immediately frozen in liquid nitrogen and stored at -80ºC until further processing. Then tissues were deep frozen homogenized by a metal mortar. The crushed tissue was lysed in either RIPA buffer (50mM Tris HCl pH=7.4, 1%NP-40, 0.5%Na-deoxycholate, 0.1%SDS, 150mM NaCl, 2mM EDTA, 50mM NaF) or in 8M Urea at room temperature. Lysis was performed until the whole tissue was homogenized. Lysates were sonified and centrifuged at 4ºC at 1300rpm for 5 minutes. The supernatant was transferred into a new Eppendorf tube and stored at -20ºC until further use.

2.7.2 Protein extraction from adherent cells

Adherent cells were washed first with PBS. Lysis of the cells was performed using RIPA buffer containing proteinase inhibitors. Tissue cultures were always kept on ice in this

process. Afterwards cells were dislodged by using a cell scraper and transferred into a microcentrifuge tube. Cells were then sonified for 10 seconds with a 50% amplitude in a Branson Sonicator. Then cell lysate was centrifuged for 5 minutes at 1500 RPM at 4ºC. For storage, the lysates were frozen at -20°C or -80°C.

2.7.3 Determination of protein concentration

Protein concentration was determined by BCA protein assay reagent kit (Pierce) according to manufacturer protocol. The extinction at 570 was determined with a microtiter plate reader. Proteins concentrations were calculated according to a BSA standard curve measured simultaneously.

2.7.4 Sample preparation

Samples derived from cell culture or mouse tissues were prepared as described before. 10µg - 30µg of protein was prepared and prior to run 1xSDS loading dye diluted in A.dest. The lysates were properly mixed and then heated for 5 minutes at 100°C for protein denaturation.

2.7.5 SDS Page

Immunoblot analyses was performed in order to separate and analyze proteins in a semi quantitative way. Proteins are separated based on their molecular weight trough a gel electrophoresis. The results are then transferred to a blotting membrane, producing a distinct band for each protein. The membrane is then incubated with the desired antibody of interest to detect specific proteins.

2.7.6 Gel preparation

Immunoblot gels were made by two layers of different types of acrylamide gel: stacking and separating gel. The stacking gel is the upper part of the gel is slightly acidic (pH 6.8). It has a lower acrylamide concentration making a porous gel, which separates protein poorly but allows them to form thin, sharply defined bands. The separating (lower gel) is basic (pH 8.8), and has a high polyacrylamide content. This makes the gel pores narrower. The proteins are separated by size, small proteins travel more easily and faster trough the separating gels than bigger ones.

4x Separating Gel Buffer: 1.5M Tris, 0.4%SDS, pH=8.8

4x Stacking Gel Buffer: 0.5M Tris, 0.4% SDS, pH=6.8

2.7.7 Electrophoresis

The proteins when loaded on the gel have a negative charge, as they have been denatured by heating, and will travel toward the positive electrode when a voltage is applied. When the samples were running through the stacking gel 60V was applied. Later when the proteins were running through the separating gel the voltage was increased to 120V. After approximately 1.5 hours the protein lysate with the dye runs off the bottom of the gel.

10xRunning Buffer: 250mM Tris, 2M Glycin, 1%SDS in A.dest

2.7.8 Membrane Transfer

After separating the protein mixture, it is transferred to a membrane. The transfer is done using an electric field, causing proteins to move out of the gel and onto the membrane. A sandwich for transfer was created as follows: 3 filter paper, membrane, gel, 2 filter papers using transfer buffer. The membrane was placed between the gel and the positive electrode. Transfer lasted for about 90 minutes when using 1.5mm gels and 1hour minutes for 0.75 thick gels.

10xTransfer Buffer: 250mM Tris, 2M Glycin in A.dest

2.7.9 Protein Detection

After membrane transfer was successful, membranes were blocked in 5% blocking milk in 0.1%SDS in PBS. After blocking, membranes were incubated overnight at 4ºC on a shaker with blotting milk including the primary. The next day the membrane was washed 3 times in washing buffer and then incubated with the secondary antibody in blocking solution.

Wash Buffer: 0.1%NP-40 in PBS; Blocking solution: 5% nonfat dried milk, 0.2% NP-40 in PBS

The proteins on the membrane are then detected with an antibody, labeled with a horseradish peroxidase (HRP), which is detected by the signal it produces corresponding to the position of the target protein. This signal is captured Immunoblot chemiluminiscence device from Peqlab (FUSION-FX7 Advance SUPER-BRIGHT).

Table 11: List of antibodies used for Immunoblot analysis			
Antibody	**Manufacturer**	**Ordering Number**	**Dilution**
Gorab	Abcam	ab128110	1:1000
Rab6	Santa Cruz	SC-310	1:1000
p-Smad2	Cell Signaling	3101	1:1000
Decorin	R&D	AF143	1:1000
Collagen I	Abcam	34710	1:500
Lamin A/C	Santa Cruz	sc-6215	1:500
Smad2	Cell Signaling	3122	1:1000
GapDH	Santa Cruz	sc-6215	1:10000
Actin	Cell Signaling	4967	1:1000

2.8 High Content Screening

2.8.1 MitoSOX Measurement by Operetta

$5x10^3$ cells were seeded in a 96 well plate (Cell Carrier, Perkin Elmer). 1 day and 7 days after seeding, cells were incubated at 37ºC in colourless DMEM containing 5µM MitoSOX (Invitrogen, M36008) and Hoechst (33342, Invitrogen,) for 10 minutes. Then the cells were washed once in PBS and fixed in 4% PFA at 4ºC for 10 minutes. In order to remove the PFA cells were washed 3-4 times with PBS.

2.8.2 CellRox Measurement by Operetta Imaging System

$5x10^3$ cells were seeded in a 96 well plate (Cell Carrier, Perkin Elmer). 1 day and 7 days after seeding, cells were incubated at 37ºC in colourless DMEM containing 5µM CellRox (Invitrogen, C10422) and Hoechst (33342, Invitrogen,). Then the cells were washed once in PBS and fixed in 4% PFA at 4ºC for 10 minutes. To remove the PFA, the cells were washed 3-4 times with PBS.

2.8.3 Co-Culture Experiments by Operetta Imaging System

$1x10^5$ control HAF cells were seeded in a 24 well culture dish (black Visiplate, TC treated). GO HAF cells were seeded in ThinCerts (Greiner Bio) with a pore size of 1µm. Cells were either cultured in normal DMEM containing 10% FCS, 1% Pens-Strep and 1% Ultraglutamine, or with additionally supplied TGF-β inhibitor (SB-431542) at a concentration of 10ng/ml. Medium and the medium containing the TGF-β inhibitor were changed ever 2-3

days. 7 days after the first TGF-β inhibitor stimulation, cells were stained with MitoSOX and Hoechst33342, as previously described. Afterwards cells were fixed in 4% PFA at 4ºC; washed and prepared for imaging.

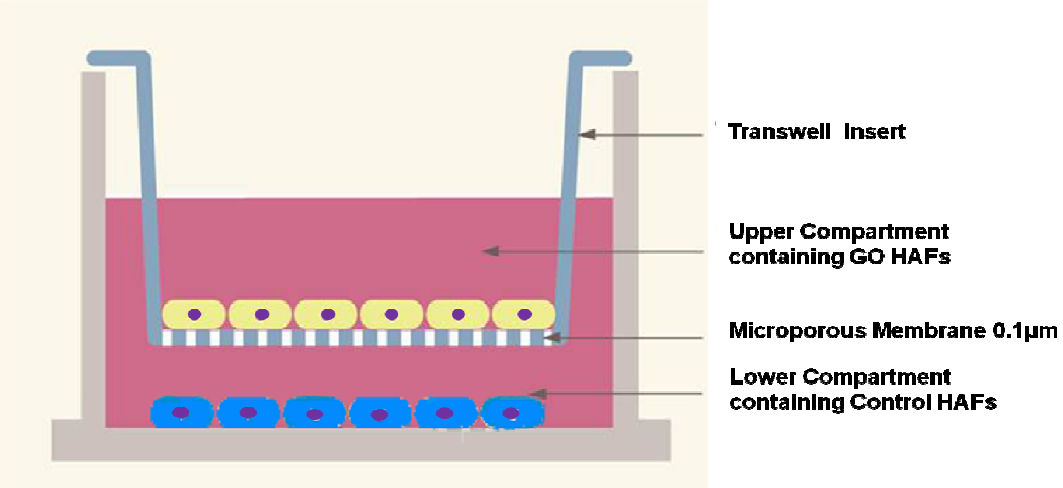

Figure 4: Co-Culture System. This system with an ultrathin glass bottom (Perkin Elmer) was used for co-culture of GO and control human fibroblasts. Control HAFs were seeded confluent in the lower compartment whereas GO HAFs were seeded in the upper compartment. The transwell insert with a microporous membrane (0.1µm) was used for separation. DMEM medium ±SB431542 TGF-β inhibitor was used. This image was modified from:
[http://www.unc.edu/depts/our/hhmi/hhmi-ft_learning_modules/2012/biologymodule/science.html]

2.8.4 High Content Imaging

24 and 96 well plates with an ultrathin glass layer botton were analyzed with the Operetta System from Perkin Elmer. The Harmony software was used to place the settings. CellRox had an excitation/emission wavelength of 485/520 nm (Green), MitoSOX 510/580 nm and Hoechst 33342 350/461 nm. A 20-fold magnification was used for imaging and following positions of the well were recorded (see Figure 5). The Perkin Elmer Software Columbus was used to quantify intensity properties of the different dyes.

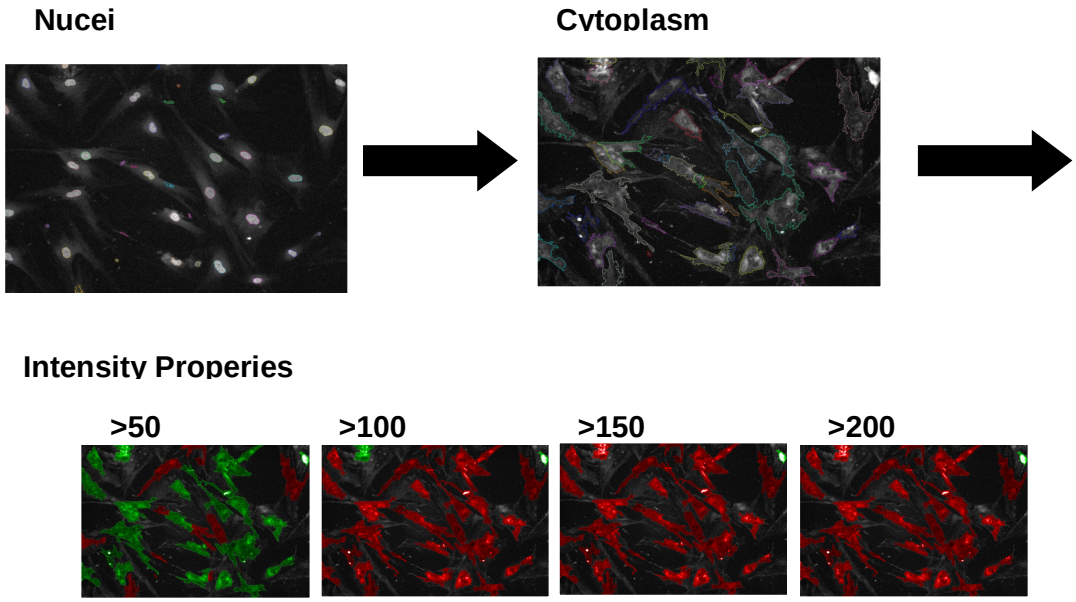

Figure 5: Workflow High Content Screener Imaging. First nuclei were selected according to Hoechst 33342 counts. The cytoplasm was selected automatically based on regions around the nuclei. Dye intensities were calculated and grouped.

2.9 Radiological Methods

2.9.1 µCT Analysis

µCT analysis was done by using the high-resolution micro-computed tomography Skyscan 1172. Long Bones and the vertebras were scanned with 80kV and 124 mA, Al 0.5 mm and a resolution of 4.9µm. Reconstruction of the files were conducted with NRecon using 0.00 as a lower threshold and 0.10 as upper threshold and a beam hardening correction of 30%. The regions of interest for the trabecular and for the cortical bone were defined with CTan due to following restrictions: 100 slices in total for the trabecular bone, starting after the growth plate below the primary spongiosa. 100 slices break followed after the trabecular bone measurement. The ROI for the cortical bone was set right afterwards, 100 slices in total. An illustration of the region of interest of the long bones is shown in Figure 6. The trabeculae of the fifth and sixth lumbar vertebra were measured between the upper and the lower growth plate.

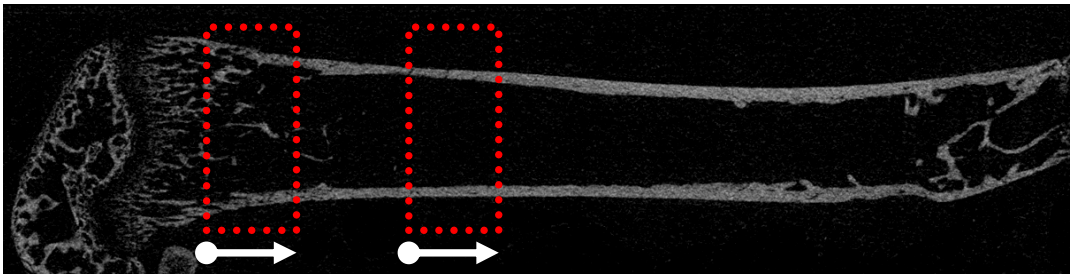

Figure 6: ROI definitions with CTan. 100 slices of trabecular bone was measured after the growth plate and primary spongiosa for 100 slices. 100 slices break and afterwards followed by 100 slices cortical bone measurement.

2.10 Histological Methods

2.10.1 Methylmethacrylate (MMA) embedding and sectioning

Tibia, Femur and Spine were embedded in MMA (Polysciences, Cat. #00843) and then sectioned for histological studies. The bone samples were first fixed in 4% PFA for 16-24 hours at 4ºC. Then the samples were dehydrated in ascending ethanol, 70% ethanol for 24 hours, 80% ethanol for 24 hours, 100% ethanol for 24 hours, ethanol:acetone=1:1 for 24 hours, 100% ethanol for another 24 hours, twice xylene for 2 hours. Then the bone samples were infiltrated with the infiltration solution for at least 24 hours at 4ºC. The polymerization was started under low pressure (200mbar) and then continued at normal pressure at 4ºC in polymerization solution. The embedded samples were then cut at 5 µm thickness using a Leica RM2255 microtome.

Infiltration solution: 10% v/v polyethylene glycerol (Sigma, Cat. # 202398), and 0.33% w/v benzoylperoxide in MMA

Polymerization solution: 10% v/v polyethylene glycerol (Sigma, Cat. # 202398) and 0.55% w/v benzoylperoxide in MMA and 0.5% v/v N,N-dimethyl-p-toluidine in MMA

2.10.2 Histological Staining

MMA sections were deplasticized by washing in 2-methoxyethylacetate thrice for each 10 minutes. Then, the sections were washed in xylene twice for 5 minutes and then rehydrated trough 2x100%, 70%, 50% ethanol for one minute in each step. Finally the sections were rinsed in A.dest and then used for the different histological stainings.

2.10.3 Von Kossa and Toluidine blue double staining

This staining is used for general bone histology. Sections were put into 1% silver nitrate solution for 3 minutes and then washed in water for 2 minutes 3 times. The staining was then developed in 5% $NaCO_3$ solution with 10% formaldehyde for 2 minutes. The sections were then washed in running tap water for at least 10 minutes. Then 5% $Na_2S_sO_7$ solution was applied to remove unwanted background staining. The sections were then washed again in running tap water for 10 minutes. Finally, the sections were counterstained with 0.05% toluidine blue solution for around 2-3 minutes.

2.10.4 Masson Goldner

This staining was used for high quality cellular histology and extracellular matrix staining. First, the sections were incubated for 2 minutes in Weigerts Haematoxylin. Afterwards, the sections were washed in running tap water for 10 minutes. The bone sections were then stained for 5 minutes with the Ponceau-Fuchsin solution (Chroma Cat. #2C149). This leads to a blue plasma staining. Then the slices were rinsed with 1% acetic acid for only a few seconds. The sections were then differentiated in Orange G solution (2% w/v Orange G in 3% phosphomolybdic acid) for 5 minutes. Then the sections were rinsed again in 1% acetic acid and then stained in light green solution (0.1% w/v light green in 2% acetic acid) for 5 minutes, for collagen fibre staining. The sections were then dehydrated and mounted for imaging. Images were taken with an Olympus Bx60 Microscope, an AxioCam Rc Zeiss camera and processed with the Axio Vision Software.

2.10.5 Von Kossa and Pikro Fuchsin double staining

This staining is generally used for osteoid staining and quantification. The protocol for the von Kossa staining can be found above. Then the sections were then stained with Picro Fuchsin solution for 10 minutes and then mounted with Entellan for imaging. Osteoid area, volume and thickness in the metaphysic were determined using the Osteomeasure ™ software.

2.10.6 Trap Staining

This enzymatic assay was used to visualize the osteoclasts in the trabecular bone region of the long bones. MMA embedded, PFA fixed sections were incubated overnight in the TRAP staining solution which consisted out of 1mg Naphtol-AS-MX-phosphat / 100µl N-N Dimethylformamid in 10ml TRAP buffer (40mM Na-acetate, 10mM Na tatrat, pH5.0). Light green was used to stain the nuclei.

2.10.7 Picosirius Red staining

Samples were deplasticized and rehydrated as described above. Then sections were incubated in 1.2% Picrosirius Red solution (Fluka/Sigma) which was always made fresh containing 1.2% saturated picric acid and 0.2g 'Direkt Rot' pH 2.0 (200ml). The samples were visualized with a polarized light microscope.

2.11 Paraffin Embedding and sectioning

Tibia, Femur and Spine were prepared and immediately fixed with PFA at 4°C overnight, followed by a decalcification step with EDTA. Then the sections were processed trough ascending ethanol (70%, 90%, 2x100%) and 2 times xylene for 30 minutes to ensure a subsequent dehydration. The samples were then infiltrated with liquid paraffin at 60°C 3 times 45 minutes each and afterwards the samples were embedded in paraffin. The paraffin embedded samples were then cut at 5 µm thickness using a Leica (2255) microtome.

2.11.1 Immunohistochemistry (IHC) on paraffin embedded tissue

The paraffin embedded section were processed trough 2x xylene for 10 minutes each, this was followed by descending ethanol steps to ensure proper rehydration. Then sections were incubated with 3% H2O2 for 10 minutes to block endogenous peroxidise activity. Then the sections were washed 3-4 times with PBS. The sections were then permeabilized using 0.1% TX-100 in 3% BSA, followed by a blocking step in 3% BSA/PBS for 30 minutes.

Then the sections were incubated for 12-16 hours with the primary antibody (Table 2) at 4°C in a humid chamber. Then sections were washed 3-4 times in PBS and incubated with a biotinylated secondary antibody for 30 minutes at room temperature. Afterwards, sections were washed 3-4 times with PBS and incubated for 40 minutes with the ABC reagent (Vectorlabs) for signal multiplication. Then the sections were incubated with the DAB substrate until the optimal colour develops (2-10 minutes). Then sections were washed in A. dest. for at least 10 minutes. A counterstaining, usually haematoxylin, was done as a final step. All primary antibodies used in this study are listed in table 12.

Table 12: List of antibodies used for Immunohistochemistry

Antibody	Manufacturer	Ordering Number	Dilution
Scerlostin	R&D	AF1589	1:200
Osterix	Abcam	ab22552	1:200
8-Oxoguanine	Abcam	ab64548	1:500
53BP1	Santa Cruz	sc-22760	1:500
Osteocalcin	Enzo Life Science	ALX-210-333	1:3000
p-Smad2	Cell Signaling	3101	1:500
P21	EuroMabNet	Hugo291H/H6	1:100
P16	EuroMabNet	Car327	1:10

3. Results

3.1 Preliminary Results

3.1.1 Gorab genetrap (GT) mouse model

A mouse model was obtained by our laboratory in which the *Gorab* gene was inactivated by a genetrap (GT) strategy. In this genetrap animal the genetrap cassette was inserted into the first intron of the gene leading to a reduction of the *Gorab* mRNA by over 90%. Preliminary analyses of GT animals were done by Dr. Heikuo Zhang a former colleague of the laboratory. However, these homozygous animals died soon after birth because of breathing difficulties. The lung of the GT animals was examined and it was found that the connective tissue in the lung and the alveoles was highly altered. Nevertheless no lung defects were reported in human GO patients. Interestingly, the skin seemed tighter comparing to littermate controls. This finding is also in contrast to human patients where the skin is lax and loose. The GT animals showed also mild delay in ossification by E14.5 which was revealed by Von Kossa staining. In E18.5 no significant difference could be detected except for a mild shortening of the long bones and a thickened and slightly disorganized bone collar. These data point into the direction of an altered osteoblast development problem. GT animals showed a highly altered gene expression of osteocyte markers in the bone as well as defects in the glycosylation in skin tissue and in the perichondrium of the long bone.

3.1.2 Conditional Knockout Mice

To prevent the lethal effect of the germline knockout and investigate the postnatal consequences of Gorab deficiency Dr. Wing Lee Chan generated conditional Gorabflox knockout mice. First, exon 2 and 3 of the Gorab allele were targeted for deletion. Exon 2 and 3 were chosen because of a.) their small size (~2.6kb) and b.) because these exons encode the majority of the first coiled-coil domain. This deletion leads to a frameshift mutation, which entails the complete loss of *Gorab*. Subsequently, *Gorab* was deleted in different cell types using transgenic lines expressing cre recombinase under the control of the Prx1, Col2a1 and DMP1 promoters in mesenchymal progenitor cells, chondrocytes, and mature osteoblasts and osteocytes, respectively. A severely osteoporotic phenotype was obtained for the resulting GorabPrx1 and GorabCol2a1 lines, but not for GorabDmp1. This indicated that the Dmp1-driven inactivation occurred after the vulnerable phase of osteoblast differentiation.

3.2 Role of Gorab in bone development

3.2.1 Generation of conditional GorabRunx2cre mouse model

GorabRunx2cre conditional mutant mice were obtained by crossing the Gorabflox strain with a *Runx2* transgenic mouse line in order to inactivate Gorab in vivo within the expression domain of the Cre transgene. In Prof. Dr. Jan Tuckerman's lab a BAC containing the *Runx2* locus was modified through ET recombination to insert a cre recombinase sequence and an ampicillin resistance gene which were flanked by two FRT sites at the translational start site of the distal promoter (P1) of the *Runx2* gene.

3.2.2 Phenotypic analysis of GorabRunx2cre animals

By crossing the conditional Gorabfl/fl mouse with the Runx2cre mouse, *Gorab* was inactivated in an early osteoblastic state. The conditional mutant mouse was viable, in contrast to the genetrap mouse model, which died at the day of birth because of lung failure. Overall, the GorabRunx2cre mouse has weak mineralization in the long bones, in the vertebrae and in the calvaria and serves as a good model to study the development of osteoporosis. Mutant mice of three postnatal stages: 4 week (juvenile), 12 week and 26 week (adult) were analysed for phenotypic abnormalities. The characterization of these animals was mainly focused on the bones of the hind limbs, the vertebrae and the calvaria.

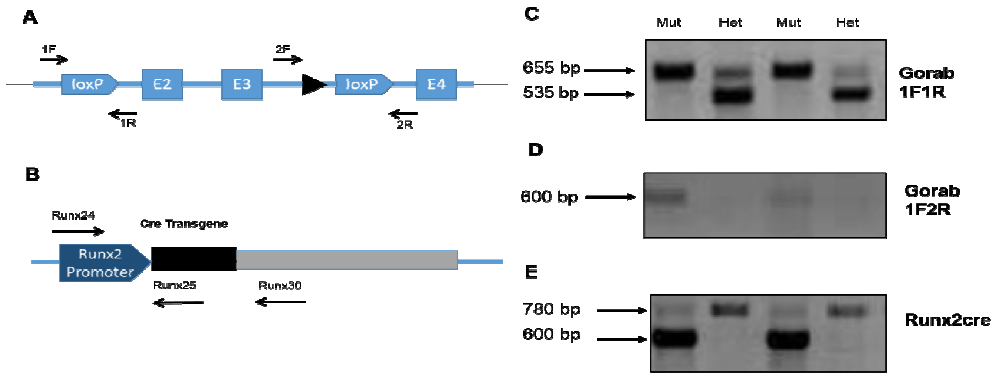

Figure 7: GorabRunx2cre genotyping strategy. (A) Schematic diagram of the Gorab locus showing the design for PCR genotyping. 1F1R primer pair flanking the first loxP site. 2F2R flanking the second loxP site (B) *Runx2* locus with the three primer strategy. By binding of the 5´primer (24) to the *Runx2* promoter of the endogenous gene and the transgene and binding of one 3´primer (25) to the cre sequence and one 3´primer (30) to the endogenous *Runx2* sequence two PCR products will result. (C) 1F1R genotyping result. Homozygous mutants Gorabfl/fl showing only one band at 655bp and the heterozygous control showing two bands, one at 535bp and an additional one at 655bp. (D) Cre-floxed mediated knockout leads to an amplification of the 1F2R product with a size of 600bp. (E) With the Runx2cre primer strategy a wt product of 780 bp (with the primer pair 24-30) and a transgene product of 600 bp (with the primer pair 24-25) will be generated.

3.2.3 Inactivation of Gorab results in size reduction and weight loss

GorabRunx2cre mice were significantly smaller and lighter compared to their littermate controls. The weight difference was most striking in 4 week old animals. In detail, by 4 weeks GorabRunx2cre conditional mice showed a reduction of 15.63g (SD±1.08) to 8.2g (SD±3.53) comparing to littermate controls which is a reduction of 48%. 12 week old GorabRunx2cre animals were significantly smaller and lighter. The weight was reduced from 19.38g (SD±3.19) to 16.12g (SD± 1.59) compared to control animals, which is in total a reduction of 17%. 26 week old GorabRunx2cre mice had around 15% less weight comparing to control animals. Since *Runx2* is only active in bone and cartilage, size reduction, weight differences and skeletal abnormalities were observed. No other striking phenotypic alterations were seen in GorabRunx2cre animals.

3.2.4 Inactivation of Gorab results in osteoporosis

Skeletal abnormalities in 4 week old GorabRunx2cre mice

To quantify bone quality of GorabRunx2cre mutant mice, X-ray radiography was performed. 3D microCT reconstruction of 4 week and 12 week old GorabRunx2cre conditional mutants showed clearly skeletal changes and phenotypic differences. The long bones were not properly mineralized; both femur and tibia were significantly shorter. Whole body X-ray scans showed that 4 week old GorabRunx2cre mutants were significantly smaller comparing to controls. The femur and tibia were shorter and thinner and showed a low mineralization rate. MicroCT analysis was performed in the distal femur, the proximal tibia and the 5^{th} and 6^{th} lumbar vertebrae. By 4 weeks the tibia and the femur of mutant mice were shorter and narrower than the control animals. This was indicated by the reduction in total bone volume and cortical bone thickness. In addition, there was a decrease in trabecular bone volume. For detailed volumetric analysis of all bones see table 2. In addition to the thinning and shortening of the bones, the overall structure was bended and appeared to be more fragile. The tibia of 4 week old mice showed a decrease in length of 14.01mm (SD±0.63) to 10.02mm (SD±0.69) comparing to controls. A similar observation was made in the femur of the animals. By 4 weeks the femur length was decreased from 13.24mm (SD±1.02) to 9.99mm (SD±0.58).

Skeletal abnormalities in 12 week old GorabRunx2cre mice

Whole body X-ray radiography showed skeletal abnormalities in 12 week old GorabRunx2cre mutants. Similar as in the case of the 4 week old animals; long bones were shorter and thinner and showed a low mineralization rate (Figure 8.A). In detail, distal femur, proximal tibia and

5th and 6th lumbar vertebrae were conducted for volumetric analysis. The femur and the tibia of 12 week old GorabRunx2cre mice was shorter and narrower indicated by a decrease in total bone volume and thickness of the cortical bone. In addition, a decrease in trabecular bone volume to tissue volume ratio as well as a reduction in trabecular thickness, number and an increase in trabecular separation was detected. The tibia of 12 week old animals showed a reduction in length from 15.28mm (SD±0.645) to 11.90mm (SD±0.52). A similar observation was made in the femur of 12 week old mice; femur length was reduced from 15.30mm (SD±0.35) to 12.98mm (SD±1.07). For detailed volumetric analysis see table 13.

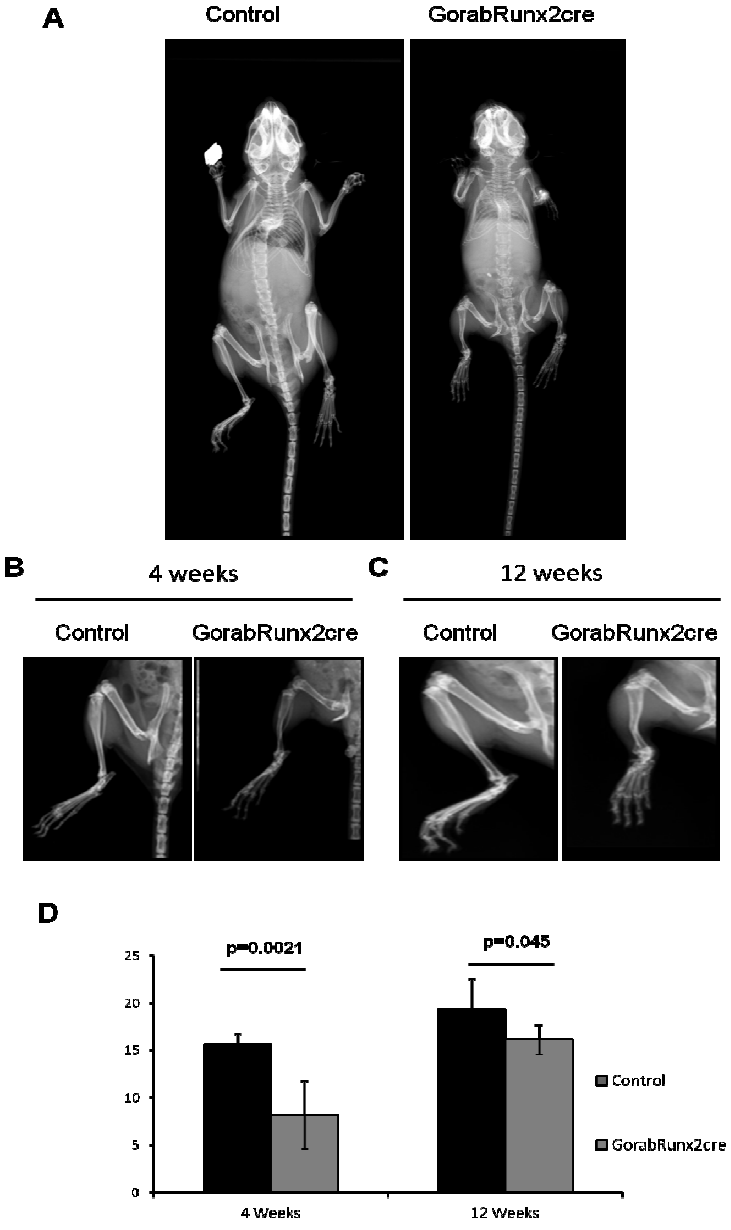

Figure 8: (A) X-ray radiography of a 4 week old GorabRunx2cre animal compared to a littermate control showing a reduction in size and a severe osteoporosis in the long bones and the spine. (B,C) X-ray radiography

on a 4 week and 12 week old control and GorabRunx2cre animal revealed a severe shortening and thinning of tibia and femur. Additionally a severe osteoporosis was observed with a low degree of mineralization. (D) GorabRunx2cre animals were significantly lighter than their littermate controls. The mean weight in 4 week animals was reduced from 15.63g (SD±1.08) to 8.2g (SD±3.53) (n=6) (p=0.0021). In 12 week old mutants the weight was reduced from 19.38±3.19 g to 16.12± 1.59 g (n=6) (p=0.045). Statistical analysis was performed by two tailed paired t-test. Error bars are representing SD.

3.2.5 Inactivation of Gorab results in bone defects and high fracture risk

The low degree of mineralization leads to a higher fracture risk in GorabRunx2cre mutants comparing to control animals. The highest fracture risk period was found between 2 weeks and 6 weeks of age (Figure 9.A). Another phenotypic abnormality of the GorabRunx2cre mutants is the malformed pelvis with a triangular obturator foramen, a short and thin pubis and a severe flatting of the ilium and ischium. The vertebra appeared to be shorter, flatter and narrower in size and had smaller processes (Figure 9.B). In all time points a significant size and weight difference could was observed. However, the size difference is most striking in 4 weeks of age. With progressing age the weight difference gets more moderate showing a regressive phenotype development.

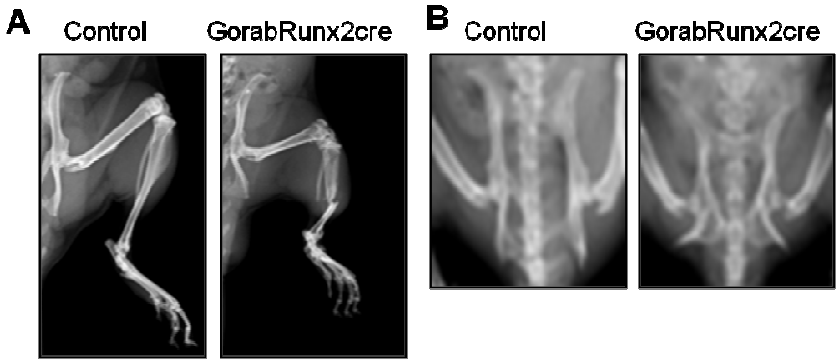

Figure 9: X-ray Radiography (A) Low degree of mineralization in GorabRunx2cre mutants compared to their littermate controls. The severe thinning of the bone leads to a higher fracture risk especially between 2 weeks and 6 weeks. (B) Malformed pelvis in the mutant. Note the thinner and more bended bone structure.

3.2.6 Inactivation of Gorab results in cortical bone thinning

Cortical tibia and femur were significantly thinner compared to controls. Cortical thickness of the tibia in 4 weeks old mutants was significantly reduced from 0.115mm (SD±0.015) to 0.069mm (SD± 0.017), in 12 week old animals from 0.123mm (SD± 0.014) to 0.084mm (SD±0.02) and in 26 weeks from 0.198 (SD±0.029) to 0.142 (SD±0.011). Femoral cortical thickness in 4 weeks old animals was reduced from 0.116mm (SD±0.002) to 0.082mm (SD± 0.026), in 12 week old animals from 0.119mm (SD± 0.019) to 0.099mm (SD±0.049) and in

26 weeks from 0.196 (SD±0.025) to 0.129 (SD±0.039) (Figure 10 and Table 13). Note that the overall structure of the bone was highly altered.

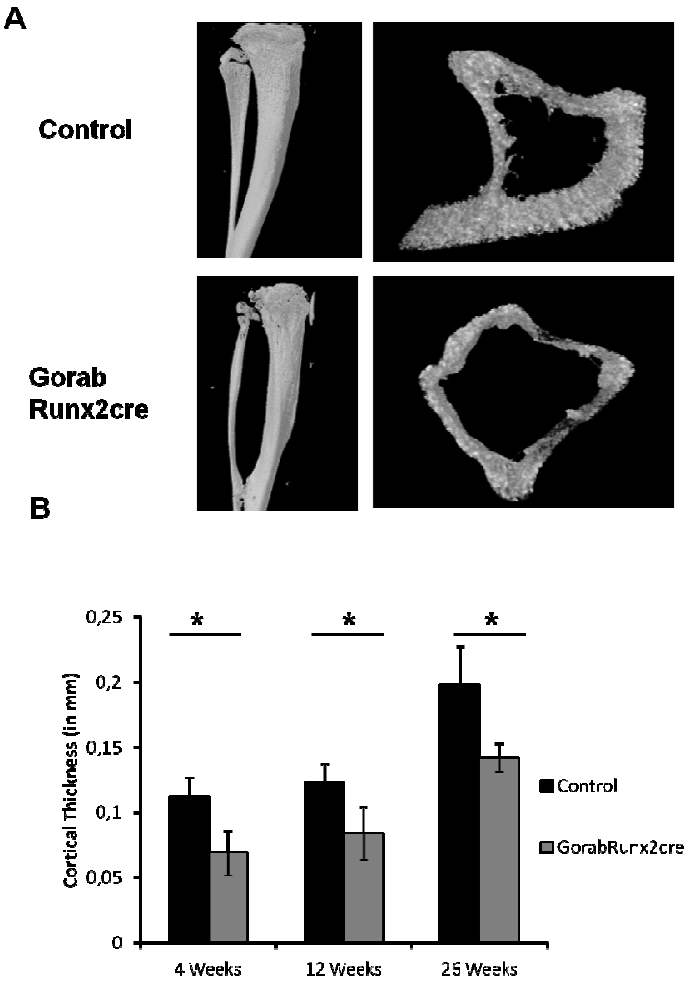

Figure 10: Cortical bone phenotype (A) µCT images showed a structural bending and a reduced cortical thickness in 4 and 12 week old Gorab Runx2cre mutants. (B) Cortical Thickness quantification revealed a significant reduction in 4 week (p=0.0009), 12 week (p=0.016) and 26 week (p=0.037) old GorabRunx2cre mutants (n=7). Statistical analysis was performed by two tailed paired t-test. Error bars are representing SD. *indicates significant differences (p<0.05).

3.2.7 Inactivation of Gorab results in trabecular bone phenotype

MicroCT analysis and quantification showed a decrease in trabecular bone volume to tissue volume ratio in 4, 12 and 26 week old animals. This resulted mainly from a decrease in trabecular number and trabecular thickness and an increase in trabecular separation. In the tibia of 12 week old GorabRunx2cre mutants a significant reduction in trabecular bone volume and number was observed. BV/TV values were significantly lower in 4 week and 12 week old GorabRunx2cre animals. Figure 11 shows in detail the tibia of 4 week and 12 week

old mutant mice compared to control animals, illustrating the thinning of the cortical bone and the reduction of the trabeculae including BV/TV quantified by microCT analysis.

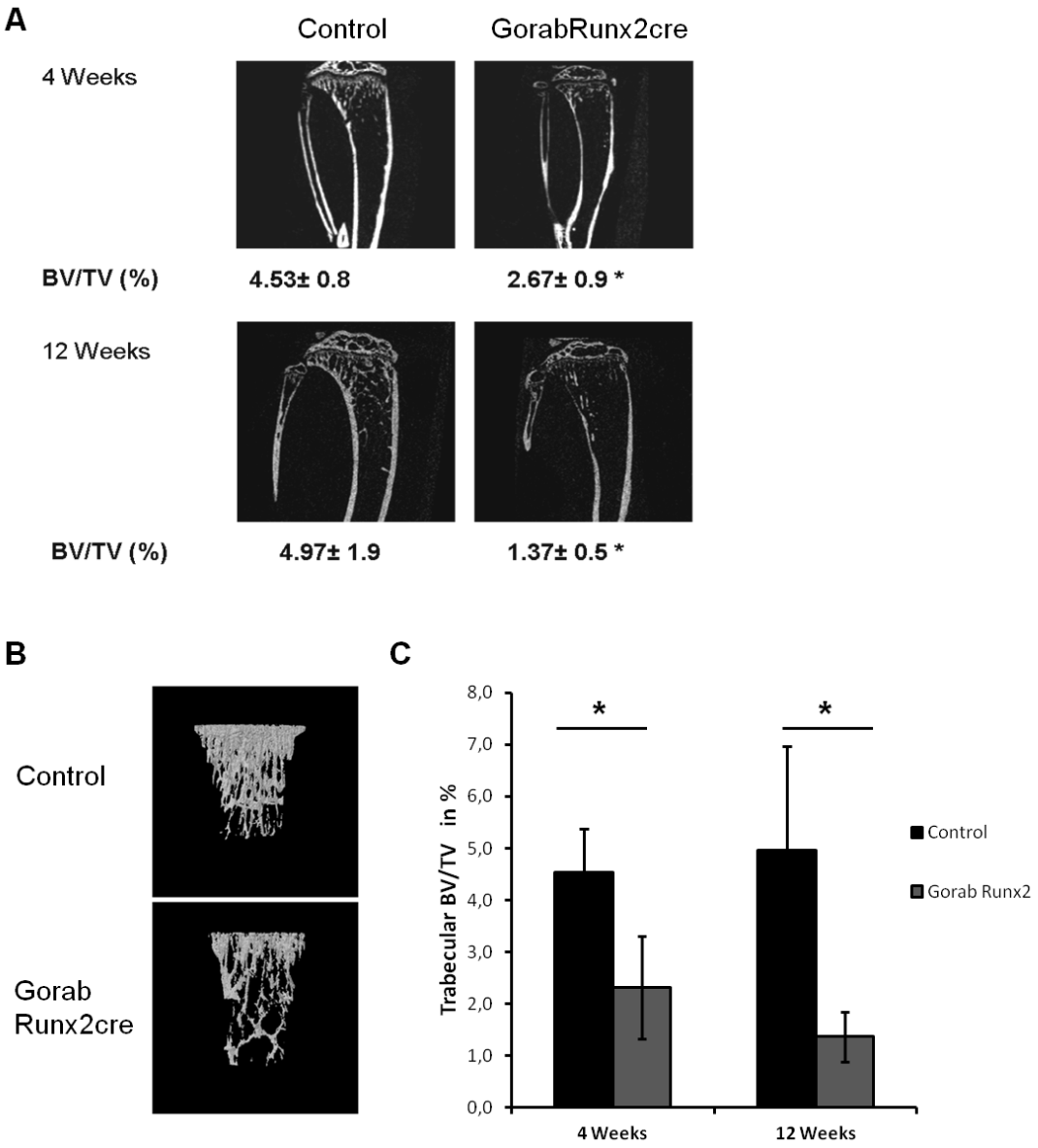

Figure 11: (A) MicroCT analysis of the tibia in 4 week and 12 week old GorabRunx2cre mutants comparing to littermate controls. The cortical bone is thinner and the trabecular bone showed a reduction of bone volume to total volume (BV/TV) ratio. (B) Three dimensional microCT reconstruction of a 4 week old tibia shows the reduction in trabecular number and thickness as well as the increase in trabecular separation. (C) BV/TV reduction in 4 week and 12 week old animals. Statistical analysis was performed by two tailed paired t-test (n=6). Error bars are representing SD. * indicates significant differences ($p<0.05$).

Trabecular bone number, thickness as well as separation were significantly changed. By 4 weeks the trabecular number (Tb.N) of the tibia was changed from 1.45 (SD±0.17) to 0.93 (SD±0.28) and by 12 weeks from 1.37 (SD±0.42) to 0.53 (SD±0.10). Trabecular thickness

(Tb.Th.) was significantly lower in GorabRunx2cre mutants. By 4 weeks the Tb.Th. was changed from 0.031mm (SD±0.002) to 0.028mm (SD±0.04) and by 12 weeks from 0.035mm (SD±0.005) to 0.029mm (SD±0.005). In the same manner, trabecular separation (Tb.S) increased since trabecular thickness and number decreased. Tb.S. was increased in the tibia of 4 week old animals from 0.261mm (SD±0.02) to 0.272mm (SD±0.04) and in 12 week animals from 0.291mm (SD±0.03) to 0.304mm (SD±0.02). 26 week old GorabRunx2cre animals displayed a similar phenotype in trabecular and cortical bone in tibia and femur. In the tibia bone volume to tissue volume ratio was decreased from 5.38% (SD±0.127) to 2.59% (SD±0.511). Tb.N was significantly decreased from 0.486 (SD±0.003) to 0.326 (SD±0.002) and Tb.Th was significantly decreased from 0.0498mm (SD±0.002) to 0.0380mm (SD±0.001). In the same manner Tb.S. was increased from 0.369 (SD±0.007) to 0.382 (SD±0.003). In the femur bone volume to tissue volume ratio was decreased from 3.41% (SD±0.36) to 1.69% (SD±0.506), Tb.N from 0.869 (SD±0.095) to 0.172 (SD±0.071) and Tb.Th from 0.0393 (SD±0.001) to 0.0374 (SD±0.012). Tb.Sp. was increased from 0.317 (SD±0.014) to 0.411 (SD±0.037).

3.2.8 Inactivation of Gorab results in vertebral bone phenotype

Since *Runx2cre* is also active in the spine, the phenotype of the lumbar spine in GorabRunx2cre animals were characterized by microCT analysis. The vertebrae of the GorabRunx2cre animals exhibited a lower mineralization rate. The vertebrae appeared to be shorter, flatter and narrower in size and had additionally smaller processes. MicroCT quantification revealed a lower bone volume to tissue volume (BV/TV) ratio in GorabRunx2cre animals. BV/TV ratio of the 5^{th} lumbar spine in 4 week old animals was reduced from 5.81% (SD±1.92) to 3.14% (SD±0.92) and in 12 week old animals from 7.08% (SD±1.67) to 3.35% (SD±0.67). BV/TV ratio of the 6^{th} lumbar spine in 4 week old animals was reduced in a similar manner. BV/TV ratio was changed from 6.02% (SD±1.64) to 3.41% (SD±0.98) and in 12 week old animals from 6.94% (SD±1.64) to 3.69% (SD±1.31). Like in the case of the tibia and femur, trabecular number and trabecular thickness were significantly decreased and trabecular separation increased. For example, in 4 week old mice trabecular number was changed from 1.65 (SD±0.38) to 0.99 (SD±0.28) and in 12 weeks from 1.09 (SD±0.57) to 0.77 (SD±0.21). Trabecular thickness was reduced from 0.035mm (SD±0.005) to 0.032mm (SD±0.004) in 4 week old animals and from 0.037mm (SD±0.011) to 0.029mm (SD±0.001) in 12 week old animals. In the same manner, the trabecular separation was increased from 0.291mm (SD±0.107) to 0.345mm (SD±0.114) in 4 week old animals but decreased from 0.421mm (SD±0.158) to 0.373mm (SD±0.079) in 12 week old animals. This

difference is most likely caused by a general reduction of the trabecular bone in 12 week old animals (see Table 2 and Figure 11). To summarize, GorabRunx2cre conditional mice show an osteoporotic phenotype in long bones of the lower limbs and in the spine. Interestingly, in the tibiae this finding was more prominent than in the femora. The osteoporosis is most pronounced in long bones of 4 week and 12 week old mice than in elderly animals, indicating a rather regressive course of disease.

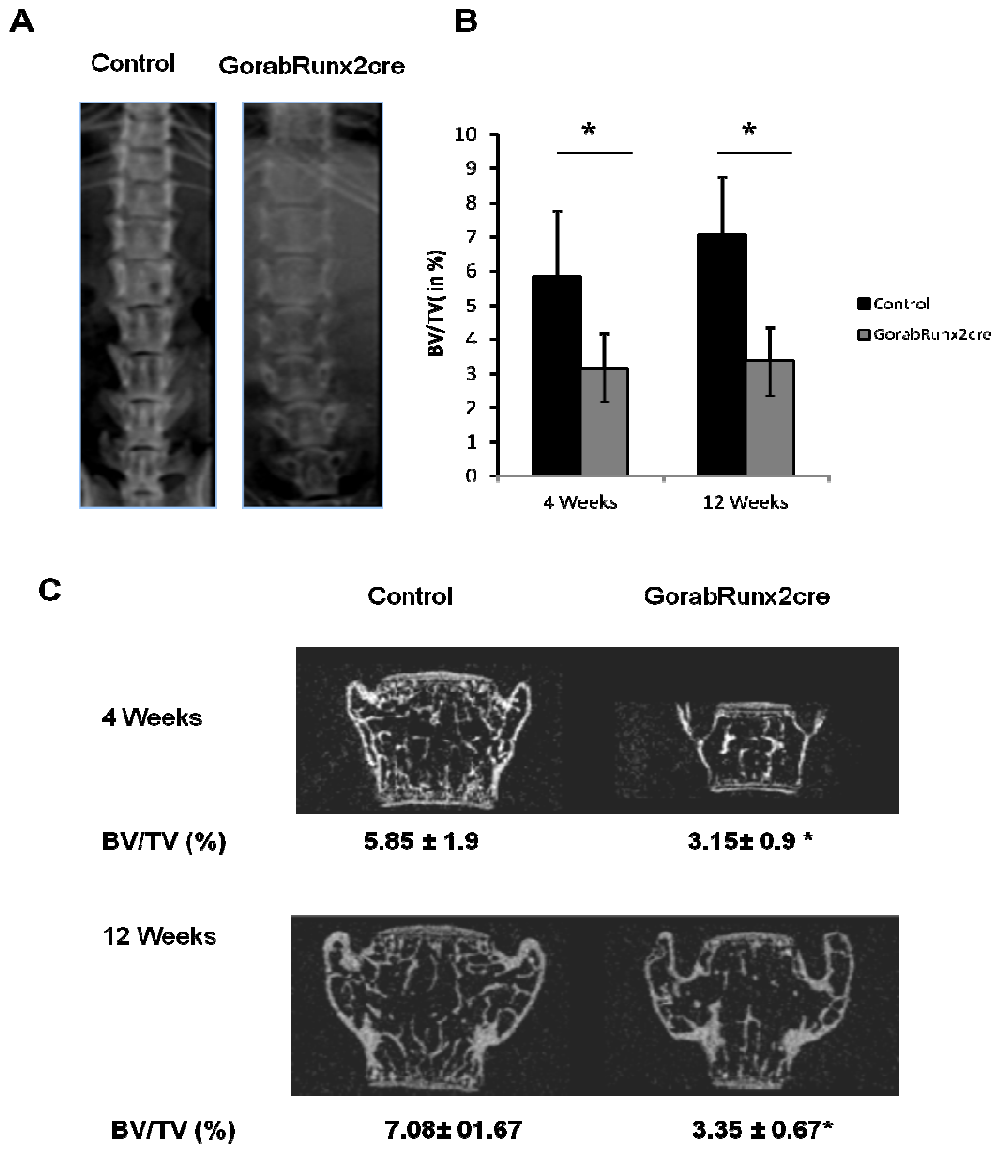

Figure 12: Vertebrae characterization (A) X-ray radiography images showed the low mineralization in the vertebral column of a 4 week old GorabRunx2cre mouse comparing to a control animal. The vertebral bodies were smaller in size with shorter processes. (B) Quantification of BV/TV ratio in the 5th lumbar spine showed a significant reduction in 4 week and 12 week old animals. (C) MicroCT images with the corresponding BV/TV values demonstrate the thinning and the reduction of the trabeculae in the vertebrae. Statistical analysis was performed by two tailed paired t-test. Error bars are representing SD. * indicates significant differences ($p<0.05$).

Table 13: Summary of microCT quantification. MicroCT scanning of the tibia, femur and vertebral column of GorabRunx2cre mutant and controls at 4 weeks (N=6) and 12 weeks of age (N=5). Mean value ± S.D. * = p<0.05. Statistical analysis was done by two-tailed, unpaired t-test.

			4 Weeks		12 Weeks		26 Weeks	
			Control	**Gorab Runx2cre**	**Control**	**Gorab Runx2cre**	**Control**	**Gorab Runx2cre**
Tibia	Trabecular Bone	BV/TV (%)	4.54 ±0.83	**2.31 ±0.99***	4.97±1.99	**1.37±0.48***	5.382±0.127	**2.59±0.511***
		Tb. N. (1/mm)	1.45±0.17	**0.93±0.28***	1.37±0.42	**0.53±0.10***	0.4864±0.003	**0.3268±0.002***
		Tb. Th (mm)	0.031±0.002	0.028±0.004	0.035±0.005	**0.029±0.005***	0.0498±0.002	**0.0380±0.001***
		Tb. Sp (mm)	0.261±0.02	**0.272±0.04***	0.291±0.03	**0.304±0.02***	0.3690±0.007	**0.3821±0.003***
	Cortical Bone	TV (mm^3)	0.609±0.124	**0.324±0.103***	0.806±0.314	**0.524±0.113***	1.114±0.026	**0.698±0.003***
		Cortical Th.	0.112±0.015	**0.069±0.017***	0.123±0.014	**0.084±0.02***	0.198±0.029	**0.142±0.011***
		Length (mm)	14.01±0.633	**10.023±0.689***	15.28±0.645	**11.896±0.524***	16.217±0.789	**13.286±0.286***
Femur	Trabecular Bone	BV/TV (%)	6.86±0.89	4.81±0.83	5.34±2.93	**1.49±1.13***	3.417±0.36	**1.691±0.506***
		Tb. N. (1/mm)	1.97±0.23	1.27±0.96	1.49±0.89	**1.26±0.11***	0.869±0.095	**0.172±0.071***
		Tb. Th (mm)	0.034±0.001	0.032±0.001	0.033±0.006	0.027±0.002	0.0393±0.001	0.0374±0.012
		Tb. Sp (mm)	0.242±0.009	0.246±0.002	0.259±0.019	**0.235±0.010***	0.317±0.014	**0.411±0.037***
	Cortical Bone	TV (mm^3)	0.687±0.156	**0.356±0.135***	0.496±1.369	**0.396±0.159***	0.523±0.003	**0.462±0.008***
		Cortical Th.	0.116±0.002	**0.082±0.026***	0.119±0.019	**0.099±0.049***	0.196±0.025	**0.129±0.039***
		Length (mm)	13.241±1.021	**9.987±0.576***	15.298±0.348	**12.978±1.069***	16.7235±1.002	**13.269±1.236***
Spine	5th Lumbar	BV/TV (%)	5.81±1.92	**3.14±0.92***	7.08±1.67	**3.35±0.67***	7.56±1.29	**5.45±0.89***
		Tb. N. (1/mm)	1.65±0.38	**0.99±0.28***	1.09±0.57*	**0.77±0.21***	1.29±0.06	**0.86±0.09***
		Tb. Th (mm)	0.035±0.005	**0.032±0.004***	0.037±0.011	**0.029±0.001***	0.041±0.001	0.023±0.005
		Tb. Sp (mm)	0.291±0.107	0.345±0.114	0.421±0.158	0.573±0.079	0.327±0.003	**0.426±0.021***
	6th Lumbar	BV/TV (%)	6.02 ± 1.64	**3.41±.0.983***	6.94±1.64	**3.69±1.31***	6.78±1.89	**4.65±0.73***
		Tb. N. (1/mm)	1.36±0.31	**1.09±0.24***	1.19±0.52*	**0.77±0.24***	1.26±0.31	**0.79±0.02***
		Tb. Th (mm)	0.030±0.001	**0.030±0.004***	0.038±0.011	**0.026±0.002***	0.059±0.002	0.059±0.003
		Tb. Sp (mm)	0.286±0.107	0.364±0.174	0.432±0.158	0.343±0.081	0.394±0.052	**0.413±0.012***

3.2.9 Inactivation of Gorab results in a skull phenotype

Runx2 is also active in the osteoblasts of the skull; therefore Gorab is deleted in the calvaria in mice. In general, the appearance of the GorabRunx2cre mouse head was characterized by a shortened snout (Figure 13). Three dimensional microCT reconstructions revealed a mineralization defect which was most prominent in the suture region of the calvaria. Von Kossa histology of MMA embedded bone sections revealed less mineralized bone (Figure 13.B and Figure 13.C) and an increased number of osteocyte-like cells (Figure 13.D).

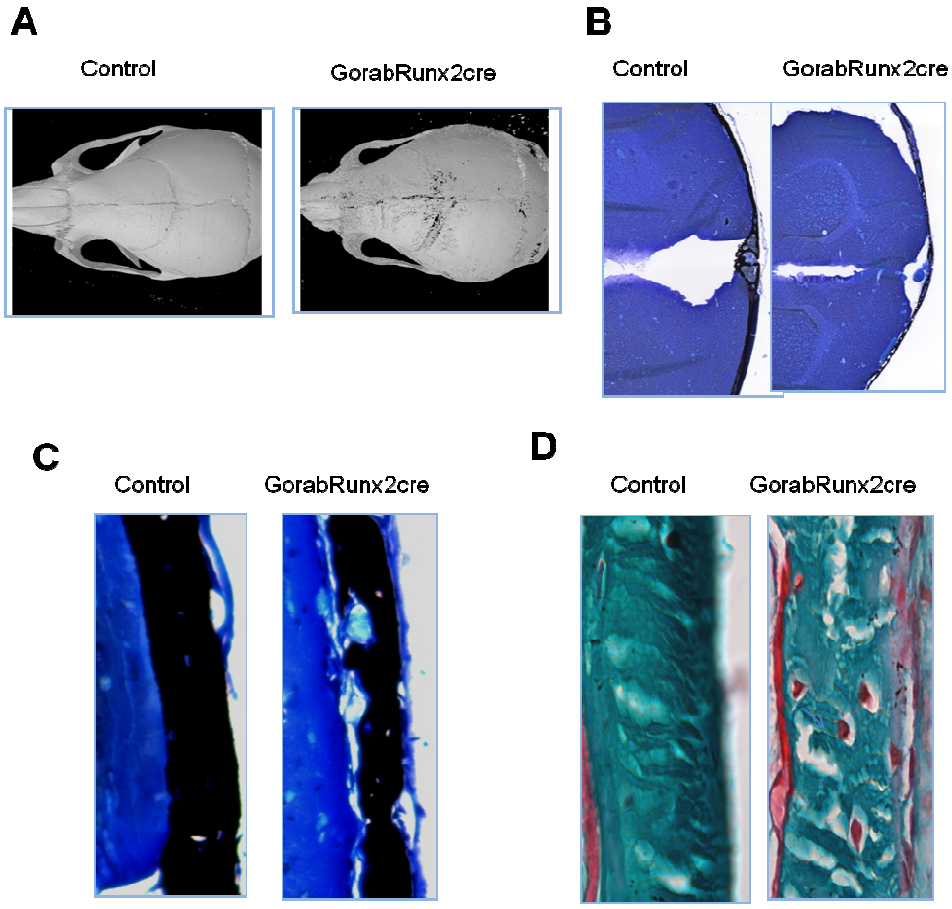

Figure 13: Calvaria phenotype. (A) Three dimensional MicroCT reconstruction shows the thinning of the calvaria with a mineralization defect in the suture region of 4 week old GorabRunx2cre animals. (B) and (C) Von Kossa/Toluidine blue histology staining on 5µm thick MMA sections exhibited less mineralized mature bone (stained in black) compared to control animals. (D) Masson Goldner staining showed an accumulation of round osteocyte-like cells (red) in mineralized (green) bone comparing to controls.

3.2.10 Loss of Gorab has no effect on osteoclast number

Tartrate-resistant acid phosphatase (TRAP or TRAPase) is highly expressed in osteoclasts, activated macrophages and neurons. To identify whether the decrease in trabecular number and thickness as well as the reduction in cortical thickness resulted from an increased osteoclast activity, TRAP enzymatic staining was performed and counterstained with light green. 5µm thick MMA sections of the tibia of four week GorabRunx2cre animals were used and TRAP positive osteoclasts were counted and normalized to the bone perimeter 1mm below the growth plate. No significant difference was found by comparing with littermate controls. Controls displayed 4.25 ± 2.01 and mutants 4.01 ± 2.68 osteoclasts per bone perimeter. 12 week old animals have only a small proportion of trabecular bone remaining; therefore TRAP staining could not be conducted in these animals.

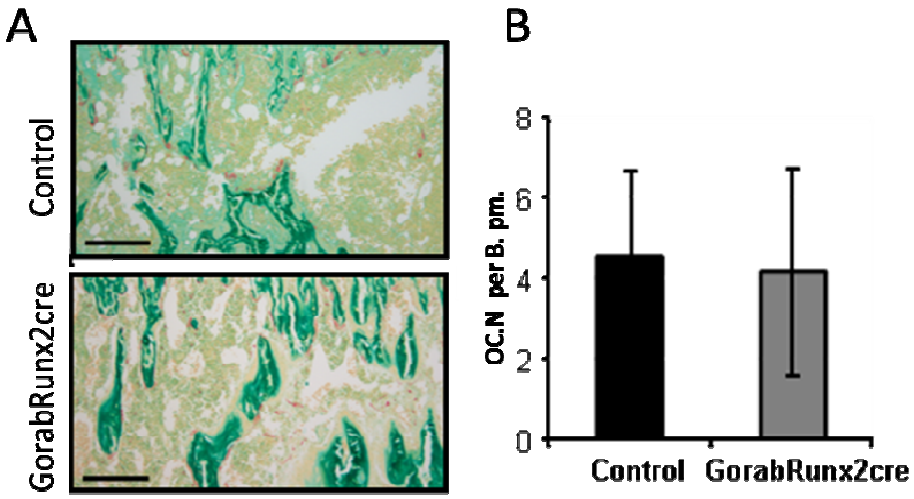

Figure 14: TRAP staining on 5µm MMA section of the tibia from 4 week old GorabRunx2cre animals. 1mm below the growth plate was the region of interest. Osteoclasts number (red) per bone perimeter (OC.N per B. pm) was counted (Scale=500µm). No significant difference could be observed (n=5). Error bars representing SD. Scale=100µm. Statistical analysis was performed by two tailed unpaired t-test.

3.2.11 Histomorphometric alterations in GorabRunx2cre mice

Von Kossa/van Giesson staining was performed to distinguish between mineralized, mature bone (black) and the osteoid which is a young, not mineralized and immature bone (red). Alterations in tibia osteoid content were detected by quantifying the trabecular bone 1mm below the growth plate. Osteoid thickness (O.th), osteoid surface

area (OS/BS) and relative osteoid volume (OV/BV) were clearly increased in GorabRunx2cre mutants. Osteoid thickness was increased from 2.05 (SD±0.21) to 2.83 (SD±0.14) indicating a 25% increase of osteoid content comparing to control animals. Other parameters like the osteoid surface area (OS/BS) showed an increase from 13.50 (SD±1.38) to 25.08 (SD± 1.98) and osteoid volume (OV/BV) from 1.62 (SD±0.17) to 4.29 (SD± 0.43). Histomorphometric analyses were performed by OsteoMeasure™ software (Figure 15).

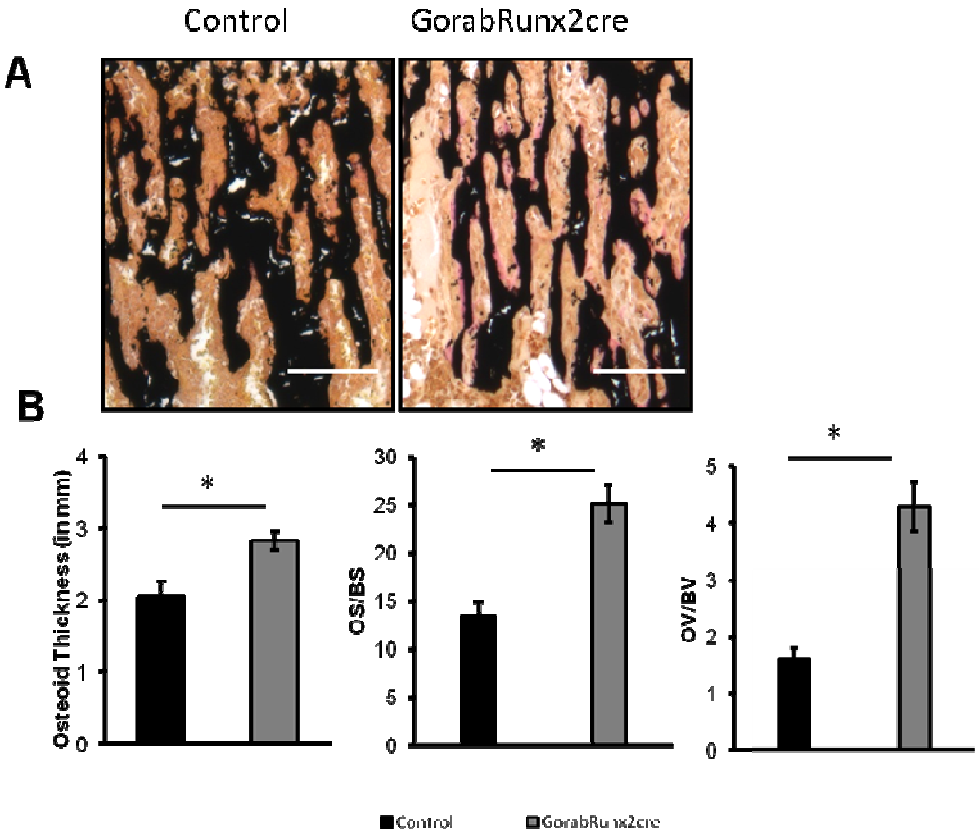

Figure 15: Histomorphometry on the trabecular bone of the tibia. (A) Histological analysis of the trabecular bone in 4 weeks old GorabRunx2cre mutants. Von Kossa/Van Giesson staining showed mineralized adult bone (black) in comparison to osteoid (immature not mineralized bone in red). (B) Significant increase in osteoid thickness, O.Th (in mm), from 2.05 (SD±0.21) to 2.83 (SD±0.14) relative osteoid surface area (p=0.0027), OS/BS, from 13.50% (SD±1.38) to 25.08% (SD± 1.98) (p=0.019) and relative Osteoid volume, OV/BV, 1.62% (SD±0.17) to 4.29% (SD± 0.43) (p=0.010) was found in the mutants (n=4). Histomorphometric analyses were performed by OsteoMeasure™. Statistical analysis was performed by two tailed, unpaired t-test. (n=3). Error bars are representing SD. * indicates significant differences ($p<0.05$).

3.2.12 Altered osteocyte network in GorabRunx2cre mice

Two different approaches were conducted to identify the quality of the osteocyte canaliculi network within the cortical bone of 4 week old GorabRunx2cre animals. Firstly, fresh bone samples were infiltrated with rhodamin 6G solution and canaliculi networks were visualized. Canaliculi are nanometer thick tunnels which connect the cells within the cortical bone. Canaliculi integrity is important for bone quality and mechanosensing of the osteocytes. Secondly, paraffin embedded bone samples were stained with silver nitrate (AgNO3) and sections were examined for the osteocyte canaliculi network. The silver nitrate staining confirmed the initial results from the rhodamin 6G infiltration. Within the cortical bone, osteocytes showed a more round shape and had less canaliculi per cell. The overall canaliculi network was highly disturbed (Figure 16).

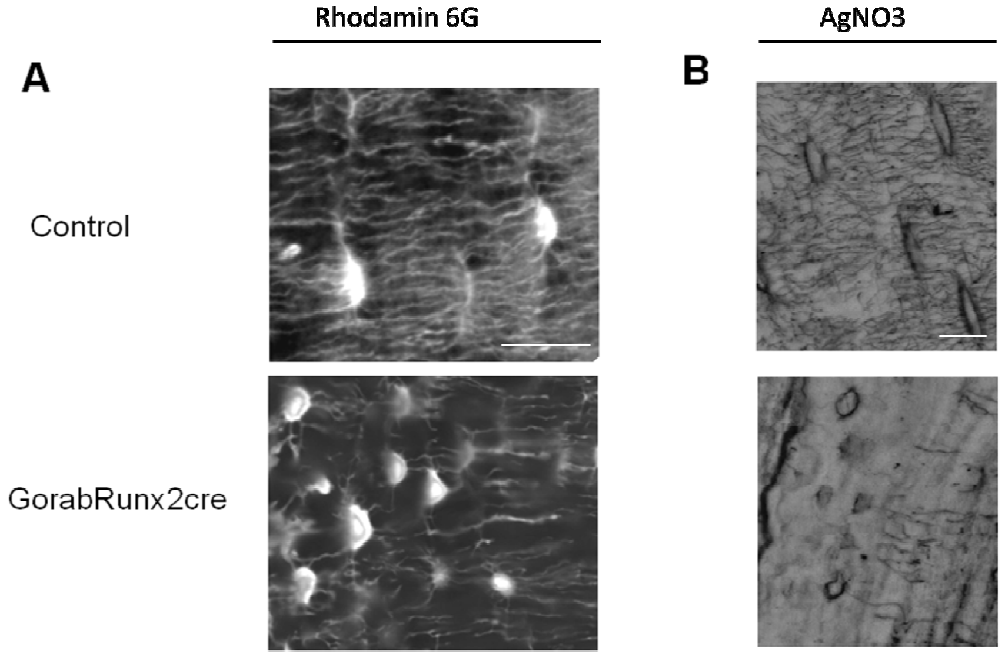

Figure 16: Structural observations in GorabRunx2cre tibia. Canaliculi network in GorabRunx2cre mouse tibia. 4 week old GorabRunx2cre showed a highly disturbed osteocyte canaliculi network in the cortical bone. (A) Rhodamin 6G and (B) AgNO3 staining on 5µm thick MMA sections (Scale is 50µm and 20µm respectively).

3.2.13 Extracellular matrix components are changed in GO

To investigate the matrix composition of the cortical bone in GorabRunx2cre mice the collagen content was inspected. MMA embedded bone samples of tibia and femur were stained with picosirius red and visualized with polarized light microscopy in order to

detect the collagen fibers within the bone. Thick and mature fibers are shown in red and immature and thin fibers in green. Control animals exhibited a thick and mature collagen network which appeared mostly in red when visualized with polarized light. Collagen fibers were highly orientated. In contrast, GorabRunx2cre animals exhibited a thin and immature collagen network with lots of fragmented fibers, which appeared in yellow-green.

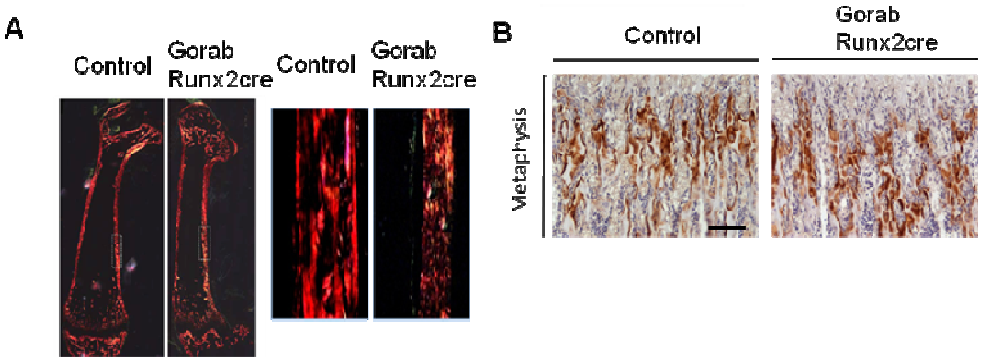

Figure 17: Matrix abnormalities in Gerodermia Osteodysplastica. (A) Cortical Bone Phenotype of 4 week old GorabRunx2cre femur. Picosirius red staining using polarized light to visualize collagen fibers in the bone exhibited disorganized collagen fibers in GorabRunx2cre animals. In addition collagen fibers were fragmented and less mature (yellow-green) comparing to control animals with thick mature (red) and well organized collagen network. (B) Immunohistochemistry staining using decorin antibody showed increased signal intensities in the metaphysis of the tibia in GorabRunx2cre. Note that highest signal intensity is more distal of the growth plate comparing to the control (Scale is 500µm).

The proteglycan decorin is known to affect the fibrillogenesis and the ultrastructure of collagen. It is highly expressed in connective tissue and matrix of the bone. Since decorin and collagen content are highly accompanying, this specific proteoglycan was investigated. Immunohistochemistry staining on the metaphysis of GorabRunx2cre tibia revealed a different expression of decorin. Mutants showed an increased staining intensity and though the intensity of staining was noted to increase more distally. Immunoblot analysis in GO HAFs showing a light increase in size of glycanated decorin. GorabRunx2cre cortical bone lysates showing an increased decorin core protein (40 kDA) and a reduction of glycanated protein (90-120 kDA) in mutants. P-Smad signals in GorabRunx2cre mutants are significantly increased (data not shown).

3.2.14 Osteoblast Differentiation delay in 4 week old GorabRunx2

Immunohistochemistry on 4 week old GorabRunx2cre animals revealed an osteoblast to osteocyte developmental defect in the trabecular bone region of the metaphysis in the tibia of 4 week mice (Figure 18.A). Cell counting in 4 week old tibia revealed a 4.5-fold increased number positive for osterix, an early osteoblast marker. In the metaphysis of control animals in average 242 ± 33.08 whereas in GorabRunx2cre mutant 884 ± 175.1 cells were counted (2.03 ± 0.45 comparing to 11.76 ± 2.27 Ob/B.pm; Figure 18.B). Immunoblot analysis confirmed this finding (Figure 18.C). However, in 12 week old GorabRunx2cre animals no significant increase of osterix signal was detected.

Since sclerostin is expressed in vivo by mineral-embedded osteocytes, its antibody was used to identify late osteoblasts or early osteocytes within the bone. In the GorabRunx2cre mutant tibia diaphysis cells positive for sclerostin were significantly increased comparing to controls. The same trend could be observed in 12 week old animals (Figure 18.D). As described above osteocyte morphology was altered. The osteocytes were more round in shape and showed less canaliculi per cell. These findings were supported by Rhodamin6G and AgNo3 (Figure 16).

To summarize, 4 week old mutant GorabRunx2cre animals exhibited a 4-fold increased osterix number compared to controls. This accumulation of early osteoblasts was vanished by 12 weeks. Sclerostin positive cells were significantly increased in the GorabRunx2cre mutant bone diaphysis and in addition osteocyte morphology was highly changed.

3.2.15 Oxidative DNA-damage in GorabRunx2cre animals

Previously it was found that GORAB knockdown in HeLA cells and human patient fibroblasts lead to an increase in DNA damages. Therefore GorabRunx2cre bone tissues were tested for 8-oxoguanine, a DNA damage marker specific for oxidative stress. In the tibia of 4 week old GorabRunx2cre mutants increased signal intensities for 8-oxoguanine were detected. This increase could be observed in the trabecular bone of the metaphysis and also in the diaphysis. This result indicated an accumulation of oxidative stress induced DNA damages in the bone of mutant mice (Figure 19).

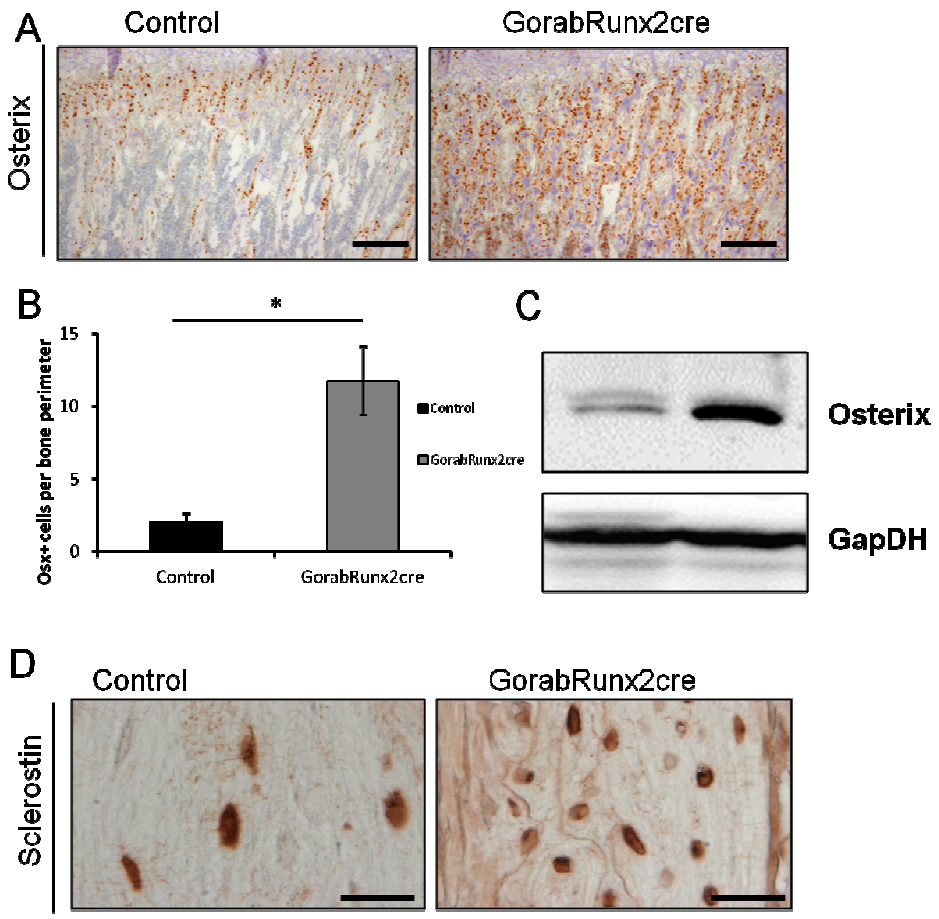

Figure 18: Differentiation delay in 4 week old GorabRunx2cre animals. (A) Immunohistochemistry images showing an increase of osterix positive cells in the tibial metaphysis region. (B) Mutant mice exhibited a 4.5-fold increase of osterix positive cells per bone perimeter (p=0.002) Error bars are representing SD. (C) Immunoblot analysis on bone lysates with increased osterix signal. (D) Sclerostin staining in the tibial diaphysis. Osteocytes morphology is altered, immunohistochemistry images show round cells with less canaliculi per cell (Scale is 500µm). Statistical analysis were performed by two tailed unpaired t-test (n=4). Error bars are representing SD. * indicates significant differences ($p<0.05$).

As shown in a previous dissertation by our collage Dr. Wing Lee Chan and in this current study we can summarize that Gorab knockout leads to an increase in DNA damages in vitro and in vivo. This current data shows increased DNA damages in the mutant mouse tibia caused by elevated oxidative stress.

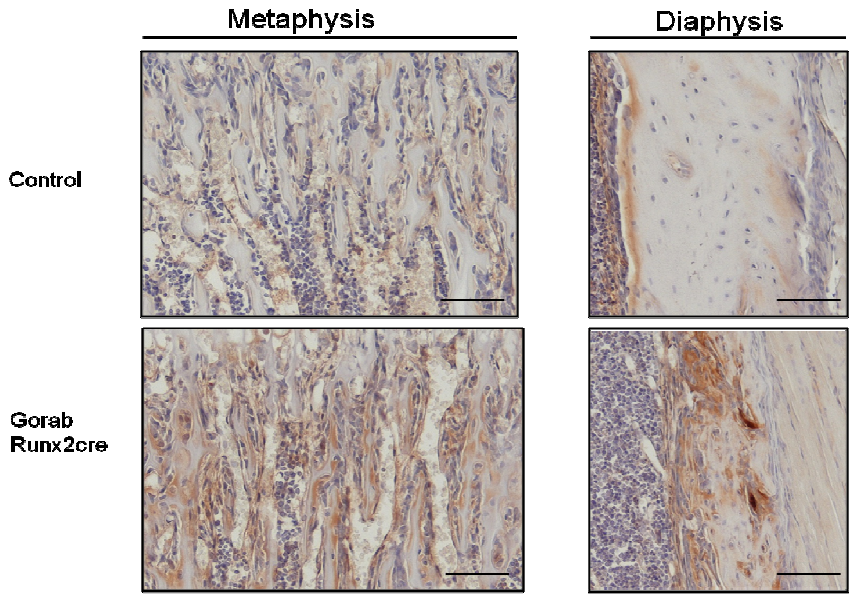

Figure 19: 8-oxoguanine immunohistochemistry on GorabRunx2cre mouse tibia. 4 week old GorabRunx2cre animals displayed increased antibody staining of 8-oxoguanine in the tibial metaphysis and diaphysis (n=4). Scale=350µm.

3.2.16 Increased TGF-β signaling and cellular senescence in GO

TGF-β is known to be elevated in several bone-related diseases like Osteogenesis Imperfecta and Marfan Syndrom. In GORAB deficient HeLa cells TGF-β and downstream targets were found upregulated in previous experiments. Therefore, GorabRunx2cre bone tissues were probed with an antibody specific for phospho-Smad (P-Smad). Smads are known to transmit TGF-β signals from the cell surface to the nucleus. GorabRunx2cre showed increased p-Smad signals within the metaphysis of the tibia. GorabRunx2cre bone tissues were tested for p21 (Cdkn1a) a well-known cell cycle regulator. By immunohistochemistriy we could show increased p21 levels in the tibial metaphysis of GorabRunx2cre mutants. In addition an upregulation of the *p21* gene was detected by rtPCR.

To summarize, tibia and femur and the lumbar spine of 4 week, 12 week and 26 week old GorabRunx2cre animals displayed reduced trabecular bone volume and thickness and a lower trabecular number. In a similar manner, trabecular separation was increased. Histology on bone sections revealed an increase of osteoid, the immature bone. The osteoclast number per bone perimeter was not changed suggesting a low bone turnover osteoporosis. GorabRunx2cre mice exhibited changes in the matrix composition, in particular collagen and decorin. Moreover histology stainings on mouse

tibia revealed that osteocytes maturation was delayed and their morphology was highly altered. This was supported by the fact that marker genes for early osteoblastic markers were upregulated and terminal osteocyte markers were downregulated. In addition, GorabRunx2cre mice exhibited increased oxidative DNA damages in the diaphysis and metaphysis of the tibia. In the same time TGF-β and the senescence marker p21 were significantly upregulated. Together this demonstrates that a deficiency of Gorab causes defects in osteoblast maturation trough the influence of TGF-β signalling and p21-mediated cellular senescence.

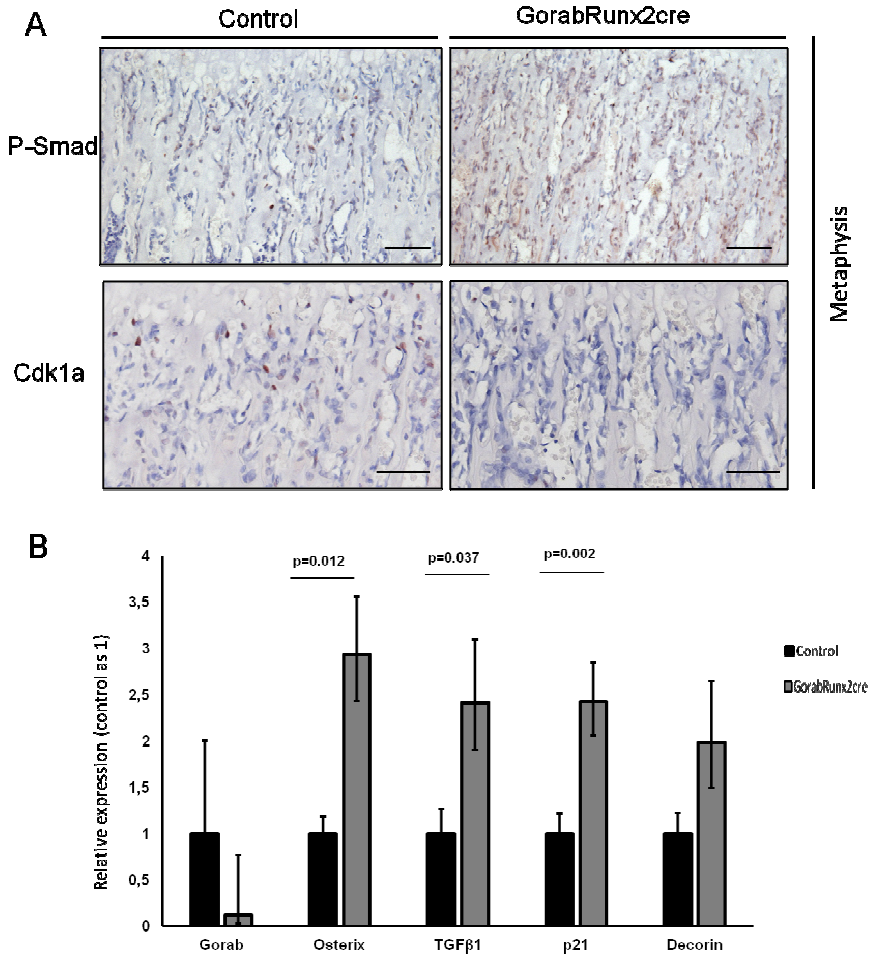

Figure 20: (A) Gorab deficiency leads to increased p-Smad and Cdkn1a (p21) signals in the tibial metaphysis. Images were taken in the metaphysis of 4 week old mice (Scale is 500µm; n=4). (B) Relative qPCR expression analysis on the epiphysis of GorabRunx2cre animals comparing to controls. Gorab expression was not significantly reduced. Osterix, TGFβ1 and p21 were significantly upregulated upregulated (p=0.012; p=0.037 and p=0.002 respectively). Decorin expression was 2-fold increased, but not significant (n=3). Statistical analysis was performed by two-tailed paired t-test. Error bars are representing SD.

3.3 In vitro Osteoblast Differentiation Assays

To study osteoblast to osteocyte differentiation in vitro; either adult mouse primary osteoblasts from the calvaria of two week old GorabRunx2cre animals or ST2 cells were taken. After reaching confluence, cells were stimulated with osteogenic medium containing 100ng/ml BMP2 in addition to vitamin C and β-glycerolphosphate to induce osteoblast differentiation. RNA samples were harvested on day 0, 1, 3, 5, 7 and 14. The samples from all individual timepoints were analyzed to indentify alterations in different stages of osteoblast development.

3.3.1 Differentiation delay in GorabRunx2cre calvaria osteoblasts

Gene expression analyses of several osteoblast and osteocyte markers were investigated at different time points between day 1 and day 14. An increase of osterix (an early osteoblast marker) was found at day 1 and day 3. Only the increase of osterix at day 1 was significant (p=0.041). A significant downregulation of osterix in GorabRunx2cre cells was observed at day 7 (p=0.045). This osterix differentiation disorder was diminished by day 14 where osterix levels of mutants were comparable to controls. Relative *Bglap* (Osteocalcin) expression was downregulated at day 5 and 7. This decrease was only at day 5 significant (p-values of day 5 and 7; p=0.0455 and p=0.35, respectively). Relative expression of *Cdkn1A* (p21) was constantly upregulated during osteogenic differentiation. A significant upregulation was only seen at day 7 (p=0.01). Relative expression of *Cdkn2a* (p16) revealed no significant alterations in GorabRunx2cre comparing to controls. TGF-β1 was significantly increased at day 0 in GorabRunx2cre animals (p=0.021). At day 7 after osteogenic induction a second peak of significant upregulation was observed (p=0.028). In addition, TGF-β2 expression was tested but no significant differences were observed (Figure 21.A).

ALP and Alizarin staining revealed a similar staining intensity in GorabRunx2cre animals and controls (Figure 21.B and C).

3.3.2 In vitro differentiation delay in siGorab ST2 cells

ST2 cells were transiently transfected with unmodified oligos specific for Gorab and one scrambled control. After reaching confluence cells were treated as described in Chapter 3.3. No significant differences in *osterix* gene expression were found. *Sclerostin* (Sost), a marker for osteocytes showed a dysregulation between day 0 and

day 7 with a significant reduction at day 7 (p=0.026). Relative *osteocalcin* (Bglap) was significantly reduced at day 7 (p=0.0455). In addition *XBP1* and *XBP1 spliced* gene expressions were analysed. However, no significant changes were found. *TGF-β2* gene expression was significantly upreguated at day 1 (p=0.011) (Figure 22.A).

Immunoblots on protein lysates from tissue culture revealed a transient knockdown of Gorab. Gorab (47kDA) levels were reduced to a minimum at day 0, day 1 and day 3 after siRNA knockdown. At day 7 Gorab levels were increased with highest levels at day 10. Moreover, osterix (45kDA) levels were increased at day 1 in Gorab siRNA treated samples. At day 7 after osteogenic induction protein levels of osterix were decreased in cells lacking Gorab. In Gorab siRNA samples Sclerostin (24kDA) protein levels were found increased at day 1 whereas at day 3 levels were decreased comparing to controls. No significant changes in sclerostin protein levels were found at day 7 and day 14 (Figure 22.B).

ALP assay on day 5, day 7 and day 14 did not reveal any significant changes comparing to controls. Nevertheless, at day 14 a minor reduction of ALP secretion was observed in cells lacking Gorab (Figure 22.C).

Taken together, these results indicate a maturation delay in Gorab deficient cell lines. Summarized, based on ALP and Alizarin staining in the well no significant changes were detected but more detailed analyses using real time PCR for relative quantification revealed an osteoblast to osteocyte maturation alteration.

In both, GorabRunx2cre osteoblasts and ST2 cells, osterix (early osteoblast marker) was initially upregulated. However, this finding was only significant in GorabRunx2cre osteoblasts. Late osteoblast markers (bglap, sost) were upregulated in early stages of osteoblast development but in late stages both markers were significantly downregulated. In accordance to previous findings, TGF-β and p21 were continuously upregulated. No contribution of the UPR machinery (XBP1, XBP1s) in osteoblast maturation was found.

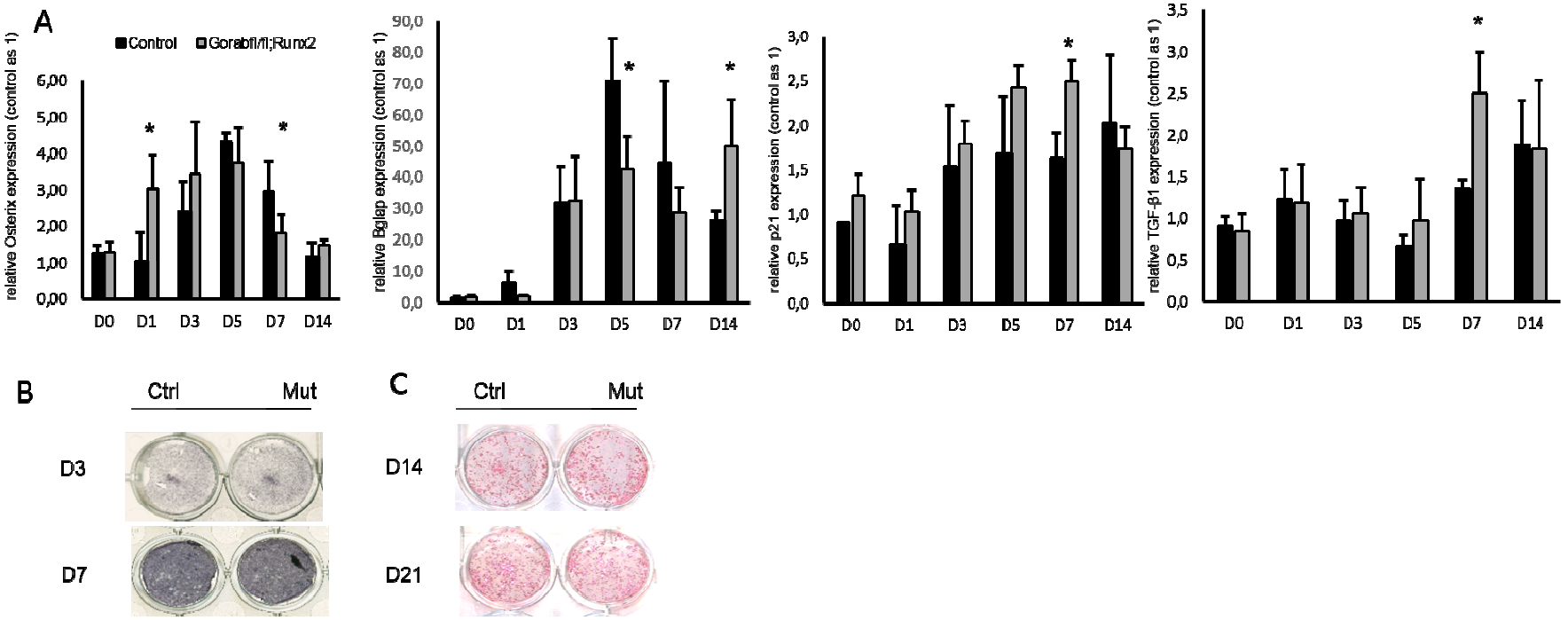

Figure 21: Osteoblast development and gene expression analysis on 2 week GorabRunx2cre primary calvaria osteoblasts. (A) Differentiation was induced by osteogenic medium containing 100ng/ml BMP2. RNA samples were harvested on day 0, 1, 3, 5, 7 and 14. Gene expression levels of several osteoblast to osteocyte markers were investigated at different time points. A significant increase of *osterix* was observed at day 1 (p=0.041) and a significant reduction of *osterix* was observed at day 7 (p=0.045). *Osterix* dysregulation was diminished by day 14. Relative *osteocalcin* (Bglap) expression was downregulated at day 5 and 7. This decrease was significant at day 5 (p-values of day 5 and 7; p=0.045 and p=0.035). Relative expression of *Cdkn1a* (p21), was constantly upregulated from day 0 till day 7 during osteogenic differentiation. A significant upregulation was only seen at day 7 (p=0.01). *TGF-β1* was significantly increased at day 7 (p=0.028), at day 14 levels were comparable to controls. (B) ALP staining on day 3 and day 7 showing no difference between control and mutant (C) Alizarin staining on day 14 and day 21 showing no difference between control and mutant (n=3). Statistical analysis was performed by two tailed paired t-test. * indicates a significant difference ($p<0.05$).

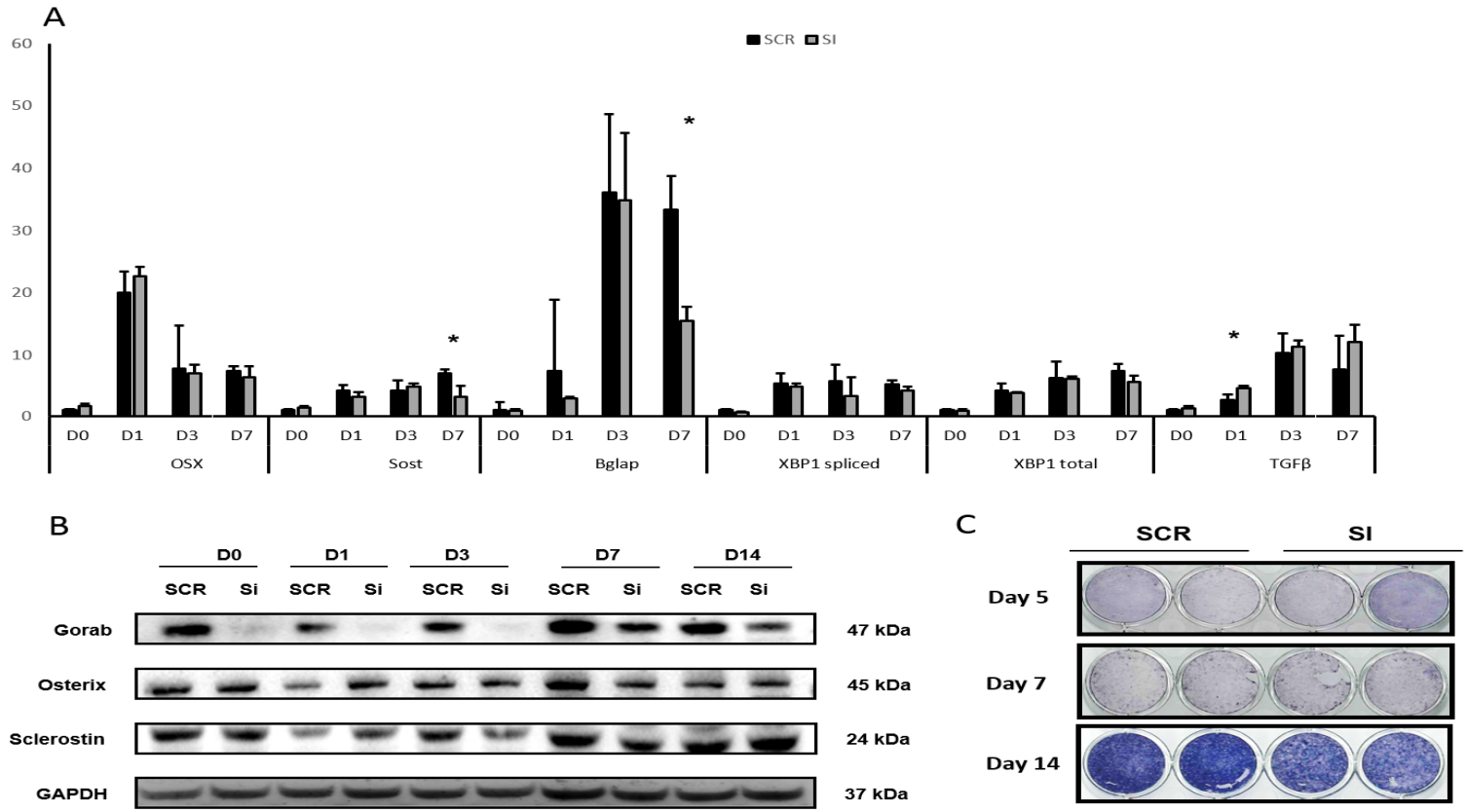

Figure 22: Osteoblast development and qPCR gene expression analysis on ST2 cells. (A) Differentiation was induced by osteogenic medium containing 100ng/ml BMP2. RNA samples were harvested on day 0, 1, 3 and 7. Gene expression of several osteoblast, osteocyte, ER Stress and TGF-β markers were investigated. An increase of *osterix* was detected at day 0, day 1 and day 3 but not significantly. Relative *osteocalcin* (Bglap) expression was downregulated at day 0, 1 and 7 (significant at day 7 p=0.031). *TGF-β1* was significantly increased at day 2 (p=0.039). No significant differences *in XBP1* and *XBP1spliced* were detected. (B) Immunoblot analysis on protein lysates from day 0 until day 14. (C) ALP staining on day 5, day 7 and day 14 showing only minor reduction at day 14 (n=3). Statistical analysis was performed by two tailed paired t-test. Error bars are representing SD. * indicates a significant difference ($p<0.05$).

3.4 Elevated Reactive Oxygen Species in GORAB-deficient cells

According to the free radical theory the process of aging is at least partially caused by damages due to increasing ROS levels with age. Therefore, it was hypothesized that GO skin fibroblasts and primary osteoblasts might suffer from increased ROS levels and DNA damages and therefore cause the GO phenotype.

3.4.1 Gorab deficiency leads to elevated mtROS in GorabRunx2cre bone marrow

Gorab deficient bone marrow cells were tested for mitochondrial reactive oxygen species (mtROS) intensities. To estimate ROS production in vivo of 4 week old GorabRunx2cre bone marrow cells; mice were exposed to MitoSOX, a fluorochrome specific to anion superoxide produced in the inner mitochondrial compartment. MitoSOX red reagent is a novel fluorogenic dye that specifically targets to the mitochondria in living cells. Oxidation of MitoSOX by superoxide produces a red fluorescence with an absorption/emission maximum of 510/580. By quantification with ImageJ we could clearly find an increase in mitochondrial ROS (mtROS) of 12.897 (SD±3.045) in control animals to 23.158 (SD±4.462) in mutant mice. Summarized, GorabRunx2cre bone marrow cells showed clearly a 2-fold increase of mtROS levels compared to controls.

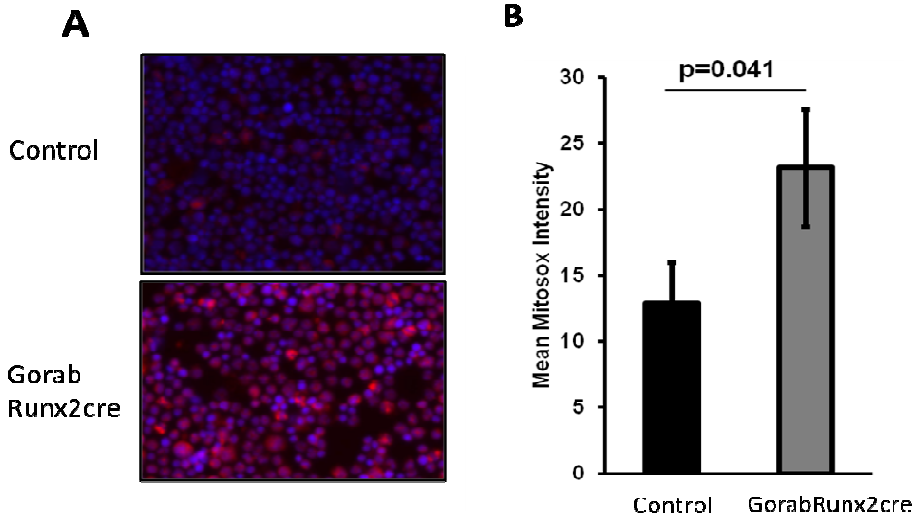

Figure 23: GorabRunx2cre bone marrow cells were incubated with MitoSOX, an anion superoxide specific dye produced in the inner mitochondria compartment. (A) MitoSOX was monitored by fluorescence microscopy and (B) signals were quantified with Image J. mtROS signals were in average 2-fold higher in GorabRunx2cre bone marrow compared to littermate controls. Control cells showed mtROS intensities of 12.897±3.045 and in GorabRunx2cre mutants mtROS intensities of 23.158±4.462 were observed (n=3). Error bars are representing SD.

3.4.2 GO HAFs show elevated mtROS levels in 7 day post confluent cells

To estimate ROS production in vitro, GORAB deficient human fibroblasts and GorabRunx2cre calvaria osteoblasts were exposed to MitoSOX, an superoxide anion dye, and CellROX, a general ROS indicator. Scanning was conducted with Operetta (HCS; PerkinElmer) and quantification by Harmony (PerkinElmer). 1 and 3 days post confluence mtROS levels were not clearly increased. Only 7 days post confluence a significant increase of mtROS could be detected indicating a potential influence of the matrix to mtROS levels (see Figure 24.A). When the cells were treated with a TGF-β specific inhibitor (SB431542) no significant difference between control and patient fibroblasts were measured. MtROS levels of GO HAFs were significantly decreased when treated with SB431542 (p=0.023) (see Figure 24.C). However, these results support the indication, that mtROS is only stably increased in 7 day post confluent cells suggesting a matrix contribution.

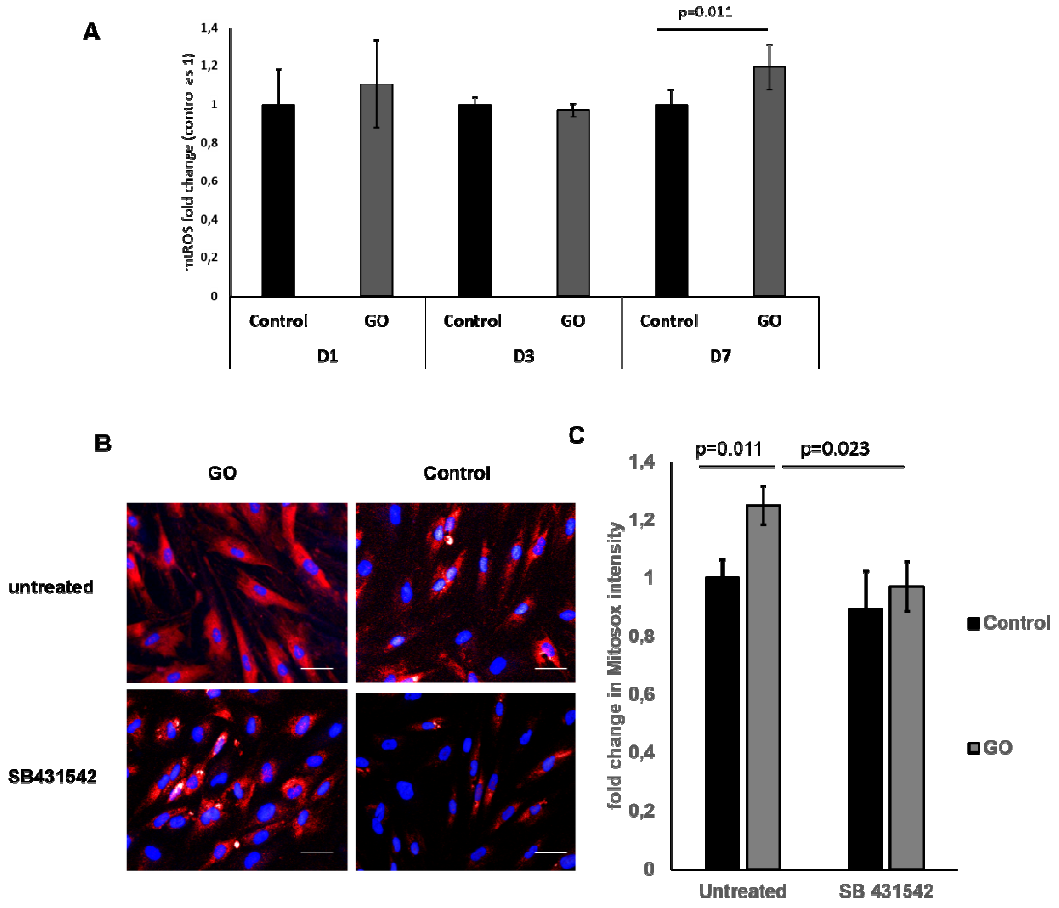

Figure 24: mtROS in human fibroblast culture (HAF). (A) HAFs were incubated with a MitoSOX specific dye. 1 and 3 day subconfluent GO and control HAFs gave inconsistent results. 7 days post confluente GO HAFs exhibited significantly increased mtROS levels. (B) Fluorescent images showing increased mtROS fluorescent intensities in GO HAFs. Treatment with a TGF-β specific inhibitor (SB431542) resulted in decreased mtROS

fluorescent intensities. (C) Quantification of the mtROS in untreated HAFs showed a significant increase in GO HAFs whereas when treated with SB431542 the cells exhibited a significant lower fluorescent intensities when comparing to untreated GO cells (p=0.023). Error bars are representing SD. Scale=20µm.

3.4.3 GO deficient mouse osteoblasts show elevated mtROS levels in vitro

To estimate ROS production in vitro; primary osteoblasts isolated from the calvaria of GorabRunx2cre and Gorab;GT mice were exposed to mtROS. Quantification showed increased mean mtROS intensities per cell. GorabRunx2cre primary osteoblasts were gained from the calvaria of 2 week old mice. Cells were seeded confluent and cultivated for 7 days before exposed to mtROS. Primary osteoblasts gained from GorabRunx2cre mouse displayed 1.4-fold increased mtROS levels comparing to littermate controls. Gorab;GT primary osteoblasts were gained from E18.5 embryonic mice and cultured confluent for 7 days after seeding. Gorab;GT animals showed 1.4-fold increased mtROS levels comparing to cells from littermate controls (see Figure 25.A and Figure 25.B).

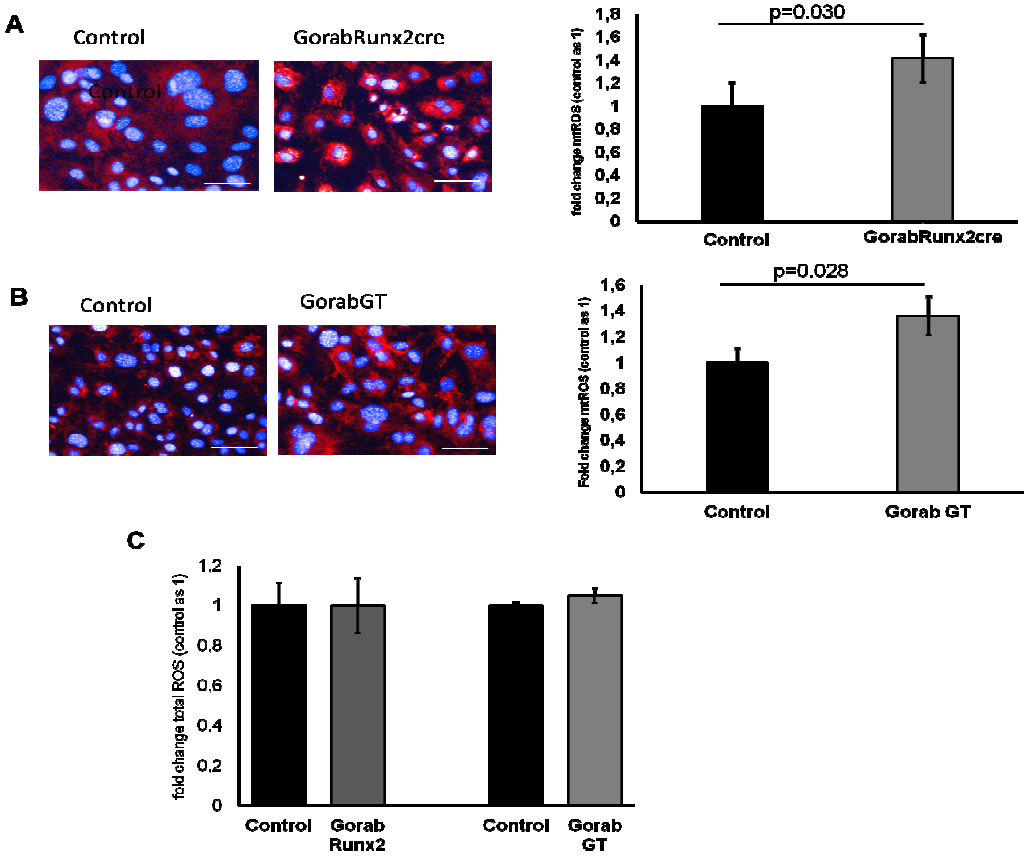

Figure 25: MtROS and total ROS in mouse primary osteoblasts. (A) Confocal Microscopy images showed an increase of mtROS in GorabRunx2cre osteoblasts. Mean fluorescent intensity were 1.4-fold increased comparing to littermate controls (p=0.030). (B) Gorab;GT embryonic osteoblasts (E18.5) showed significantly increased mtROS levels. Mean fluorescent intensities were 1.37-fold higher than in controls (p=0.028). (C) Mean CellRox intensities were comparable to littermate controls (n=7). Statistical analysis by two tailed unpaired t-test. Error bars are representing SD. Scale=20µm.

3.4.4 GO deficient mouse osteoblasts show no increase in total ROS

In addition to mtROS experiments, mouse primary osteoblasts were exposed to CellROX. This reagent is a novel fluorogenic probe for measuring oxidative stress in living cells. It is weakly fluorescent active while it's in a reduced state but it exhibits bright green fluorescent light as soon as it is oxidized by ROS. It subsequently binds to DNA and has an absorption/emission of 485/520 nm. No differences in total ROS between GorabRunx2cre and control cells were revealed. A similar result was gained by quantifying and comparing Gorab;GT animals to controls. No significant differences in totalROS was observed (see Figure 25.C).

3.4.5 GO patient fibroblasts show elevated TGF-β - Nox4 signaling

Since the TGF-β pathway was found overactivated in GorabRunx2cre mice human patient fibroblasts were tested. GO HAFs showed an increase in p-Smad and Nox4 protein levels when cultivated for 7 days post confluence. TGF-β signals are passed on to specific intracellular mediators known as Smad proteins P-Smad protein levels were 2-fold upregulated comparing to littermate controls (p=0.037). Nox4 levels were 1.7-fold higher in GO HAFs comparing to controls (p=0.0422; Figure 26.A and B). These results support the indication, that mtROS is increased due to increased TGF-β and Nox4 signaling in GO.

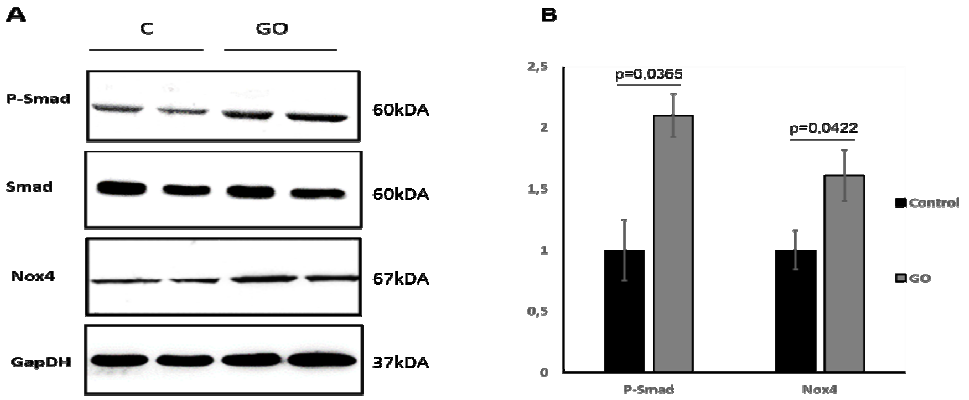

Figure 26: Upregulation of p-Smad and Nox4 in HAFs. (A) Immunoblots showing a 2-fold upregulation of p-Smad protein in GO comparing to controls. In GO HAFs Nox4 was 1.7-fold upregulated comparing to controls. (B) ImageJ quantification of p-Smad protein normalized to Smad. Nox4 was normalized to Gapdh. Error bars are representing SD. Statistical analysis was performed by two tailed paired t-test (n=4).

3.4.6 TGF-β inhibitor leads to a rescue effect in GO

TGF-β is a secreted factor and is upregulated in GO. Therefore the role of TGF-β in the GO pathomechanism was further investigated. Control and patient HAFs were cultivated for 7 days post confluence in the presence of the TGF-β inhibitor kinase SB431542.

Immunoblots were performed in order to verify a dysregulation of key proteins. GO patient HAFs were compared to controls and cultivated in the presence of 10µM of TGF-β inhibitor SB 431542. As shown before P-Smad and Nox4 were upregulated in patient fibroblasts. When mutant cells were treated with the TGF-β inhibitor SB 431542 P-Smad and Nox4 were decreased suggesting a direct regulatory effect. P-Smad protein levels were found 1.4-fold increased in patient fibroblasts (see Figure 27.C). After SB431542 treatment patient fibroblasts exhibited significantly lower p-Smad levels in comparison to untreated patient fibroblasts. In addition, Nox4 was in average 1.2-fold upregulated in GO HAFs comparing to controls. When cultivated with SB431542 Nox4 were significantly reduced in comparison to untreated patient fibroblasts.

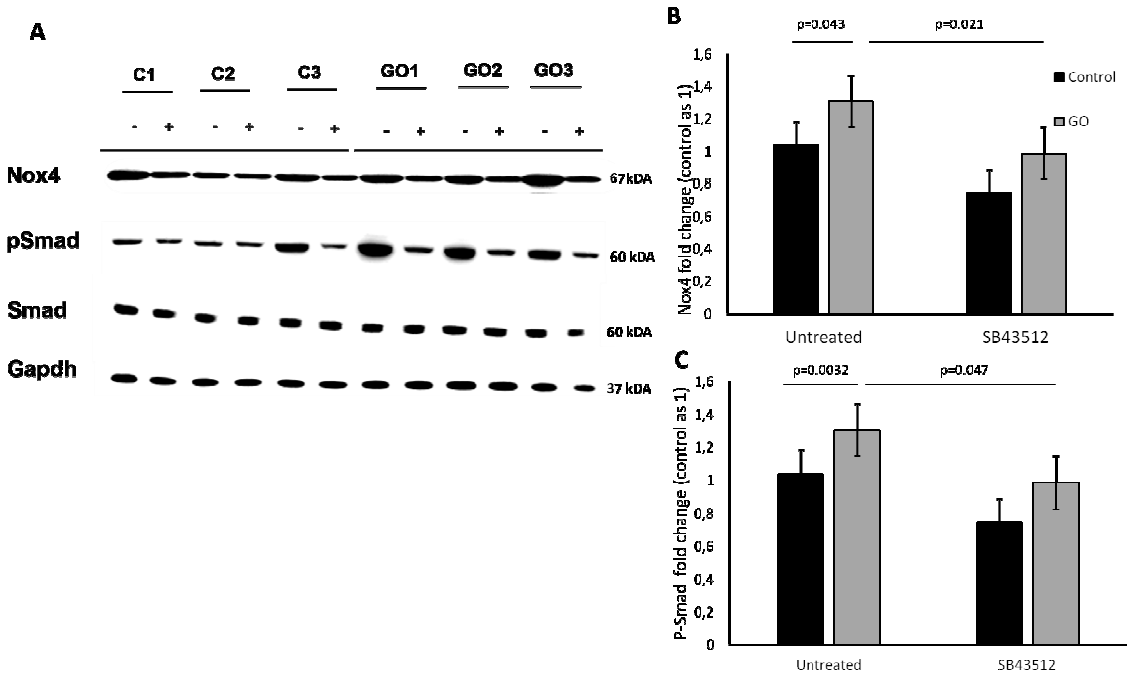

Figure 27: Immunoblot on GO fibroblasts with or without TGF-β inhibitor. Protein lysates are probed for Nox4, pSmad, Smad and Gapdh. Nox4 and pSmad are both increased in GO HAFs comparing to controls. Cultivation for 7 days in the presence of the TGF-β inhibitor SB 431542 leads to a reduction of Nox4 and pSmad levels. (N=5) Error bars are representing SD. Statistical analysis was performed by two tailed paired t-test (n=3).

To further investigate the cell specific response to the TGF-β inhibitor SB431542, different key regulator genes were analysed. *DNA-damage transcript 4* (DDIT4) was in average 3-fold upregulated in GO patient fibroblasts compared to controls. This upregulation was diminished by cultivating the cells in the presence of SB431542. *NADPH Oxidase 4* (Nox4) is an enzyme known to generate intracellular superoxides. Nox4 was found in average 2-fold upregulated in GO HAFs whereas after SB431542 treatment *Nox4* was significantly downregulated. However, no upregulation was observed when GO cells were cultivated in the presence of SB431542. *Superoxide dismutase 2* (SOD2), an enzyme known to transform toxic superoxide into H2O2 and diatomic oxygen, was reduced in GO HAFs. Nevertheless, this reduction was not significant. The same effect was seen when the cells were cultivated in the presence of SB431542. No difference in *TGF-β 1* gene expression was observed. Gene expression of *TGF-β 2* was in average 3-fold upregulated in GO HAFs comparing to controls. This effect was weakened when cultivated in the presence of SB431542. *Serpine1*, a downstream target of TGF-β was significantly upregulated in mutants whereas after TGF-β inhibitor treatment Serpine1 gene expression was significantly downregulated. The cell cycle regulators *p21* (CDKN1A) and *p16* (CDKN2A) were both significantly upregulated in GO HAFs whereas TGF-β inhibitor treated samples showed lower levels (Figure 27).

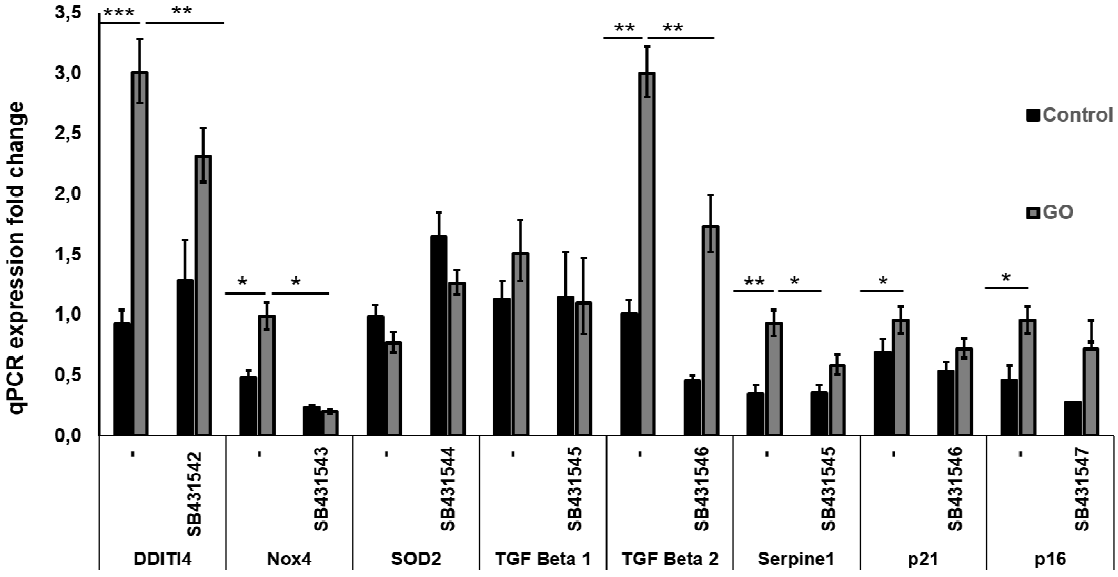

Figure 28: Relative qPCR expression analyses on human fibroblasts. GO patient fibroblasts comparing to control human fibroblasts with or without TGF-β inhibitor (10µM SB 431542). Results indicate an upregulation of *DDIT4* in GO human fibroblasts which could be partially rescued by the presence of SB 431542. Nox4 showed a significant upregulation in GO. However, this upregulation could be significantly downregulated by the presence of TGF-β inhibitor. *SOD2* levels were lower in GO comparing to control fibroblasts. *TGF-β 2* was significantly upregulated in GO fibroblasts but not *TGF-β 1*. Statistical analysis was performed by two tailed paired t-test (n=4). Error bars are representing SD. (* $p<0.05$).

3.4.7 Co-culture with GO lead to elevated mtROS levels in controls

Control human fibroblasts were cultured in a special co-culture system described in (Chapter: Methods, Co-Culture System). One day after co-culture was started in the presence of the TGF-β inhibitor SB431542. MtROS levels of control cells (seeded in the lower compartments) were measured 7 days after the start of co-culture. MtROS levels of control cells were 1.2-fold increased when cultured with GO HAFs in comparison to a co-culture with control cells (Figure 29). When control fibroblasts were cultivated with GO fibroblasts in the presence of SB431542 kinase no significant mtROS increase was observed suggesting a direct connection of TGF-β levels and mtROS.

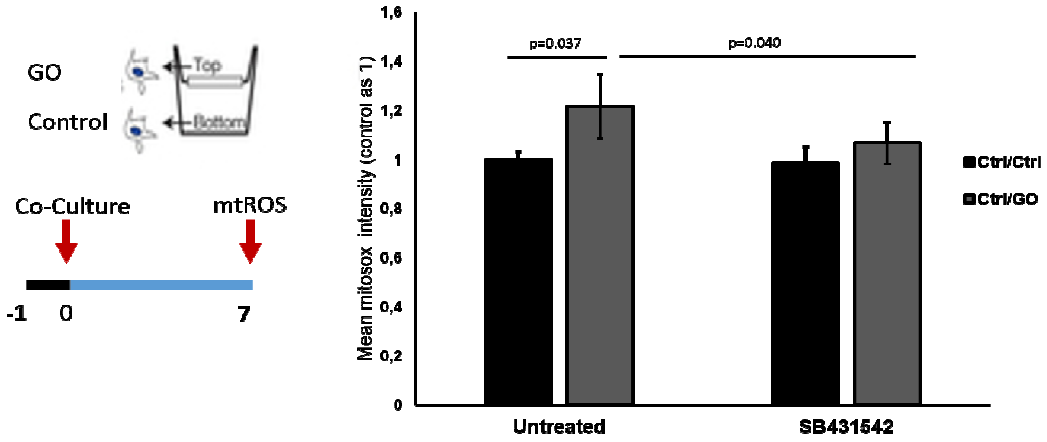

Figure 29: HAF co-culture system. Co-Culture of control HAFs with GO HAFs for 7 days resulted in increased mtROS levels in control cells. (p=0.037). When the cells were treated with TGF-β inhibitor (SB431542) mtROS of Ctrl/GO was significantly decreased (p=0.040). Ctrl/GO did not show higher mtROS levels compared to Ctrl/Ctrl when treated with TGF-β inhibitor. Modified and adopted from [100]. N=6 Error bars are representing SD.

3.5 Influence of oxidative stress on GORAB subcellular localization

HeLA cells were treated with ROS producing substances in order to test the sensitivity of GORAB to different chemicals. Untreated cells were compared to cells treated with hydrogen peroxide (200µM), paraquat (1mM) and CCCP (10µM). Untreated cells showed a distinct fluorescent signal of GORAB at the Golgi apparatus. This could be shown by colocalization with GM130, a well known cis-Golgi matrix protein. When HeLa cells were treated with 200µM H2O2 the fluorescent signal at the Golgi apparatus diminishes whereas paraquat or CCCP treatment did not show any differences compared to untreated cells. However, UV-light, gamma-irradiation and bleomycin did not lead to any phenotypic alterations in HeLA cells (data not shown).

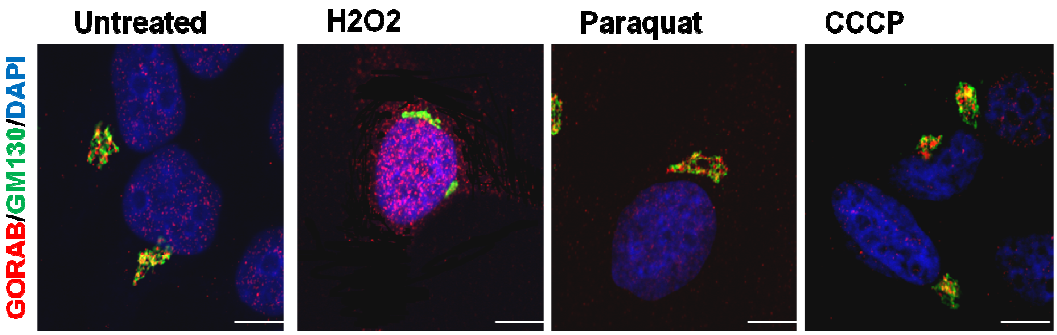

Figure 30: GORAB response to different ROS inducing chemicals. HeLa cells were treated with different chemicals to trigger a specific response of GORAB. In untreated HeLa cells GORAB (red) was located at the Golgi apparatus (GM130 in green) leading to a yellow signal. When HeLa cells were treated with 200µM H2O2 the signal at the Golgi diminishes. Treatment with paraquat (1mM) or CCCP (50µM) did not lead to any phenotypical differences comparing to the untreated cells. (Scale = 5µm)

3.5.1 GORAB detaches from the Golgi apparatus after H2O2 treatment

In order to test this hypothesis, HeLA cells were treated with increasing doses H2O2. GORAB localization was checked after 30 and 60 minutes post-treatment and compared to untreated cells. After H2O2 treatment GORAB detaches from the Golgi apparatus. Higher fluorescent intensities could be observed in the nucleus and cytoplasm of the cells. Within these 60 minutes the Golgi apparatus stays intact and Rab6 still localizes to the Golgi apparatus. Nevertheless, delocalization of GORAB from the Golgi apparatus is concentration depended. Low concentration of H2O2 (2 µM) leads only to a partial delocalization of GORAB of about 10-15%. Intermediate concentration, 20 µM, showed a higher delocalization potential of about 50%. 200 µM H2O2 leads to a complete GORAB delocalization from the Golgi apparatus after 30 minutes (Figure 31). Since 200µM H2O2 resulted in the strongest effect, this condition was selected for further investigations.

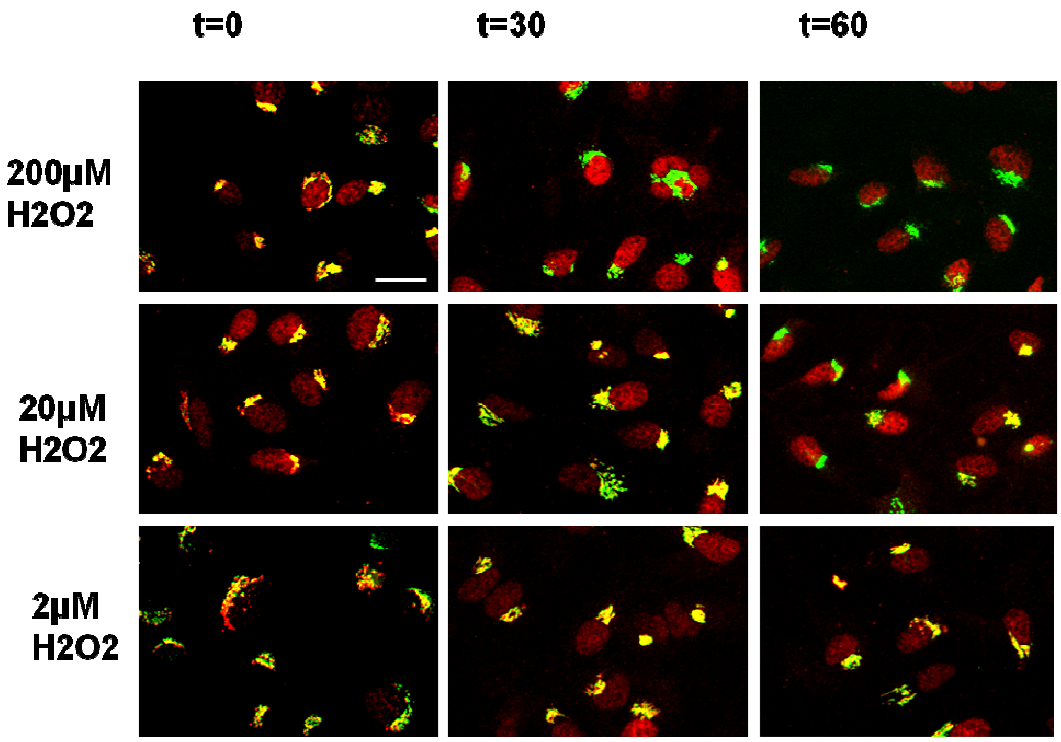

Figure 31: GORAB delocalization is concentration depended. Low concentration of H2O2 (2 µM) lead to a partial delocalization of about 10-15%. Intermediate (20 µM) H2O2 concentration lead to a complete Gorab delocalization from the Golgi apparatus. 200 µM H2O2 resulted in a complete delocalization of Gorab from the Golgi apparatus in all cells. Nevertheless, the Golgi apparatus stayed intact, here shown by GM130 staining (Gorab=red, GM130=green, Co-staining=yellow; Scale = 20 µm).

To get a better understanding of the stress specific response of GORAB, high magnification images were conducted by laser scanning microscopy and z-stack images were processed with maximum intensity projection mode. In HeLa cells a clear delocalization from the Golgi apparatus to the nucleus was observed. Most fluorescent signals were detected within the nuclear region of the cell. No fluorescent signal of GORAB remained at the Golgi. Nevertheless, the Golgi apparatus itself stayed intact, this was shown by GM130 staining.

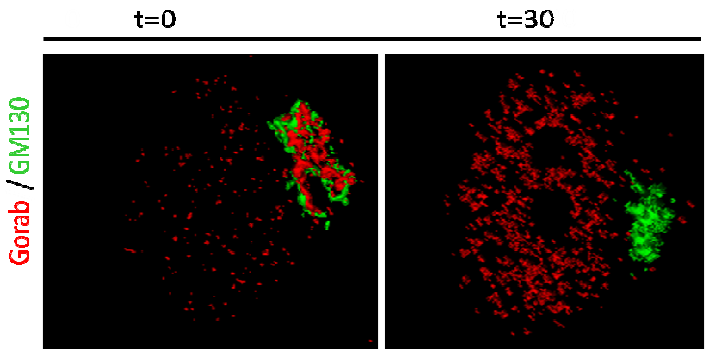

Figure 32: Gorab delocalization HeLa cells stained for GORAB (red) and GM130 (green) were exposed to 200µM H2O2. After 30 minutes, Gorab delocalized from the Golgi apparatus and signal high fluorescence intensities could be observed in the nucleus.

To identify the location of GORAB after H2O2 treatment several colocalization stainings were performed using different makers for cellular sub compartments. LaminA/C a nuclear lamina marker showed clearly an increased GORAB signal within the nucleus. The signal of GORAB at the Golgi apparatus was completely diminished after 30 minutes of 200 µM H2O2 treatment. Increased signals were observed in the nucleus but also in the cytoplasm. In addition, other subcompartments were tested for colocalization. Moreover, GORAB did not show any colocalization with markers specific for lysosomes, endosomes, mitochondria and cytoskeleton (data not shown).

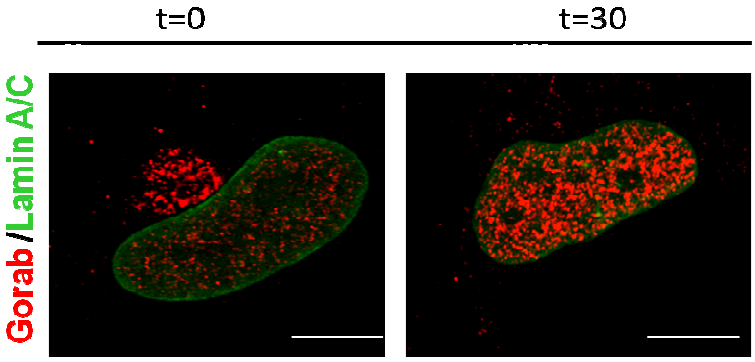

Figure 33: Gorab delocalization HeLa cells were treated with 200µM H2O2 for 30 minutes. GORAB (red) is under normal conditions located at the Golgi apparatus. After H2O2 treatment, increased fluorescent intensity of Gorab could be detected in the nuclear region within the nuclear lamina **(**Scale is 5µm).

3.5.1 Gorab delocalization in PC12 cells after NGF induced differentiation

PC12 cells were stimulated with 100ng/ml NGF for 3 days. Cells were stained each day after NGF induced differentiation. Untreated cells displayed a Gorab signal mainly at the Golgi apparatus. Nevertheless, 3 days after osteogenic induction Gorab was found mainly located in

the nucleus of the cells. To get a better understanding about the role of Gorab in the differentiation process of cells, MC3T3-E1 cells were stimulated with BMP2 to induce osteoblast differentiation. Gorab was found at the Golgi apparatus before and after BMP2 stimulation. No increased signal intensities in the nucleus or cytoplasm were observed.

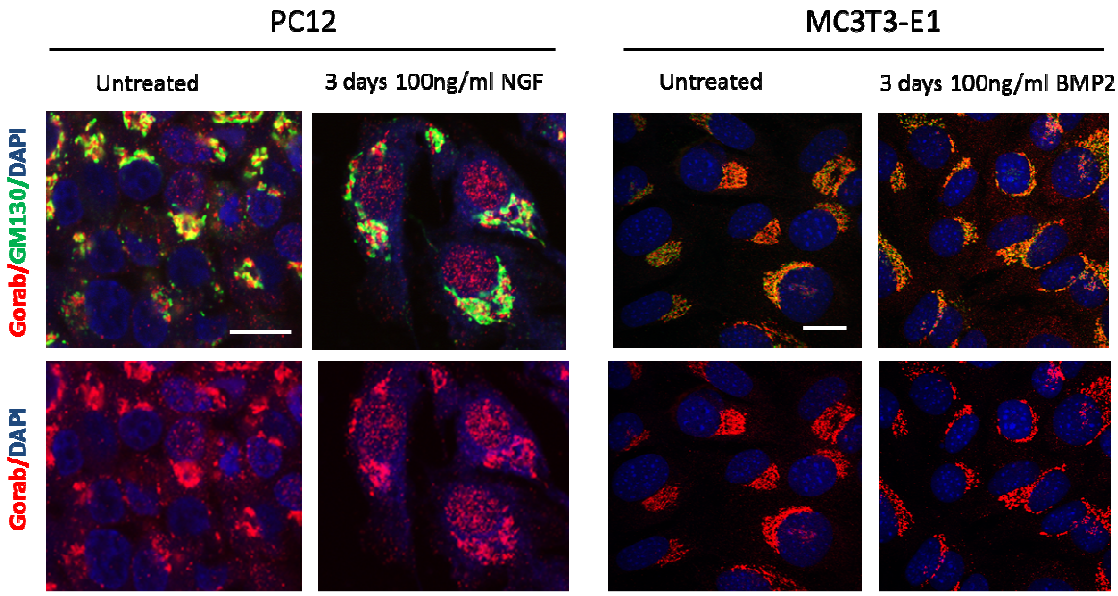

Figure 34:PC12 and MC3T3 before and after differentiation. PC12 cells were treated with 100ng/ml NGF in order to induce differentiation. Gorab was mainly located at the Golgi apparatus before stimulation whereas increased signal intensities of Gorab were found in the nucleus after NGF treatment. In MC3T3-E1 cells Gorab was located at the Golgi apparatus before and after 100ng/ml BMP2 stimulation (Scale=20µm).

To sum up, the findings of this section demonstrate that Gorab location changes after H2O2 treatment in several human and mouse cell lines. Moreover, Gorab signal was more intense in the nucleus in PC12 cells after NGF induction.

Cells from GorabRunx2cre mice and GO HAFs exhibited increased mtROS levels whereas totalROS levels remained unchanged. Treatment with a specific TGF-β kinase inhibitor (SB431542) led to lower mtROS levels. Furthermore, it was found that *p-Smad* and *Nox4*, both downstream targets of *TGF-β*, were significantly upregulated but in the presence of SB431542 expression of these genes was significantly decreased. Furthermore, co-culture experiments show clearly that the soluble factor TGF-β is responsible for increased mtROS levels in control fibroblasts. These findings suggests that a.) Gorab is a sensor for H2O2 and b.) Gorab knockdown leads to increased TGF-β - Nox4 signaling which is in charge for the increased mtROS levels in GO.

4. Discussion

4.1 Bone phenotype of GorabRunx2cre mutants

Inactivation of *Gorab* by Runx2cre mice led to a bone phenotype not only in all major parts of the skeleton (cranial, axial, and appendicular), but also in the two compartments in long bones, the cortical and the trabecular bone. An important part of the prematurely aged appearance of gerodermia osteodisplastica (GO) patients is the hypoplasia of maxilla and mandibula with variable malformation of the teeth. Three dimensional microCT reconstructions on 2 and 4 week old GorabRunx2cre mice showed poor mineralization in the suture region with a delayed closure of the fontanels. However, no malformation of the teeth was seen in our animals.

Moreover, one major characteristic of GO patients is the early onset osteoporosis which is more pronounced in the spine than in the long bones. The GorabRunx2cre animals generated in the course of this study reflected the bone phenotype found in GO patients. In 4 and 12 week old GorabRunx2cre tibia and femur a reduced bone volume to total volume ratio, a reduced trabecular number and trabecular thickness as well as a cortical bone thinning were observed. Moreover, the spine of GorabRunx2cre animals showed a severe osteoporosis with a decrease in number of vertebral trabeculae.

In summary, the phenotype of GorabRunx2cre mutants corresponds to a severe variant of the GO bone phenotype.

4.1.1 The primary affected cell type leading to the GO bone phenotype

Since the GorabRunx2cre model recapitulates faithfully the GO bone phenotype it can be assumed that the inactivation of *Gorab* occurs in those cell types and the time point at which *Gorab* is physiologically most relevant. The inactivation was driven by the *Runx2* promoter. Therefore, in the GorabRunx2cre mouse model investigated here *Gorab* is likely to be inactivated at the early stage of osteoblast and at the later stage of chondrocyte differentiation.

Previously Dr. WL Chan generated GorabPrx1cre, GorabCol2a1cre and GorabDmp1cre mice to study the knockout of *Gorab* at different stages of chondrocyte and osteoblast differentiation.

In GorabCol2a1cre mutants, in which *Gorab* is specifically deleted in chondrocytes, a trabecular bone phenotype and a pronounced shortening were observed, but the cortical bone was not affected. This finding suggests a contribution of the chondrocytic lineage to the

shortening of the long bones and the trabecular bone phenotype but not to the cortical bone phenotype. These findings could be due to lack of specificity of the Col2a1 promoter. Several recent publications have shown a transdifferentiation of growth plate chondrocytes into osteoblasts. Interestingly, these chondrocyte-derived osteoblasts were found on the trabecular bone and the endocortical surfaces, but not at the periosteum. Therefore, the strinking difference between the cortical phenotype of GorabCol2a1cre and GorabRunx2cre mutants can possibly be explained by a defect in periosteal bone apposition in GorabRunx2. This is also in line with the abnormal modelling of the growing bone, which is largely due to periosteal bone apposition.

GorabDmp1cre mutants showed a reduced trabecular bone volume, but no changes in cortical bone thickness or long bone length. Dmp1 starts to be expressed in late osteoblasts and remains active in bone-embedded mature osteocytes. Although in GorabRunx2cre the osteocytes showed strong alterations, inactivation in this cell type by *Dmp1* has only mild effects. Therefore, the most relevant physiological function of *Gorab* must take place at earlier stages of osteoblast differentiation.

The mouse line most closely resembling the GorabRunx2cre bone phenotype is GorabPrx1cre. In GorabPrx1cre animals *Gorab* is deleted in the limb bud mesenchyme very early in development of the long bones and therefore affects osteoblasts, chondrocytes, the muscle, and probably also to some degree the vessels. Although in GorabPrx1cre mutants the knockout in the appendicular skeleton is broader the bone phenotype of GorabRunx2cre animals was more pronounced. This might indicate that the *Runx2*cre-driven inactivation perturbs the osteoblasts at a more vulnerable point. An alternative hypothesis is simply that the efficiency of *Gorab* inactivation in osteoblasts and chondrocytes is higher in GorabRunx2cre than in GorabPrx1cre animals.

Further studies have to be performed in order to test this hypothesis. Nevertheless, immunohistochemistry would serve as an ideal method to verify the efficiency of *Gorab* inactivation. Unfortunalety, up do date, no specific Gorab antibodies for immunohistochemistry on mouse bone samples are available.

4.1.2 Irregular extracellular matrix in Gerodermia Osteodysplastica

Since we found an osteoblast to osteocyte maturation delay we speculated if these osteoblasts secrete an altered extracellular matrix which impairs the differentiation into osteocytes. Indeed, we were able to show that decorin and collagen, two major matrix proteins, were highly changed in the mutant bone. Polarized light images on MMA tibia sections of

GorabRunx2cre and GorabPrx1cre mice revealed an increased fragmentation and thinning of collagen fibres.

Osteogenesis Imperfecta (OI) is caused by mutations in *COL1A1* and *COL1A2* and causes a bone phenotype characterized by brittle bones, extracellular matrix manifestations and abnormal TGF-β function [54]. Mutations in collagen type II cause a spectrum of diseases called type II collagenopathies [55]. Moreover other collagens like collagen IX, X, XI, XII are known but have minor roles.

It is known that TGF-βI binds to type I, II, and IV collagens, as well as to biglycan and decorin and plays important roles in cell-to-cell, cell-to-collagen, and cell-to-matrix interactions and regulates the synthesis of ECM throughout the body [56], [57]. Stamov et al. could clearly show the relationship of glycosylated decorin to collagen fibril diameter. A collagen type I to glycosylated Decorin ratio of 200:1 clearly resulted in a thick and oriented collagen network in vitro. A ratio change of 20:1 resulted in a fragmented collagen structure, whereas a ratio of 2:1 resulted in a total loss of linear collagen fibers [58], [59], [40].

Decorin is only one member of the small leucine-rich proteoglycan family. Other examples are: Biglycan, Lumican, Fibromodulin, Keratocan, Osteoadherin and others. All the other leucine-rich proteoglycans can be described in a similar way as decorin. Hence, biglycan and lumicans are associated to collagen fibers in bone, lung and skin [56],[57],[60],[61].

Collagen alterations and elastic fiber abnormalities leading to impaired glycanation of proteoglycans were also described in the progeroide form of Ehlers-Danlos syndrome [62]. Our group could show a significant reduction in the amount of dermatan sulfate but not in other glycosaminoglycans in Gorab Genetrap animals. In GorabRunx2cre and GorabPrx1cre bone samples decreased levels of glycanated decorin were found. In addition decorin staining was increased more distally in the metaphysis of the tibia in GorabRunx2cre mice. This finding indicates a specific defect in dermatan sulfate glycanation of proteoglycans.

Homozygous decorin knockout mice are viable; they show a thinning and fragility of the skin and abnormal collagen fibrils. However, no bone phenotype was described in $Dcn^{-/-}$ animals [56]. Biglycan knockout mice have a reduced bone mass with a progressive phenotype with increasing age. These mice have a reduced capacity to produce stroma cells which are the important bone cell precursors. Homozygous animals show a reduced response to TGF-β, a reduced collagen synthesis and an increase in apoptosis. This phenotype is completed by a reduced expression of terminal osteocyte markers in mouse calvaria [63]. Based on these studies, the biglycan knockout mice with their pronounced bone phenotype recapitulate our

findings in the GorabRunx2cre and GorabPrx1cre animals. Nevertheless, in GorabRunx2cre and GorabPrx1cre mice no abnormalities in biglycan was found.

Biglycan/Decorin double knockout animals show a phenotype which is even more prominent than in homozygous biglycan animals [63]. GorabRunx2cre animals displayed rather an improper glycosylation defect than a complete loss of decorin therefore a knockout of glycosyltransferase gene knockout mice would reflect the GO bone phenotype better.

4.1.3 Osteoblast to osteocyte differentiation delay in GorabRunx2cre

Immunohistochemistry on 4 week old GorabRunx2cre and GorabPrx1cre animals revealed a significant increase of osterix (Sp7) positive cells in the tibia metaphysis. By 12 weeks the tremendous increase of premature osteoblasts is no longer detectable suggesting a differentiation delay instead of a complete block. Moreover, in the cortical diaphysis; more sclerostin positive cells were found. However, in cultured osteoblastic cells these findings cannot be fully reproduced.

This indicates a) GorabRunx2cre mutant primary osteoblasts are able to differentiate into mature osteoblasts, they produce a similar amount ALP and Alizarin as controls but with an altered osteoblast and osteocyte marker genes expression b) since the calvaria is formed through the direct ossification, no intermediate chondrocytes are formed. This suggests that the chondrocyte influence in the GO pathomechanism is subtle and most of the problems in the GO phenotype arise from the differentiation delay of osteoblasts.

To identify the reason for the osteoblast to osteocyte differentiation delay we followed different hypotheses. Firstly, the unfolded protein response machinery (UPR) in GO was investigated. It was reported that the UPR is a key regulator in the osterix mediated differentiation process. Typically, in osteoblast maturation and development, the capacity of the endoplasmatic reticulum (ER) is exceeded and ER stress is triggered. ER stress is followed by a response of the UPR, which signals to XBP1, IRE1α and subsequently to osterix in order to induce osteoblast maturation. However, this interesting hypothesis could not be confirmed in GorabRunx2cre and *Gorab* siRNA transfected ST2 cells. In both systems no significant changes in XBP1, XBP1-spliced and IRE1 α was found [64].

Secondly, in order to test if the osteoblast to osteocyte maturation deficiency is caused by increased cell death, immunohistochemical detection of indicator proteins for apoptosis was performed. To stain for apoptosis different markers were used: a.) cleaved caspase 3, which is a critical executor of apoptosis b.) Parp and c.) TUNEL fluorescent staining. By 4 and 12

weeks no significant changes in apoptosis in the metaphysis of GorabRunx2cre mutants was observed. Nevertheless, the lack of a proper positive control and the weak staining intensity make a final conclusion difficult. In vitro culture of GO patient fibroblasts displayed rather a reduced proliferation potential with a senescent phenotype than an increase in apoptosis. For future studies, it is necessary to improve the conditions or to find a better technique and a positive control to detect apoptosis in bone tissues. Additionally it would be important to use an intermediate timepoint, for example 8 and/or 10 weeks.

Thirdly, TGF-β and its downstream target p-Smad were found significantly increased in the mutant mouse tibia by rtPCR and immunoblots. Moreover, we were able reproduce this increase in mouse primary osteoblasts and human patient fibroblasts culture suggesting a leading role of TGF-β in GO.

4.1.4 The role of TGF-β in Gerodermia Osteodysplastica

TGF-β upregulation was found in a variety of cells and tissues lacking Gorab. We detected an increased gene expression of TGF-β in human patient fibroblasts, GorabRunx2cre mouse primary osteoblasts and in GorabRunx2cre tibia lysates. The downstream target p-Smad was found increased in immunoblots of GorabRunx2cre mouse diaphysis.

Bone and cartilage contain large amounts of TGF-β. It is a known chemoattractant for osteoprogenitor cells to recruit them to the site of new bone formation or bone remodelling [65], [66], [67], [68], [69]. Increased TGF-β signaling enhances cell proliferation and accumulation in different tissues [70], [71] (Figure 35). Moreover, TGF-β is important for the differentiation of monocytes into osteoclasts and couples osteoblast and osteoclast function. A mouse model overexpressing TGF-β2 results in an osteoporotic bone phenotype [72].

Marfan syndrome is caused by defective fibrillin-1 that cannot bind to TGF-β and therefore leading to increased activated TGF-β tissue levels [53], [73]. This accelerated TGF-β signaling leads on the one hand to an overactivation of osteoclasts. On the other hand, high TGF-β levels in the stem cell niche lead to a depletion of mesenchymal stem cells in a Marfan mouse model [74]. The different phenotype in GorabPrx1cre and GorabRunx2cre mutants can possibly be explained by the fact that in both mouse models bone is the main source of abnormally high TGF-β, thereby attracting osteoblasts to the bone surfaces, where their differentiation is blocked.

Interstingly, Gorab genetrap mice die neonatally because of respiratory failure, which is in contrast to the GO patomechanism in humans. It was previously reported that exceeded TGF-

β signaling results in marked lung fibrosis, which could be significantly reduced by accompanying overexpression of decorin and by inhibition of Nox4 [75], [76].

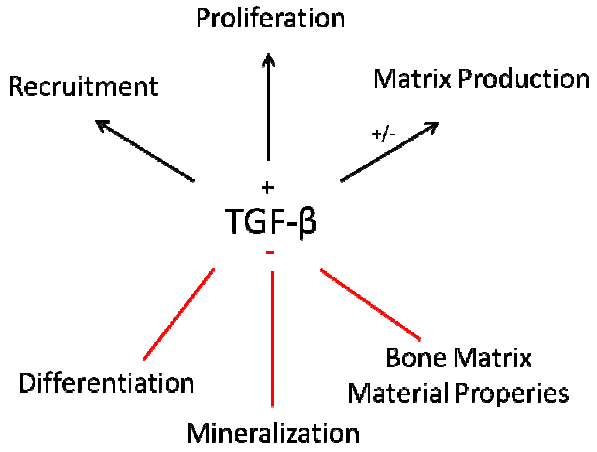

Figure 35: Different Roles of TGF-β. TGF-β regulates the recruitment, proliferation, differentiation and matrix production in the developing osteoblast as well as the mineralization and bone matrix material properties in osteocytes. (Please not: black arrow is positive regulation; red line is negative regulation).

Moreover, TGF-β upregulation has also been reported in a number of autosomal dominant cutis laxa cases and also OI [77],[78]. In OI type I and II higher ratio of phospho-Smad2 to total Smad2 protein was measured. In addition, higher in vivo Smad2 reporter activity, as well as a reduced binding capacity of the proteoglycan decorin was found. Anti TGF-β treatment (Antibody: 1D11) corrected the bone phenotype in both forms of OI [79], [80].

The osterix accumulation, the delayed differentiation and mineralization found in GorabRunx2cre and GorabPrx1re animals in vivo and in vitro can be tracked back to accelerated TGF-β signaling.

4.1.5 Emerging role of reactive oxygen species in GO

The free radical theory of aging states that an organisms ages because free radicals lead to permanent oxidative damages in cells. Studies in C. elegans showed that an organism needs a certain amount of stress in order to perform better. High levels tough can damage an organism seriously resulting in accelerated aging [81]. Oxidative stress is triggered by reactive oxygen species (ROS) that generally comprises superoxide anions (O2-) and hydrogen peroxide (H_2O_2) and also Nitric oxide (NO) [82]. Mitochondria generate damaging ROS during oxidative phosphorylation [83]. ROS and the resulting damages can drive a cell into senescence [84]. Nevertheless, besides the harmful potential of ROS it is also an important second messenger in lower doses. For example low doses of H2O2 is needed for collagen

crosslinking in the bone [85]. In order to test the influence of ROS in the premature ageing process of GO several different approaches to answer this question were performed.

Firstly, totalROS and mtROS dyes were used to stain all the cells of bone marrow. A significant increase of mtROS but no increase in totalROS was detected. Since the mouse bone marrow contains a very heterogeneous group of cells a more specific approach was performed next.

Secondly, mouse primary osteoblasts isolated from the calvaria of genetrap (E18.5) and GorabRunx2cre (P10) mutant mice were cultivated for 1, 3 and 7 days post confluence and stained with MitoSOX. Interestingly, most consistent results were obtained by cultivating the cells 7 days post confluence. This showed evidence that matrix secretion plays a role in mtROS signaling. Nevertheless, totalROS measurements using two different markers (CellROX, CDFDA) remained variable. Presumably, the markers were not as stable for high content screening as for example MitoSOX and therefore strong variations in the wells were observed.

Thirdly, to address how the increase in mtROS but not in totalROS is emerging we tested enzymes that are involved in the ROS production and degrading process. In a cell, ROS is produced as a side product in mitochondria or peroxisomes. Ubiquinone and NADH dehydrogenase are the enzymatic ROS producers. One family that is known to produce superoxide and hydrogen peroxide are the NADPH oxidases (Nox). They are integral membrane proteins that enable the transport of electrons and produce ROS in order to regulate specifically signal transduction [86], [87]. Nox1, Nox2 and Nox4 are expressed in bone cells like osteoblasts and osteoclasts [88]. In undifferentiated mesenchymal stem cells low expression levels of Nox4 can be found but in contrast, mature cells express high levels of Nox4. Therefore, Nox4 has been suggested to drive the differentiation process in cells [89]. $Nox4^{-/-}$ mice displayed higher bone mass and a reduced number of osteoclasts [90].

Moreover, Nox4 is strongly induced by TGF-β [91], [92], [93]. Hence we speculated if exceeding TGF-β - Nox4 signaling happens in GO. Indeed, we were able to show the importance of TGF-β in the accumulation of mtROS in GO. TGF-β inhibitor treatment resulted in a significant downregulation of mtROS. Since TGF-β is a secreted factor we speculated if we could increase mtROS levels in control fibroblasts by co-culturing them with patient cells. After 7 days of co-culture with patient fibroblasts, controls exhibited elevated mtROS levels in comparison to a co-culture with control cells. When control and GO cells were co-cultured in the presence a specific TGF-β inhibitor no elevated mtROS levels in

control cells was observed. These data suggests a direct role of TGF-β in promoting mtROS in GO.

In collaboration with the University of Hong Kong, a Talen approach to knockout *Gorab* in zebrafish was performed. In vivo mtROS staining and FACS sorting revealed a 10-fold increase of mtROS intensities comparing to controls. Importantly, gene expression of Nox4 was again upregulated (manuscript in preparation).

Superoxide is in general reduced by an enzyme called superoxide dismutase (SOD) which converts superoxide to hydrogen peroxide and molecular oxygen. Antioxidant systems and ROS degrading enzymes, for example catalase, SODs and glutathione, are important systems to neutralize harmful ROS molecules within a cell. Similar as in GO, SOD1 deficient mice showed high levels of intracellular ROS and a severe bone loss with impaired collagen cross linking resulting in a fragile bone structure. Antioxidant treatment could rescue the bone phenotype in mice significantly [94]. We did not find significant changes in SOD1 but the lack of an appropriate antibody make a final conclusion difficult. SOD2 is the main antioxidant enzyme that scavenges ROS, particularly superoxide, in the inner mitochondria matrix. Mice that lack SOD2 develop severe pathologies soon after birth that are associated with increased mtROS levels, premature ageing and cellular senescence. Embryonic fibroblasts from SOD2 deficient mice proliferate slowly and have in total more chromosomal breaks than healthy control cells [95], [96]. Gene expression of *SOD2* was found decreased in patient fibroblasts comparing to controls. However, this reduction was not significant (see Figure 36).

To finally prove the contribution of ROS to the GO phenotype in our group, an in vivo rescue experiment was performed using N-Acetyl-Cysteine (NAC), an antioxidant, to treat the bone phenotype in GorabPrx1cre animals. NAC treatment in 4 week old GorabPrx1cre animals, for 8 weeks, led to a significant improvement of the trabecular bone phenotype. Nevertheless, cortical bone thinning was not changed using NAC as a treatment strategy (manuscript in preparation).

To sum up, we were able to demonstrate the increase of ROS in different in vitro and in vivo systems in human, mouse and zebrafish. To date there is much evidence that the increased ROS levels are playing a major role in the GO pathomechanism. We believe that excessive TGF-β – Nox4 signaling causes the accumulation of superoxides within GO cells.

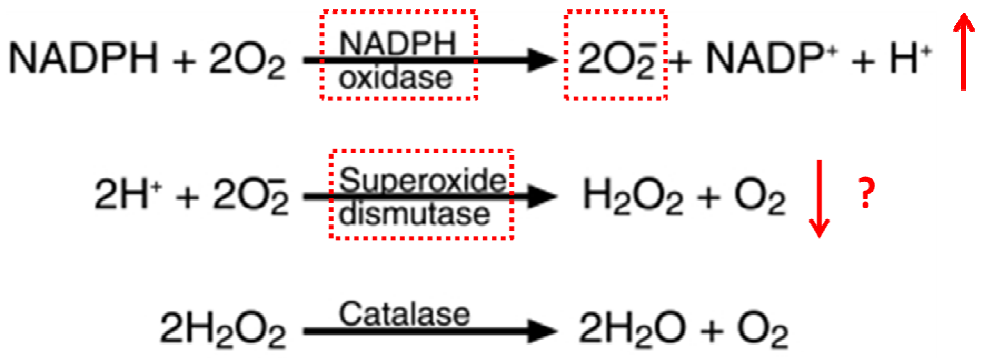

Figure 36: Relationship between ROS and reaction enzymes. Molecular oxygen is reduced by NADPH oxidase (Nox4) which produces superoxide anions as an end product. Superoxide is reduced by superoxide dismutase to H2O2 and molecular oxygen. H2O2 is subjected by catalase to become water and molecular oxygen. Red arrows and squares indicate the changes found in patient fibroblasts. Nox4, an NADPH oxidase and superoxide anions were significantly increased whereas SOD2 was found decreased (not significantly). Picture modified and adapted from [124].

4.2 Cellular senescence in GO

Cellular senescence is the irreversible replication arrest in mitotic cells. There are three known causes of cellular senescence: a) telomere dysfunction, b) DNA damages and c) oncogens [97], [98]. Since we found elevated mtROS levels we speculated if this ultimately leads to increased DNA damages and subsequently to cellular senescence in our system. Indeed, GO patient fibroblasts exhibited increased DNA damages and reduced DNA damage response (DDR), lower proliferating potential with increased cell size in combination with an increased beta-galactosidase activity and increased p16 and p21 marker gene expression.

With immunohistochemistry we found a mild increase of p21 in the trabecular bone of 4 week old mutant mice. Since the number of cells positive for p21 was rather small we speculated if these senescent cells affect their surrounding through increased TGF-β - Nox4 signaling. In a recent study it was found that conditioned medium from cells undergoing senescence contain high levels of interleukins and TGF-β. Trough paracrine signaling ROS and DNA damage response was affected in neighboring cells. Inhibition of either TGF-β/SMAD or IL1/NFκB pathway resulted in decreased ROS production, DDR as well as in senescence [99], [100], [101]. A decline of TGF-β signaling suppressed the development of premature senescence in a p21 dependent manner [102], [103], [104].

Comparing to other publications p21 was mostly increased due to elevated ROS levels through p53. Up to date we did not find altered p53 expression in vivo or in vitro.

Nevertheless, it was previously shown that p21 induced senenscence can also develop independently of p53 [105].

Cellular senescence is associated with telomere shortening and by damages specifically in the telomere regions resulting in a senescent cell phenotype. According to our current knowledge it is unlikely that telomere dysfunction or damages in the telomere region play a role in GO development. For future studies, it is necessary to improve the conditions, find better antibodies or a better technique to detect telomere dysfunctions and/or DNA damages in the telomere regions in patient fibroblasts.

To summarize, we believe that excessive TGF-β – Nox4 signaling causes elevated mtROS levels. This leads to increased DNA damages within the cells which cause ultimately cellular senescence.

4.2.1 GO and other premature ageing disorders

Gerodermia Osteodysplastica (GO) belongs to the group of progeroid syndromes (PS) which are rare genetic disorders wherein symptoms resembling aspects of aging. Patients that suffer from PS appear to be older than the normal physiological age. Progeroid syndromes can be categorized in segmental progeroid syndromes with multiple affected organs, and unimodal progeroid syndromes with only one affected organ [106]. Mutations in a heterogeneous group of genes like, *Lamin A/C, Werner syndrome ATP-dependent helicase* (WRN), *Cockayne syndrome protein A* (CSA), and *CSB* and repair genes like *Xeroderma Pigmentosum group B* complementary (XBP), *XPD* and *TTDA*, lead to premature ageing in humans. Longevity in humans is caused by a defect in following genes: *TOR, S6kinase1 and tumor protein 53* (p53) [107].

At first glance no overlap of these genes can be found. The reason why this heterogeneous group of genes causes premature ageing can be only in the molecular downstream processes that they have in common. Universal molecular mechanisms are the enhanced DNA damages and the defective DNA damage repair, altered cell proliferation behavior, increase in ROS, and the increase in cellular senescence [108].

The three premature ageing disorders GO, Werner syndrome (‘progeria of adults’, OMIM 277700) and HGPS (‘progeria of childhood’, OMIM 176670) share many similar features but can be distinguished by some others. They all have in common a severe bone phenotype. This includes a short stature and osteoporosis. In Werner syndrome the onset of the phenotypes starts much later in adolescence. GO and HGPS develop the bone phenotype at birth and both

of them have in addition a maxillary hypoplasia and mandibular prognathism. The skin phenotype is diverse in these premature ageing disorders. In GO and in HGPS the onset of the skin phenotype is at birth whereas the skin phenotype in Werner syndrome develops at adolescence. The GO skin phenotype is characterized with wrinkled skin on the dorsum, the hands and the feet. HGPS patients lose their skin appendages and their hair and they have reduced subcutaneous fat tissue. The onset of the skin phenotype at adolescence is characterized with a scleroderma like skin, loss of subcutaneous fat tissue and a premature loss of hair and graying [109], [1], [110], [111].

Hutchinson-Gilford is caused by a defect in Lamin A/C. A mouse model defective in the pre-lamin A processing enzyme ZMPSTE24 reproduced the progeroid phenotype. Hutchinson-Gilford mutant mice displayed a phenotype similar as in GorabRunx2cre and GorabPrx1cre mutant mice. In 5 week old ZMPSTE24$^{-/-}$ mice, growth retardation, imbalanced gait, low bone mass and spontaneous fractures were observed [112]. Interestingly, the periosteum in HGPS mutant mice shows an analogous phenotype as in GorabRunx2cre and GorabPrx1cre animals. In HGPS the thickened periosteum is buildup of several layers of lining osteoblasts which replicates the bone phenotype in GO mutant mice. Moreover, in HGPS an increase in DNA damages and a delayed recruitment of DNA damage repair proteins was reported which was confirmed in *Gorab* deficient animals [113], [114]. Upon ZPMSTE knockdown cancer cells showed significant increase of genes involved in proteoglycan synthesis (chondroitin sulphate and/or heparan sulphate). The authors suggested a rescue of ZMPSTE $^{-/-}$ cells by the presence of wildtype ECM [115]. This proposes a common proteoglycan synthesis alteration in HGPS and GO. Nevertheless HGPS mutant mice exhibited much higher number of DNA damages in comparison to GO. However, three major findings in the HGPS mouse phenotype were different to findings in *Gorab* deficient mice:

a) HGPS mutant mice showed a massive increase of empty osteocyte lacunae in the cortical bone. In GorabRunx2cre and GorabPrx1cre animals osteocyte shape and canaliculi network was highly altered. Moreover, osteocyte-like cells were round surrounded by large and unmineralized lacunae.
b) In HGPS mutant mice TRAP and MMP9, which are both markers for osteoclasts, were significantly downregulated. In *Gorab* conditional animals no significant difference in osteoclasts number per bone perimeter was detected. Nevertheless, the biological variations in 4 week old controls and mutants were tremendous. One human bone sample that was tested in the lab of Prof. Dr. Amling in Hamburg revealed a mild increase in TRAP positive cells. The low patient number (n=1) limits the significance of this finding.

c) In HGPS animals an increase in white adipocytes was found. In the case of HGPS it seems there is an imbalanced differentiation potential starting from mesenchymal stem cells. In GorabRunx2cre and GorabPrx1cre animals no increase in adipocyte number is found [116]. Cell lineage tracing recently revealed that bone marrow adipocytes are largely derived from Osx+ cells [117]. However in our model these cells become rather commited to the osteoblast lineage.

Resveratrol and NAC, two well-known antioxidants, increased the binding capacity of Lamin A and SIRT1 and therefore leading to an increase in colony forming capacity, bone mineral density and life span in ZMPSTE24$^{-/-}$ mice [118]. As mentioned earlier, our group was able to show a significant improvement of the trabecular bone phenotype in 4 week old GorabPrx1cre animals upon NAC treatment.

4.3 Molecular basis of GO

4.3.1 The role of Gorab in the secretory pathway

GORAB is primarily a trans-Golgi-localized protein that interacts with Rab6 and ARF5 [6]. The loss of correct Golgi targeting was reported to be an essential aspect in the GO pathomechanism [9].

Secreted and transmembrane proteins have to pass through the endoplasmic reticulum (ER) and the Golgi apparatus where they are synthesized, folded and subjected to covalent modifications, most particularly glycosylation [119]. Mutations in specific glycosylation enzymes, nucleotide sugar transporters or recycling/reorganization components (Golgins, COG Proteins) can affect glycosylation. For review see [120].

In this process, GORAB might play an essential role in the glycosylation cargo of the Golgi apparatus since a loss of GORAB results in glycosylation defects in the bone and most presumably also in the skin and lung. GORAB expression is particularly high in dividing cells (basal cells, perichondrium) in tissues that are responsible for growth and regeneration. The tissues that are affected in GO have to secrete tremendous amounts of matrix therefore they are affected by the loss of Gorab.

However, loss of the trans-Golgi-localized V-type H+-ATPase subunit a2 leads to a wrinkly skin syndrome called ARCL2A with a phenotype similar to GO. ARCL2A shows a distinctive N- and O-glycosylation defect. However, up to date no N- and O-glycosilation defect could be found in GO patients [2], [6], [121], [122].

4.3.2 The puzzling role of Gorab in the nucleus

In this study, we examined the subcellular localization of GORAB under different circumstances. GORAB was originally described by our group as a Golgi interacting protein [6], whereas other groups reported GORAB in the cytoplasm of hepatoma cells (SMMC-7721) [123] or in the nucleus of neuronal PC12 cells [21]. Therefore, we assume the location of GORAB might be cell type, cell cylcle and stress level dependend.

In our hands colocalization studies under different conditions showed that GORAB is mostly located at the Golgi apparatus but as soon as the cell undergoes oxidative stress (triggered by H2O2) the location of GORAB changes and via an unknown mechanism immunofluorescence signals appear stronger in the nucleus and cytoplasm. We were able to reproduce this phenomenon in several human and mouse cell lines. It has not been possible to confirm a nuclear accumulation of GORAB by any other method. Since nuclear background staining often also gets stronger in GORAB-deficient cells an alternative explanation is that GORAB changes its conformation upon oxidative stress and is therefore no longer recognized by the antibody. In either case it can be stated that GORAB reacts to H2O2, which implies a function as a sensor.

In a recent publication GORAB was describes a nuclear interacting protein in PC12 cells and cortical neurons. The authors concluded that GORAB inhibits neurite outgrowth in PC12 cells affecting morphogenesis of primary cortical neurons by decreasing p53 expression. Furthermore, they found that GORAB can directly induce MDM2 transcription, whereas inhibiting the function of Mdm2 [21]. These results are questionable since 1. we found GORAB localizing at the Golgi apparatus in PC12 cells but after NGF stimulation the signal became more prominent in the nucleus. 2. ChIP – Seq experiments performed in our laboratory using HeLa cells and human fibroblasts before and after hydrogen peroxide treatment did not show a specific chromatin interaction but rather a very unspecific interaction with the whole genome. One explanation for this different result might be that our group worked mainly with the endogenous GORAB protein whereas in the other publication overexpression systems were used. In our experience, overexpression of GORAB results in the formation of fibrous structures possibly because of unspecific aggregation of the coiled-coil domains [9]. This mislocalization of GORAB in overexpression systems might cause problems in interaction experiments.

In a previous study of our lab it was shown that HeLA cells and U2OS cells exhibited increased *TGF-β* gene expression after GORAB knockdown (unpublished data). We believe

that the upregulation of *TGF-β* was independent of the matrix composition because a) the cells were semi-confluent and b) HeLa cells and U2OS cells are known to secrete a minimal amount of matrix. Considering this, we speculate if GORAB acts as a transcriptional regulator leading to an upregulation of *TGF-β*. Further studies have to be conducted in order to get insight into the role of *Gorab* inside the nucleus.

4.3.3 Summary and Outlook

In this study we characterized the skeletal phenotype of GorabRunx2cre animalsand found skeletal abnormalities and premature osteoporosis reflecting the human GO syndrome. Mutant mice displayed altered osteoblastogenesis, matrix abnormalities, an overactivated TGF-β - Nox4 signaling, increased mtROS levels and an accumulation of DNA damages. Up to date two mechanisms after *Gorab* knockdown are possible:

- Firstly, loss of *Gorab* results in glycosylation defects leading subsequently to matrix abnormalities and exceeded TGF-β – Nox4 signaling. This causes high mtROS levels leading subsequently to DNA damages. As a consequence osteoblast maturation is delayed from terminal differentiation and in this process cells might undergo cell cycle arrest and senescence.

- Secondly, loss of transcriptional regulator *Gorab* might lead to a direct osteoblast to osteocyte differentiation delay. This results in an altered matrix secretion by undifferentiated osteoblasts leading to accelerated TGF-β – Nox4 signaling. Therefore cells accumulate mtROS and DNA damages which subsequently lead to cellular senescence.

One major point to address in the future will be the contribution of TGF-β to the bone phenotype in GO. To answer this, GorabPrx1cre and GorabRunx2cre will be treated postnatally either by Losartan or by 1D11. Losartan and the antibody 1D11 were both described to inhibit TGF-β and therefore increases bone mass and quality [37].

In addition, a currently ongoing project in our lab using GorabPrx1creCdkn2a and ideally also GorabPrx1creCdkn1a mice will get insight into the contribution of cellular cellular senescence to the bone phenotype in GO. To study the chondrocyte trans-differentiation impact on the bone phenotype different reporter mice (Osx, Col2a) should be used to understand the source of the accumulating osteocytes in the trabecular bone in 4 week old mice.

5. Bibliography

[1] R. Lisker, A. Hernández, M. Martínez-Lavin, O. Mutchinick, C. Armas, P. Reyes, and J. Robles-Gil, "Gerodermia osteodysplastica hereditaria: report of three affected brothers and literature review.," *Am. J. Med. Genet.*, vol. 3, no. 4, pp. 389–95, Jan. 1979.

[2] L. I. Al-Gazali, L. Sztriha, F. Skaff, and D. Haas, "Gerodermia osteodysplastica and wrinkly skin syndrome: are they the same?," *Am. J. Med. Genet.*, vol. 101, no. 3, pp. 213–20, Jul. 2001.

[3] F. Bamatter, A. Franceschetti, D. Klein, and A. Sierro, "Gerodermie osteodysplastique hereditaire," *Ann Pediat*, 1950.

[4] "OMIM Entry - # 219200 - CUTIS LAXA, AUTOSOMAL RECESSIVE, TYPE IIA; ARCL2A." [Online]. Available: http://www.omim.org/entry/219200. [Accessed: 16-Feb-2015].

[5] E. Morava, M. Guillard, D. J. Lefeber, and R. A. Wevers, "Autosomal recessive cutis laxa syndrome revisited.," *Eur. J. Hum. Genet.*, vol. 17, no. 9, pp. 1099–110, Sep. 2009.

[6] H. C. Hennies, U. Kornak, H. Zhang, J. Egerer, X. Zhang, W. Seifert, J. Kühnisch, B. Budde, M. Nätebus, F. Brancati, W. R. Wilcox, D. Müller, P. B. Kaplan, A. Rajab, G. Zampino, V. Fodale, B. Dallapiccola, W. Newman, K. Metcalfe, J. Clayton-Smith, M. Tassabehji, B. Steinmann, F. A. Barr, P. Nürnberg, P. Wieacker, and S. Mundlos, "Gerodermia osteodysplastica is caused by mutations in SCYL1BP1, a Rab-6 interacting golgin.," *Nat. Genet.*, vol. 40, no. 12, pp. 1410–2, Dec. 2008.

[7] M. Al-Dosari and F. S. Alkuraya, "A novel missense mutation in SCYL1BP1 produces geroderma osteodysplastica phenotype indistinguishable from that caused by nullimorphic mutations.," *Am. J. Med. Genet. A*, vol. 149A, no. 10, pp. 2093–8, Oct. 2009.

[8] Y. Di, J. Li, J. Fang, Z. Xu, X. He, F. Zhang, J. Ling, X. Li, D. Xu, L. Li, Y.-Y. Li, and K. Huo, "Cloning and characterization of a novel gene which encodes a protein interacting with the mitosis-associated kinase-like protein NTKL.," *J. Hum. Genet.*, vol. 48, no. 6, pp. 315–21, Jan. 2003.

[9] J. Egerer, D. Emmerich, B. Fischer-Zirnsak, W. Lee Chan, D. Meierhofer, B. Tuysuz, K. Marschner, S. Sauer, F. A. Barr, S. Mundlos, and U. Kornak, "GORAB Missense Mutations Disrupt RAB6 and ARF5 Binding and Golgi Targeting.," *J. Invest. Dermatol.*, May 2015.

[10] J. L. Burman, L. Bourbonniere, J. Philie, T. Stroh, S. Y. Dejgaard, J. F. Presley, and P. S. McPherson, "Scyl1, mutated in a recessive form of spinocerebellar neurodegeneration, regulates COPI-mediated retrograde traffic.," *J. Biol. Chem.*, vol. 283, no. 33, pp. 22774–86, 2008.

[11] J. L. Burman, J. N. R. Hamlin, and P. S. McPherson, “Scyl1 regulates Golgi morphology.,” *PLoS One*, vol. 5, no. 3, p. e9537, 2010.

[12] M. Kato, K. Yano, K. Morotomi-Yano, H. Saito, and Y. Miki, “Identification and characterization of the human protein kinase-like gene NTKL: mitosis-specific centrosomal localization of an alternatively spliced isoform.,” *Genomics*, vol. 79, no. 6, pp. 760–7, Jun. 2002.

[13] W. M. Schmidt, C. Kraus, H. Höger, S. Hochmeister, F. Oberndorfer, M. Branka, S. Bingemann, H. Lassmann, M. Müller, L. I. Macedo-Souza, M. Vainzof, M. Zatz, A. Reis, and R. E. Bittner, “Mutation in the Scyl1 gene encoding amino-terminal kinase-like protein causes a recessive form of spinocerebellar neurodegeneration.,” *EMBO Rep.*, vol. 8, no. 7, pp. 691–7, Jul. 2007.

[14] S. Pelletier, S. Gingras, S. Howell, P. Vogel, and J. N. Ihle, “An early onset progressive motor neuron disorder in Scyl1-deficient mice is associated with mislocalization of TDP-43.,” *J. Neurosci.*, vol. 32, no. 47, pp. 16560–73, 2012.

[15] R. P. Leng, Y. Lin, W. Ma, H. Wu, B. Lemmers, S. Chung, J. M. Parant, G. Lozano, R. Hakem, and S. Benchimol, “Pirh2, a p53-induced ubiquitin-protein ligase, promotes p53 degradation,” *Cell*, vol. 112, no. 6, pp. 779–791, 2003.

[16] A. Hakem, M. Bohgaki, B. Lemmers, E. Tai, L. Salmena, E. Matysiak-Zablocki, Y.-S. Jung, J. Karaskova, L. Kaustov, S. Duan, J. Madore, P. Boutros, Y. Sheng, M. Chesi, P. L. Bergsagel, B. Perez-Ordonez, A.-M. Mes-Masson, L. Penn, J. Squire, X. Chen, I. Jurisica, C. Arrowsmith, O. Sanchez, S. Benchimol, and R. Hakem, “Role of Pirh2 in mediating the regulation of p53 and c-Myc.,” *PLoS Genet.*, vol. 7, no. 11, p. e1002360, 2011.

[17] L. Zhang, J. Li, C. Wang, Y. Ma, and K. Huo, “A new human gene hNTKL-BP1 interacts with hPirh2.,” *Biochem. Biophys. Res. Commun.*, vol. 330, no. 1, pp. 293–7, Apr. 2005.

[18] U. Thirumurthi, J. Shen, W. Xia, A. M. LaBaff, Y. Wei, C.-W. Li, W.-C. Chang, C.-H. Chen, H.-K. Lin, D. Yu, and M.-C. Hung, “MDM2-mediated degradation of SIRT6 phosphorylated by AKT1 promotes tumorigenesis and trastuzumab resistance in breast cancer.,” *Sci. Signal.*, vol. 7, no. 336, p. ra71, Jan. 2014.

[19] M. A. Suico, R. Fukuda, R. Miyakita, K. Koyama, M. Taura, T. Shuto, and H. Kai, “The transcription factor MEF/Elf4 is dually modulated by p53-MDM2 axis and MEF-MDM2 autoregulatory mechanism.,” *J. Biol. Chem.*, vol. 289, no. 38, pp. 26143–54, Sep. 2014.

[20] J. Yan, Y. Di, H. Shi, H. Rao, and K. Huo, “Overexpression of SCYL1-BP1 stabilizes functional p53 by suppressing MDM2-mediated ubiquitination,” *FEBS Lett.*, vol. 584, no. 20, pp. 4319–4324, Oct. 2010.

[21] Y. Liu, Y. Chen, X. Lu, Y. Wang, Y. Duan, C. Cheng, and A. Shen, “SCYL1BP1 modulates neurite outgrowth and regeneration by regulating the Mdm2/p53 pathway.,” *Mol. Biol. Cell*, vol. 23, no. 23, pp. 4506–14, Dec. 2012.

[22] B. Wanschers, R. van de Vorstenbosch, M. Wijers, B. Wieringa, S. M. King, and J. Fransen, “Rab6 family proteins interact with the dynein light chain protein DYNLRB1.,” *Cell Motil. Cytoskeleton*, vol. 65, no. 3, pp. 183–96, Mar. 2008.

[23] B. Short, A. Haas, and F. A. Barr, “Golgins and GTPases, giving identity and structure to the Golgi apparatus,” *Biochim. Biophys. Acta - Mol. Cell Res.*, vol. 1744, no. 3, pp. 383–395, Jul. 2005.

[24] G. Li and M. C. Marlin, “Rab family of GTPases.,” *Methods Mol. Biol.*, vol. 1298, pp. 1–15, Jan. 2015.

[25] J. M. Lucocq, “A mitotic form of the Golgi apparatus in HeLa cells,” *J. Cell Biol.*, vol. 104, no. 4, pp. 865–874, Apr. 1987.

[26] V. Popoff, J. D. Langer, I. Reckmann, A. Hellwig, R. a. Kahn, B. Brügger, and F. T. Wieland, “Several ADP-ribosylation factor (Arf) isoforms support COPI vesicle formation,” *J. Biol. Chem.*, vol. 286, no. 41, pp. 35634–35642, 2011.

[27] S. F. Gilbert, “Osteogenesis: The Development of Bones.” Sinauer Associates, 2000.

[28] N. Ono, W. Ono, T. Nagasawa, and H. M. Kronenberg, “A subset of chondrogenic cells provides early mesenchymal progenitors in growing bones.,” *Nat. Cell Biol.*, vol. 16, no. 12, pp. 1157–1167, Nov. 2014.

[29] P. Milovanovic, E. A. Zimmermann, M. Hahn, D. Djonic, K. Püschel, M. Djuric, M. Amling, and B. Busse, “Osteocytic Canalicular Networks: Morphological Implications for Altered Mechanosensitivity,” *ACS Nano*, vol. 7, no. 9, pp. 7542–7551, Sep. 2013.

[30] T. J. Martin, K. W. Ng, and T. Suda, “Bone cell physiology.,” *Endocrinol. Metab. Clin. North Am.*, vol. 18, no. 4, pp. 833–58, Dec. 1989.

[31] F. F. Safadi, M. F. Barbe, S. M. Abdelmagid, M. C. Rico, R. A. Aswad, J. Litvin, and S. N. Popoff, *Bone Pathology*, vol. 2. Totowa, NJ: Humana Press, 2009.

[32] T. Komori, H. Yagi, S. Nomura, A. Yamaguchi, K. Sasaki, K. Deguchi, Y. Shimizu, R. . Bronson, Y.-H. Gao, M. Inada, M. Sato, R. Okamoto, Y. Kitamura, S. Yoshiki, and T. Kishimoto, “Targeted Disruption of Cbfa1 Results in a Complete Lack of Bone Formation owing to Maturational Arrest of Osteoblasts,” *Cell*, vol. 89, no. 5, pp. 755–764, May 1997.

[33] G. Karsenty, “Transcriptional control of skeletogenesis.,” *Annu. Rev. Genomics Hum. Genet.*, vol. 9, pp. 183–96, Jan. 2008.

[34] S. Stricker, R. Fundele, A. Vortkamp, and S. Mundlos, “Role of Runx genes in chondrocyte differentiation.,” *Dev. Biol.*, vol. 245, no. 1, pp. 95–108, May 2002.

[35] M. Ding, Y. Lu, S. Abbassi, F. Li, X. Li, Y. Song, V. Geoffroy, H.-J. Im, and Q. Zheng, “Targeting Runx2 expression in hypertrophic chondrocytes impairs endochondral ossification during early skeletal development.,” *J. Cell. Physiol.*, vol. 227, no. 10, pp. 3446–56, Oct. 2012.

[36] M. Hirata, F. Kugimiya, A. Fukai, T. Saito, F. Yano, T. Ikeda, A. Mabuchi, B. R. Sapkota, T. Akune, N. Nishida, N. Yoshimura, T. Nakagawa, K. Tokunaga, K. Nakamura, U. Chung, and H. Kawaguchi, "C/EBPβ and RUNX2 cooperate to degrade cartilage with MMP-13 as the target and HIF-2α as the inducer in chondrocytes.," *Hum. Mol. Genet.*, vol. 21, no. 5, pp. 1111–23, Mar. 2012.

[37] T. M. Schroeder, E. D. Jensen, and J. J. Westendorf, "Runx2: a master organizer of gene transcription in developing and maturing osteoblasts.," *Birth Defects Res. C. Embryo Today*, vol. 75, no. 3, pp. 213–25, Sep. 2005.

[38] Y. Zhang, R.-L. Xie, C. M. Croce, J. L. Stein, J. B. Lian, A. J. van Wijnen, and G. S. Stein, "A program of microRNAs controls osteogenic lineage progression by targeting transcription factor Runx2.," *Proc. Natl. Acad. Sci. U. S. A.*, vol. 108, no. 24, pp. 9863–8, Jun. 2011.

[39] S. L. Dallas and L. F. Bonewald, "Dynamics of the transition from osteoblast to osteocyte.," *Ann. N. Y. Acad. Sci.*, vol. 1192, pp. 437–43, Mar. 2010.

[40] Y. Nomura, "Structural change in decorin with skin aging.," *Connect. Tissue Res.*, vol. 47, pp. 249–255, 2006.

[41] D. R. Keene, J. D. San Antonio, R. Mayne, D. J. McQuillan, G. Sarris, S. A. Santoro, and R. V. Iozzo, "Decorin binds near the C terminus of type I collagen," *J. Biol. Chem.*, vol. 275, pp. 21801–21804, 2000.

[42] S. C. Manolagas, "Birth and death of bone cells: basic regulatory mechanisms and implications for the pathogenesis and treatment of osteoporosis.," *Endocr. Rev.*, vol. 21, no. 2, pp. 115–37, Apr. 2000.

[43] T. Katagiri and N. Takahashi, "Regulatory mechanisms of osteoblast and osteoclast differentiation.," *Oral Dis.*, vol. 8, pp. 147–159, 2002.

[44] V. Kartsogiannis and K. W. Ng, "Cell lines and primary cell cultures in the study of bone cell biology.," *Mol. Cell. Endocrinol.*, vol. 228, no. 1–2, pp. 79–102, Dec. 2004.

[45] F. Barrère, C. A. van Blitterswijk, and K. de Groot, "Bone regeneration: molecular and cellular interactions with calcium phosphate ceramics.," *Int. J. Nanomedicine*, vol. 1, no. 3, pp. 317–32, Jan. 2006.

[46] L. F. Bonewald, "The amazing osteocyte.," *J. Bone Miner. Res.*, vol. 26, no. 2, pp. 229–38, Feb. 2011.

[47] G. C. Nicholson, J. M. Moseley, P. M. Sexton, F. A. Mendelsohn, and T. J. Martin, "Abundant calcitonin receptors in isolated rat osteoclasts. Biochemical and autoradiographic characterization.," *J. Clin. Invest.*, vol. 78, no. 2, pp. 355–60, Aug. 1986.

[48] G. Chen, C. Deng, and Y.-P. Li, "TGF-β and BMP signaling in osteoblast differentiation and bone formation.," *Int. J. Biol. Sci.*, vol. 8, no. 2, pp. 272–88, Jan. 2012.

[49] M. Centrella, M. C. Horowitz, J. M. Wozney, and T. L. McCarthy, “Transforming growth factor-beta gene family members and bone.,” *Endocr. Rev.*, vol. 15, no. 1, pp. 27–39, Feb. 1994.

[50] K. Kitisin, T. Saha, T. Blake, N. Golestaneh, M. Deng, C. Kim, Y. Tang, K. Shetty, B. Mishra, and L. Mishra, “Tgf-Beta signaling in development.,” *Sci. STKE*, vol. 2007, no. 399, p. cm1, Aug. 2007.

[51] I. Grafe, T. Yang, S. Alexander, E. Homan, C. Lietman, M. M. Jiang, T. Bertin, E. Munivez, Y. Chen, B. Dawson, Y. Ishikawa, M. A. Weis, T. K. Sampath, C. Ambrose, D. Eyre, H. P. Bächinger, and B. Lee, “Supplementary Figure 1.”

[52] C. Li, Q. Wang, and J.-F. Wang, “Transforming growth factor-β (TGF-β) induces the expression of chondrogenesis-related genes through TGF-β receptor II (TGFRII)-AKT-mTOR signaling in primary cultured mouse precartilaginous stem cells.,” *Biochem. Biophys. Res. Commun.*, vol. 450, no. 1, pp. 646–51, Jul. 2014.

[53] K. Benke, B. Ágg, B. Szilveszter, F. Tarr, Z. B. Nagy, M. Pólos, L. Daróczi, B. Merkely, and Z. Szabolcs, “The role of transforming growth factor-beta in Marfan syndrome.,” *Cardiol. J.*, vol. 20, no. 3, pp. 227–34, Jan. 2013.

[54] M. S. Kocher and F. Shapiro, “Osteogenesis imperfecta.,” *J. Am. Acad. Orthop. Surg.*, vol. 6, pp. 225–36, 1998.

[55] S. Mundlos and B. R. Olsen, “Heritable diseases of the skeleton. Part II: Molecular insights into skeletal development-matrix components and their homeostasis.,” *FASEB J.*, vol. 11, no. 4, pp. 227–33, Mar. 1997.

[56] Y. Mochida, D. Parisuthiman, S. Pornprasertsuk-Damrongsri, P. Atsawasuwan, M. Sricholpech, A. L. Boskey, and M. Yamauchi, “Decorin modulates collagen matrix assembly and mineralization.,” *Matrix Biol.*, vol. 28, no. 1, pp. 44–52, Jan. 2009.

[57] R. V Iozzo, “The family of the small leucine-rich proteoglycans: key regulators of matrix assembly and cellular growth.,” *Crit. Rev. Biochem. Mol. Biol.*, vol. 32, no. 2, pp. 141–74, Jan. 1997.

[58] C. C. Reed and R. V Iozzo, “The role of decorin in collagen fibrillogenesis and skin homeostasis.,” *Glycoconj. J.*, vol. 19, no. 4–5, pp. 249–55, Jan. .

[59] D. R. Stamov, A. Müller, Y. Wegrowski, S. Brezillon, and C. M. Franz, “Quantitative analysis of type I collagen fibril regulation by lumican and decorin using AFM.,” *J. Struct. Biol.*, vol. 183, no. 3, pp. 394–403, Sep. 2013.

[60] R. V. Iozzo, “The Biology of the Small Leucine-rich Proteoglycans: FUNCTIONAL NETWORK OF INTERACTIVE PROTEINS,” *J. Biol. Chem.*, vol. 274, no. 27, pp. 18843–18846, Jul. 1999.

[61] D. Nikitovic, A. Berdiaki, A. Zafiropoulos, P. Katonis, A. Tsatsakis, N. K. Karamanos, and G. N. Tzanakakis, “Lumican expression is positively correlated with the differentiation and negatively with the growth of human osteosarcoma cells.,” *FEBS J.*, vol. 275, no. 2, pp. 350–61, Jan. 2008.

[62] A. Hernández, M. G. Aguirre-Negrete, S. González-Flores, M. C. Reynoso-Luna, R. Fragoso, Z. Nazará, G. Tapia-Arizmendi, and J. M. Cantú, “Ehlers-Danlos features with progeroid facies and mild mental retardation. Further delineation of the syndrome.,” *Clin. Genet.*, vol. 30, no. 6, pp. 456–61, Dec. 1986.

[63] M. F. Young, Y. Bi, L. Ameye, and X.-D. Chen, “Biglycan knockout mice: new models for musculoskeletal diseases.,” *Glycoconj. J.*, vol. 19, no. 4–5, pp. 257–62, Jan. .

[64] T. Tohmonda, Y. Miyauchi, R. Ghosh, M. Yoda, S. Uchikawa, J. Takito, H. Morioka, M. Nakamura, T. Iwawaki, K. Chiba, Y. Toyama, F. Urano, and K. Horiuchi, “The IRE1α-XBP1 pathway is essential for osteoblast differentiation through promoting transcription of Osterix.,” *EMBO Rep.*, vol. 12, pp. 451–457, 2011.

[65] P. A. Lucas, “Chemotactic Response of Osteoblast-Like Cells to Transforming Growth Factor Beta,” vol. 463, no. 1989, pp. 459–463, 1990.

[66] P. A. Lucas and A. I. Caplan, “Chemotactic response of embryonic limb bud mesenchymal cells and muscle-derived fibroblasts to transforming growth factor-beta.,” *Connect. Tissue Res.*, vol. 18, pp. 1–7, 1988.

[67] Y. Tang, X. Wu, W. Lei, L. Pang, C. Wan, Z. Shi, L. Zhao, T. R. Nagy, X. Peng, J. Hu, X. Feng, W. Van Hul, M. Wan, and X. Cao, “TGF-beta1-induced migration of bone mesenchymal stem cells couples bone resorption with formation.,” *Nat. Med.*, vol. 15, no. 7, pp. 757–765, 2009.

[68] M. P. Bostrom and P. Asnis, “Transforming growth factor beta in fracture repair.,” *Clin. Orthop. Relat. Res.*, no. 355 Suppl, pp. S124–S131, 1998.

[69] R. N. Rosier, R. J. O’Keefe, and D. G. Hicks, “The potential role of transforming growth factor beta in fracture healing.,” *Clin. Orthop. Relat. Res.*, pp. S294–S300, 1998.

[70] D. Pohlers, J. Brenmoehl, I. Löffler, C. K. Müller, C. Leipner, S. Schultze-Mosgau, A. Stallmach, R. W. Kinne, and G. Wolf, “TGF-beta and fibrosis in different organs - molecular pathway imprints.,” *Biochim. Biophys. Acta*, vol. 1792, no. 8, pp. 746–56, Aug. 2009.

[71] S. Y. Tang and T. Alliston, “Regulation of postnatal bone homeostasis by TGFβ.,” *Bonekey Rep.*, vol. 2, no. October 2012, p. 255, Jan. 2013.

[72] A. Erlebacher, E. H. Filvaroff, J. Q. Ye, and R. Derynck, “Osteoblastic responses to TGF-beta during bone remodeling.,” *Mol. Biol. Cell*, vol. 9, no. 7, pp. 1903–18, Jul. 1998.

[73] V. Kaartinen and D. Warburton, “Fibrillin controls TGF-beta activation.,” *Nat. Genet.*, vol. 33, no. 3, pp. 331–2, Mar. 2003.

[74] A. R. Tan, G. Alexe, and M. Reiss, “Transforming growth factor-beta signaling: emerging stem cell target in metastatic breast cancer?,” *Breast Cancer Res. Treat.*, vol. 115, no. 3, pp. 453–95, Jun. 2009.

[75] M. Kolb, P. J. Margetts, P. J. Sime, and J. Gauldie, “Proteoglycans decorin and biglycan differentially modulate TGF-beta-mediated fibrotic responses in the lung.,” *Am. J. Physiol. Lung Cell. Mol. Physiol.*, vol. 280, no. 6, pp. L1327–34, Jul. 2001.

[76] L. Hecker, N. J. Logsdon, D. Kurundkar, A. Kurundkar, K. Bernard, T. Hock, E. Meldrum, Y. Y. Sanders, and V. J. Thannickal, “Reversal of persistent fibrosis in aging by targeting Nox4-Nrf2 redox imbalance.,” *Sci. Transl. Med.*, vol. 6, no. 231, p. 231ra47, May 2014.

[77] Y. Yamabe, A. Shimamoto, M. Goto, J. Yokota, M. Sugawara, and Y. Furuichi, “Sp1-mediated transcription of the Werner helicase gene is modulated by Rb and p53.,” *Mol. Cell. Biol.*, vol. 18, no. 11, pp. 6191–200, Nov. 1998.

[78] J.-M. Lee, E.-H. Lee, I.-S. Kim, and J.-E. Kim, “Tgfbi deficiency leads to a reduction in skeletal size and degradation of the bone matrix.,” *Calcif. Tissue Int.*, vol. 96, no. 1, pp. 56–64, Jan. 2015.

[79] I. Grafe, T. Yang, S. Alexander, E. P. Homan, C. Lietman, M. M. Jiang, T. Bertin, E. Munivez, Y. Chen, B. Dawson, Y. Ishikawa, M. A. Weis, T. K. Sampath, C. Ambrose, D. Eyre, H. P. Bächinger, and B. Lee, “Excessive transforming growth factor-β signaling is a common mechanism in osteogenesis imperfecta.,” *Nat. Med.*, vol. 20, no. 6, pp. 670–5, Jun. 2014.

[80] J. R. Edwards, J. S. Nyman, S. T. Lwin, M. M. Moore, J. Esparza, E. C. O’Quinn, A. J. Hart, S. Biswas, C. a Patil, S. Lonning, A. Mahadevan-Jansen, and G. R. Mundy, “Inhibition of TGF-β signaling by 1D11 antibody treatment increases bone mass and quality in vivo.,” *J. Bone Miner. Res.*, vol. 25, no. 11, pp. 2419–26, Nov. 2010.

[81] S. I. Liochev, “Reactive oxygen species and the free radical theory of aging.,” *Free Radic. Biol. Med.*, vol. 60, pp. 1–4, Jul. 2013.

[82] K. Schröder, “NADPH Oxidases in Redox Regulation of Cell Adhesion and Migration,” *Antioxid. Redox Signal.*, 2013.

[83] F. M. Yakes and B. Van Houten, “Mitochondrial DNA damage is more extensive and persists longer than nuclear DNA damage in human cells following oxidative stress.,” *Proc. Natl. Acad. Sci. U. S. A.*, vol. 94, no. 2, pp. 514–9, Jan. 1997.

[84] T. Kuilman, C. Michaloglou, W. J. Mooi, and D. S. Peeper, “The essence of senescence.,” *Genes Dev.*, vol. 24, no. 22, pp. 2463–79, Nov. 2010.

[85] A. Elgawish, M. Glomb, M. Friedlander, and V. M. Monnier, “Involvement of hydrogen peroxide in collagen cross-linking by high glucose in vitro and in vivo.,” *J. Biol. Chem.*, vol. 271, no. 22, pp. 12964–71, May 1996.

[86] D. I. Brown and K. K. Griendling, “Nox proteins in signal transduction,” *Free Radical Biology and Medicine*, vol. 47. pp. 1239–1253, 2009.

[87] R. P. Brandes, N. Weissmann, and K. Schröder, “NADPH oxidases in cardiovascular disease,” *Free Radical Biology and Medicine*, vol. 49. pp. 687–706, 2010.

[88] J. L. Wilkinson-Berka, I. Rana, R. Armani, and A. Agrotis, “Reactive oxygen species, Nox and angiotensin II in angiogenesis: implications for retinopathy.,” *Clin. Sci. (Lond).*, vol. 124, pp. 597–615, 2013.

[89] K. Schröder, M. Zhang, S. Benkhoff, A. Mieth, R. Pliquett, J. Kosowski, C. Kruse, P. Luedike, U. R. Michaelis, N. Weissmann, S. Dimmeler, A. M. Shah, and R. P. Brandes, “Nox4 is a protective reactive oxygen species generating vascular NADPH oxidase.,” *Circ. Res.*, vol. 110, no. 9, pp. 1217–25, Apr. 2012.

[90] C. Goettsch, A. Babelova, O. Trummer, R. G. Erben, M. Rauner, S. Rammelt, N. Weissmann, V. Weinberger, S. Benkhoff, M. Kampschulte, B. Obermayer-Pietsch, L. C. Hofbauer, R. P. Brandes, and K. Schröder, “NADPH oxidase 4 limits bone mass by promoting osteoclastogenesis,” *J. Clin. Invest.*, vol. 123, pp. 4731–4738, 2013.

[91] J. Wu, J. Niu, X. Li, X. Wang, Z. Guo, and F. Zhang, “TGF-β1 induces senescence of bone marrow mesenchymal stem cells via increase of mitochondrial ROS production.,” *BMC Dev. Biol.*, vol. 14, no. 1, p. 21, Jan. 2014.

[92] I. Carmona-Cuenca, C. Roncero, P. Sancho, L. Caja, N. Fausto, M. Fernández, and I. Fabregat, “Upregulation of the NADPH oxidase NOX4 by TGF-beta in hepatocytes is required for its pro-apoptotic activity.,” *J. Hepatol.*, vol. 49, no. 6, pp. 965–76, Dec. 2008.

[93] K. Schröder, A. Kohnen, A. Aicher, E. A. Liehn, T. Büchse, S. Stein, C. Weber, S. Dimmeler, and R. P. Brandes, “NADPH oxidase Nox2 is required for hypoxia-induced mobilization of endothelial progenitor cells,” *Circ. Res.*, vol. 105, pp. 537–544, 2009.

[94] H. Nojiri, Y. Saita, D. Morikawa, K. Kobayashi, C. Tsuda, T. Miyazaki, M. Saito, K. Marumo, I. Yonezawa, K. Kaneko, T. Shirasawa, and T. Shimizu, “Cytoplasmic superoxide causes bone fragility owing to low-turnover osteoporosis and impaired collagen cross-linking,” *J. Bone Miner. Res.*, vol. 26, pp. 2682–2694, 2011.

[95] M. C. Velarde, J. M. Flynn, N. U. Day, S. Melov, and J. Campisi, “Mitochondrial oxidative stress caused by Sod2 deficiency promotes cellular senescence and aging phenotypes in the skin,” vol. 4, no. 1, pp. 3–12, 2012.

[96] S. Melov, P. Coskun, M. Patel, R. Tuinstra, B. Cottrell, A. S. Jun, T. H. Zastawny, M. Dizdaroglu, S. I. Goodman, T. T. Huang, H. Miziorko, C. J. Epstein, and D. C. Wallace, “Mitochondrial disease in superoxide dismutase 2 mutant mice.,” *Proc. Natl. Acad. Sci. U. S. A.*, vol. 96, pp. 846–851, 1999.

[97] J. Campisi and F. d’Adda di Fagagna, “Cellular senescence: when bad things happen to good cells.,” *Nat. Rev. Mol. Cell Biol.*, vol. 8, no. 9, pp. 729–40, Sep. 2007.

[98] F. Rodier and J. Campisi, “Four faces of cellular senescence.,” *J. Cell Biol.*, vol. 192, no. 4, pp. 547–56, Feb. 2011.

[99] S. Hubackova, K. Krejcikova, J. Bartek, and Z. Hodny, “IL1- and TGFβ-Nox4 signaling, oxidative stress and DNA damage response are shared features of replicative, oncogene-induced, and drug-induced paracrine ‘bystander senescence’.,” *Aging (Albany. NY).*, vol. 4, no. 12, pp. 932–51, Dec. 2012.

[100] J. C. Acosta, A. Banito, T. Wuestefeld, A. Georgilis, P. Janich, J. P. Morton, D. Athineos, T.-W. Kang, F. Lasitschka, M. Andrulis, G. Pascual, K. J. Morris, S. Khan, H. Jin, G. Dharmalingam, A. P. Snijders, T. Carroll, D. Capper, C. Pritchard, G. J. Inman, T. Longerich, O. J. Sansom, S. A. Benitah, L. Zender, and J. Gil, "A complex secretory program orchestrated by the inflammasome controls paracrine senescence.," *Nat. Cell Biol.*, vol. 15, no. 8, pp. 978–90, Aug. 2013.

[101] J. F. Passos, G. Nelson, C. Wang, T. Richter, C. Simillion, C. J. Proctor, S. Miwa, S. Olijslagers, J. Hallinan, A. Wipat, G. Saretzki, K. L. Rudolph, T. B. L. Kirkwood, and T. von Zglinicki, "Feedback between p21 and reactive oxygen production is necessary for cell senescence.," *Mol. Syst. Biol.*, vol. 6, no. 1, p. 347, Jan. 2010.

[102] S. Lin, J. Yang, A. G. Elkahloun, A. Bandyopadhyay, L. Wang, J. E. Cornell, I.-T. Yeh, J. Agyin, G. Tomlinson, and L.-Z. Sun, "Attenuation of TGF-β signaling suppresses premature senescence in a p21-dependent manner and promotes oncogenic Ras-mediated metastatic transformation in human mammary epithelial cells.," *Mol. Biol. Cell*, vol. 23, no. 8, pp. 1569–81, Apr. 2012.

[103] A. L. Fitzgerald, A. A. Osman, T.-X. Xie, A. Patel, H. Skinner, V. Sandulache, and J. N. Myers, "Reactive oxygen species and p21Waf1/Cip1 are both essential for p53-mediated senescence of head and neck cancer cells," *Cell Death Dis.*, vol. 6, no. 3, p. e1678, Mar. 2015.

[104] K. H. Vousden, "ROS and senescence in the control of aging," vol. 2, no. 8, pp. 71–74.

[105] K. F. Macleod, N. Sherry, G. Hannon, D. Beach, T. Tokino, K. Kinzler, B. Vogelstein, and T. Jacks, "p53-Dependent and independent expression of p21 during cell growth, differentiation, and DNA damage," *Genes Dev.*, vol. 9, pp. 935–944, 1995.

[106] D. Lessel, J. Oshima, and C. Kubisch, "[Werner syndrome. A prototypical form of segmental progeria.]," *Medizinische Genet. Mitteilungsblatt des Berufsverbandes Medizinische Genet. e.V*, vol. 24, no. 4, pp. 262–267, Dec. 2012.

[107] C. R. Burtner and B. K. Kennedy, "Progeria syndromes and ageing: what is the connection?," *Nat. Rev. Mol. Cell Biol.*, vol. 11, pp. 567–578, 2010.

[108] J. Gotzmann and R. Foisner, "A-type lamin complexes and regenerative potential: a step towards understanding laminopathic diseases?," *Histochem. Cell Biol.*, vol. 125, no. 1–2, pp. 33–41, Jan. 2006.

[109] J. K. Sinha, S. Ghosh, and M. Raghunath, "progeria : A rare genetic premature ageing disorder," no. May, pp. 667–674, 2014.

[110] R. C. M. Hennekam, "Hutchinson – Gilford Progeria Syndrome : Review of the Phenotype," vol. 2624, pp. 2603–2624, 2006.

[111] L. Chen and J. Oshima, "Werner syndrome," *Journal of Biomedicine and Biotechnology*, vol. 2002. pp. 46–54, 2002.

[112] I. Varela, J. Cadiñanos, A. M. Pendás, A. Gutiérrez-Fernández, A. R. Folgueras, L. M. Sánchez, Z. Zhou, F. J. Rodríguez, C. L. Stewart, J. A. Vega, K. Tryggvason, J. M. P. Freije, and C. López-Otín, "Accelerated ageing in mice deficient in Zmpste24 protease

is linked to p53 signalling activation.," *Nature*, vol. 437, no. 7058, pp. 564–8, Sep. 2005.

[113] B. Liu, J. Wang, K. M. Chan, W. M. Tjia, W. Deng, X. Guan, J. Huang, K. M. Li, P. Y. Chau, D. J. Chen, D. Pei, A. M. Pendas, J. Cadiñanos, C. López-Otín, H. F. Tse, C. Hutchison, J. Chen, Y. Cao, K. S. E. Cheah, K. Tryggvason, and Z. Zhou, "Genomic instability in laminopathy-based premature aging.," *Nat. Med.*, vol. 11, no. 7, pp. 780–5, Jul. 2005.

[114] B. Liu, S. Ghosh, X. Yang, H. Zheng, X. Liu, Z. Wang, G. Jin, B. Zheng, B. K. Kennedy, Y. Suh, M. Kaeberlein, K. Tryggvason, and Z. Zhou, "Resveratrol rescues SIRT1-dependent adult stem cell decline and alleviates progeroid features in laminopathy-based progeria.," *Cell Metab.*, vol. 16, no. 6, pp. 738–50, Dec. 2012.

[115] J. de la Rosa, J. M. P. Freije, R. Cabanillas, F. G. Osorio, M. F. Fraga, M. S. Fernández-García, R. Rad, V. Fanjul, A. P. Ugalde, Q. Liang, H. M. Prosser, A. Bradley, J. Cadiñanos, and C. López-Otín, "Prelamin A causes progeria through cell-extrinsic mechanisms and prevents cancer invasion.," *Nat. Commun.*, vol. 4, p. 2268, Jan. 2013.

[116] E. Schmidt, O. Nilsson, A. Koskela, J. Tuukkanen, C. Ohlsson, B. Rozell, and M. Eriksson, "Expression of the Hutchinson-Gilford progeria mutation during osteoblast development results in loss of osteocytes, irregular mineralization, and poor biomechanical properties.," *J. Biol. Chem.*, vol. 287, no. 40, pp. 33512–22, Sep. 2012.

[117] Y. Liu, S. Strecker, L. Wang, M. S. Kronenberg, W. Wang, D. W. Rowe, and P. Maye, "Osterix-cre labeled progenitor cells contribute to the formation and maintenance of the bone marrow stroma.," *PLoS One*, vol. 8, no. 8, p. e71318, Jan. 2013.

[118] P. R. Musich and Y. Zou, "Genomic instability and DNA damage responses in progeria arising from defective maturation of prelamin A.," *Aging (Albany. NY).*, vol. 1, no. 1, pp. 28–37, Jan. 2009.

[119] C. Rosnoblet, R. Peanne, D. Legrand, and F. Foulquier, "Glycosylation disorders of membrane trafficking.," *Glycoconj. J.*, vol. 30, no. 1, pp. 23–31, Jan. 2013.

[120] H. H. Freeze and B. G. Ng, "Golgi glycosylation and human inherited diseases.," *Cold Spring Harb. Perspect. Biol.*, vol. 3, no. 9, p. a005371, Sep. 2011.

[121] U. Kornak, E. Reynders, A. Dimopoulou, J. van Reeuwijk, B. Fischer, A. Rajab, B. Budde, P. Nürnberg, F. Foulquier, D. Lefeber, Z. Urban, S. Gruenewald, W. Annaert, H. G. Brunner, H. van Bokhoven, R. Wevers, E. Morava, G. Matthijs, L. Van Maldergem, and S. Mundlos, "Impaired glycosylation and cutis laxa caused by mutations in the vesicular H+-ATPase subunit ATP6V0A2.," *Nat. Genet.*, vol. 40, no. 1, pp. 32–4, Jan. 2008.

[122] B. Fischer, A. Dimopoulou, J. Egerer, T. Gardeitchik, A. Kidd, D. Jost, H. Kayserili, Y. Alanay, I. Tantcheva-Poor, E. Mangold, C. Daumer-Haas, S. Phadke, R. I. Peirano, J. Heusel, C. Desphande, N. Gupta, A. Nanda, E. Felix, E. Berry-Kravis, M. Kabra, R. A. Wevers, L. van Maldergem, S. Mundlos, E. Morava, and U. Kornak, "Further characterization of ATP6V0A2-related autosomal recessive cutis laxa.," *Hum. Genet.*, vol. 131, no. 11, pp. 1761–73, Nov. 2012.

[123] Y. Di, J. Li, J. Fang, Z. Xu, X. He, F. Zhang, J. Ling, X. Li, D. Xu, L. Li, Y.-Y. Li, and K. Huo, “Cloning and characterization of a novel gene which encodes a protein interacting with the mitosis-associated kinase-like protein NTKL.,” *J. Hum. Genet.*, vol. 48, pp. 315–321, 2003.

[124] T. Yamazaki, C. Kawai, A. Yamauchi, and F. Kuribayashi, “A highly sensitive chemiluminescence assay for superoxide detection and chronic granulomatous disease diagnosis.,” *Trop. Med. Health*, vol. 39, no. 2, pp. 41–5, Jun. 2011.

6. Abbreviations

% .....Percent
µ .....Micro
µCT .....Micro Computed Tomography
A.dest .....Acqua destilled
AgNO3 .....Silver nitrate
ARCL .....Autosomal recessive cutis laxa
ATP6V0A2.....ATPase, H+ transporting, lysosomal V0 subunit a2
Bglap .....Osteocalcin
BPO.....benzoylperoxide
BS .....Bone surface
BSA.....Bovine Serum Albumine
BV .....Bone Volume
cDNA .....complementary DNA+B45
Cort .....Cortical Bone
d .....day
DAPI .....4',6-Diamidin-2-phenylindol
DMEM .....Dulbecco's Modified Eagle Medium
DMP1.....Dentin matrix acidic phosphoprotein 1
DNA.....Deoxyribonucleic acid
ECM.....Extracellular matrix
EDTA.....Ethylenediaminetetraacetic acid
EM .....Electron Microscopy
ER .....Endoplasmatic Reticulum
FBS .....Fetal Bovine Serum
fl.....flox
g .....gram
g/L.....gram per Liter
GAGs .....Glycosaminoglycans
GAPDH.....Glycerinaldehyde-3-phosphate Dehydrogenase
GO.....Gerodermia Osteodysplastica
GORAB.....Golgin RAB6-interacting Protein
h .....hour

H2O.....water
H2O2.....Hydrogen Peroxide
HAF.....Human Fibroblast
HGPS .....Hutchinson-Gilford Progeria Syndrome
IF.....Immunofluorescence
kDA.....kilo Dalton
M.....Molar
max .....maximum
mg .....milligram
min .....minutes
ml .....milliliter
MMA.....Methylmethacrylate
n .....number
nm .....nanometer
O.th.....Osteoid thickness
o/n .....overnight
Obs .....Osteoblasts
oC.....Degree Celsius
Ocn.....Osteocalcin
OS .....Osteoid surface
Osx .....Osterix
p .....p value
PBS .....Phosphate buffered saline
PFA .....Paraformaldehyde
PGs.....Proteoglycans
POBs .....Primary Osteoblasts
p-Smad .....Phospho Smad
Px .....Passage X
PYCR1 .....Pyroline-5-carboxylate reductase
qPCR.....quantitative PCR
RNA .....Ribonucleic acid
ROI.....Region of Interest
ROS .....Reactive Oxygen Species
SD .....Standard Deviation
SOST.....Sclerostin

TGF-β.....Transforming growth factor β

Trab.....Trabeculae

TRAP .....Tartrate-resistant acid phosphatase

TV .....Tissue Volume

TX-100.....Tritox 100

UG.....Ultraglutamine

7. Acknowledgements

Zu allererst möchte ich mich bei Prof. Dr. Uwe Kornak und Prof. Dr. Stefan Mundlos für die Überlassung des hochinteressanten Themas und die Bereitstellung des Arbeitsplatzes herzlich bedanken. Ich verdanke euch jede erdenklich hilfreiche Unterstützung und viele anregende Diskussionen im Zuge unserer Gorab Meetings. Jede Phase dieser Arbeit wurde stets intensiv und professionell begleitet und der kompetente Rat kam mir stets zugute. Besonders aber möchte ich mich für die Freiheit bedanken die mir während des gesamten Projekts gewährt wurde. Mein ganz besonderer Dank gilt auch Dr. Winglee (Hardy) Chan. Jederzeit war er mir eine Stütze bei der Planung, Durchführung und Auswertung der Arbeit. Zudem war er mit wegweisenden und kreativen Ideen stets eine wertvolle Unterstützung.

Ein ganz besonderer Dank gilt Sabine Stumm. Danke für deine unermüdliche, geduldige und immer freundliche Art und deine Begeisterung für die Maushistologie. Du warst immer eine wichtige Stütze im Labor. Großen Dank an Anja für die Genotypisierung der verschiedenen Mausstämme.

Großer Dank gebührt meinen lieben Kollegen sowie allen Mitarbeitern des Instituts. Claire, Denise, Anja, Björn, Philippe, Raghu, Johannes E., Johannes G, Alexej, Mohammed - ihr habt mich liebevoll und freundschaftlich in euer Team aufgenommen und mich mit großer Unterstützung in alle wichtigen Prozesse im Labor eingearbeitet. Bei unseren Diskussionen die oft auch über die Grenzen des Laboralltags hinaus gingen hatten wir immer sehr viel Spaß. Leider war die gemeinsame Zeit im Labor mit Daniela und Michael viel zu kurz aber ich habe euch von Anfang an sehr lieb gewonnen.

Ich möchte mich auch bei Dr. Daniel Ibrahim bedanken der mich in die Methode des *ChIP Sequencings* eingearbeitet hat und mir bei vielen Fragen eine große Hilfe war.

Ein ganz besonderer Dank geht an meine Eltern, die mich immer unterstützen. Danke dafür, dass ihr für meine Geschwister und mich alles erdenkliche bereit seid zu geben. Ich möchte mich auch bei meinem Freund Paul bedanken. Danke, dass du immer an meiner Seite bist und mich immer unterstützt und ermutigst. Allen meinen lieben Freunden danke ich für die Ausdauer, Ruhe und Geduld, und für die aufmunternden Worte wenn diese nötig waren.

Bei der Österreichischen Akademie der Wissenschaften möchte ich mich für die finazielle Unterstützung und bei der *Berlin School for Regenerative Therapies* für die begleitenden Doktorandenseminare und inhaltlichen Anregungen bedanken.